SIGNAL AND IMAGE PROCESSING ALGORITHMS USING INTERVAL CONVEX PROGRAMMING AND SPARSITY

A DISSERTATION SUBMITTED TO

THE DEPARTMENT OF ELECTRICAL AND ELECTRONICS ENGINEERING

AND THE GRADUATE SCHOOL OF ENGINEERING AND SCIENCE

OF BILKENT UNIVERSITY

IN PARTIAL FULFILLMENT OF THE REQUIREMENTS

FOR THE DEGREE OF

DOCTOR OF PHILOSOPHY

By

Kıvanç Köse

September, 2012

I certify that I have read this thesis and that in my opinion it is fully adequate, in scope and in quality, as a dissertation for the degree of Doctor of Philosophy.

Prof. Dr. Ahmet Enis Çetin(Advisor)

I certify that I have read this thesis and that in my opinion it is fully adequate, in scope and in quality, as a dissertation for the degree of Doctor of Philosophy.

Prof. Dr. Orhan Arıkan

I certify that I have read this thesis and that in my opinion it is fully adequate, in scope and in quality, as a dissertation for the degree of Doctor of Philosophy.

Assoc. Prof. Uğur Güdükbay

I certify that I have read this thesis and that in my opinion it is fully adequate, in scope and in quality, as a dissertation for the degree of Doctor of Philosophy.

Prof. Dr. Ömer Morgül

I certify that I have read this thesis and that in my opinion it is fully adequate, in scope and in quality, as a dissertation for the degree of Doctor of Philosophy.

Asst. Prof. Behçet Uğur Töreyin

Approved for the Graduate School of Engineering and Science:

Prof. Dr. Levent Onural
Director of the Graduate School

ABSTRACT

SIGNAL AND IMAGE PROCESSING ALGORITHMS USING INTERVAL CONVEX PROGRAMMING AND SPARSITY

Kıvanç Köse
Ph.D. in Electrical and Electronics Engineering
Supervisor: Prof. Dr. Ahmet Enis Çetin
September, 2012

In this thesis, signal and image processing algorithms based on sparsity and interval convex programming are developed for inverse problems. Inverse signal processing problems are solved by minimizing the ℓ_1 norm or the Total Variation (TV) based cost functions in the literature. A modified entropy functional approximating the absolute value function is defined. This functional is also used to approximate the ℓ_1 norm, which is the most widely used cost function in sparse signal processing problems. The modified entropy functional is continuously differentiable, and convex. As a result, it is possible to develop iterative, globally convergent algorithms for compressive sensing, denoising and restoration problems using the modified entropy functional. Iterative interval convex programming algorithms are constructed using Bregman's D-Projection operator. In sparse signal processing, it is assumed that the signal can be represented using a sparse set of coefficients in some transform domain. Therefore, by minimizing the total variation of the signal, it is expected to realize sparse representations of signals. Another cost function that is introduced for inverse problems is the Filtered Variation (FV) function, which is the generalized version of the Total Variation (VR) function. The TV function uses the differences between the pixels of an image or samples of a signal. This is essentially simple Haar filtering. In FV, high-pass filter outputs are used instead of differences. This leads to flexibility in algorithm design adapting to the local variations of the signal. Extensive simulation studies using the new cost functions are carried out. Better experimental restoration, and reconstructions results are obtained compared to the algorithms in the literature.

Keywords: Interval Convex Programming, Sparse Signal Processing, Total Variation, Filtered Variation, D-Projection, Entropic Projection, Inverse Problems.

ÖZET

ARALIK DIŞBÜKEY PROGRAMLAMA VE SEYREKLİK KULLANAN İMGE VE SİNYAL İŞLEME ALGORİTMALARI

Kıvanç Köse
Elektrik ve Elektronik Mühendisliği, Doktora
Tez Yöneticisi: Prof. Dr. Ahmet Enis Çetin
Eylül 2012

Bu tezde ters problemleri çözmek için kullanılabilecek aralık dışbükey programlama ve seyreklik bilgilerini kullanan algoritmalar geliştirilmiştir. Sinyal işleme literatüründe ters problemler ℓ_1 normu ya da Toplam Değişinti bazlı maliyet fonksiyonları kullanılarak çözülür. Bu tezde mutlak değer fonksiyonunu yaklaşıklayan değiştirilmiş entropi fonksiyonelini tanımladık. Bu fonksiyonel aynı zamanda seyrek sinyal işleme konusunda en sıklıkla kullanılan maliyet fonksiyonu olan ℓ_1 normunuda yaklaşıksamaktadır. Önerdiğimiz değiştirilmiş entropi fonksiyoneli sürekli, dışbükey ve her yerde türevlenebilirdir. Bu özelliklerinden dolayı değiştirilmiş entropi fonksiyonelini kullanarak sıkıştırmalı algılama, gürültü temizleme ve geri çatım gibi problemlere döngülü, her yerde yakınsayan algoritmalar geliştirmek mümkündür. Bregman tarafından bulunan D-İzdüşümü işletmeni kullanılarak döngülü aralık dışbükey programlama algoritmaları geliştirilebilir. Seyrek sinyal işlemede, bir sinyalin herhangi bir dönüşüm uzayında seyrek olduğu varsayılır. Bu varsayımdan yola çıkarak, bir sinyalin Toplam Değişintisinin enküçüklenmesi ile sinyalin seyrek temsillerinin gerçellenmesi sağlanması umulmaktadır. Biz bu tezde Filtrelenmiş Değişinti adını verdiğimiz, yeni bir maliyet fonksiyonu önermekteyiz. Bu fonksiyon aynı zamanda Toplam Değişinti fonksiyonunun genelleştirilmiş halidir. Toplam Değişinti sinyalin sadece yanyana iki örneğinin ya da yanyana iki pikselinin farkını kullanır. Bu aslında basit bir Haar filtrelemesinden başka birşey değildir. Filtrelenmiş Değişinti ise farklar yerine yüksek geçirgenli filtre çıktıları kullanılır. Bu bize sinyal içindeki farklı yerel değişintilere adaptasyon olanağı sağlar. Bu tez kapsamında önerilen yeni maliyet fonksiyonlarını kullanan kapsamlı simülasyon yapılmıştır. Bu önerilen yeni maliyet fonksiyonları sinyal geri çatımı, sinyallerin gürültüden arındırılması, ve birden fazla boğumlu ağlarda, boğum çıktılarının gürültüden arındırılması ve tahmin edilmesi problemleri kullanılarak test edilmiştir. Literatürdeki yöntemlere kıyasla daha başarılı sinyal geri çatımı ve oluşturulması sonuçları gözlemlenmiştir.

Anahtar sözcükler: Aralık Dışbükey programlama, Seyrek Sinyal İşleme, Toplam Değişinti, Filterelenmiş Değişinti, D-izdüşüm, Entropik İzdüşüm, Ters Problemler.

Acknowledgement

First of all I would like to thank Prof Cetin for bringing light to my path in the dark labyrinth of research. Sometimes he believed in me more than myself and motivated me like a father. He has showed a patience of job against me. I would like to thank him for all his patience and belief in me.

I would also like to specially thank to Dr. Gudukbay for not only his suggestions during my research but also treating me like a colleague and being a so good travel mate.

I would like to thank Prof Arikan, Prof Morgul and Dr. Toreyin for reading this thesis and giving me very fruitful feedback about my research.

I dedicate a big portion of this thesis to my significant other, best friend, and love Bilge. She supported me at every day of my Ph.D., believed in me and my research even if she does not understand a single equation of it. In my most desperate days, she cheered me up and put up with my all caprices. She became the complementary part of my life and soul.

I also would like to thank to my father Mustafa, mom Guler and brother Uygur for their support and encouragement. Especially, I would like to thank my mom for calling me every day and giving daily tips about protecting myself from cold, hunger and more importantly reminding me nothing is more important than my health.

Thanks to Ali and Sevgi Kasli for treating me like a mad scientist and acknowledge all my absurdity.

I would like to specially thank to Ayca and Mehmet for helping and supporting me not only in academic but also other aspects of my life and be very close friends. Thanks to Alican, Namik, and Serdar for the Tabldot and afternoon break sessions during which we talk about everything but nothing.

Thanks to Alex for supporting me at my darkest hours, and passing me his wisdom. He also deserves a special thanks to put up with minutely ringing telephones to me. I also would like to thank Erdem, Elif, Asli, Erdem S, Ali Ozgur, Gokhan Bora, Yigitcan, Fahri, and all my other Bilkent EE friends for not only considering me as a colleague but also as a part of their life.

Bilkent SPG team members especially Osman, Serdar, Ihsan and Ahmet, also deserves a special thanks for being so supportive and sharing.

Also Muruvet Parlakay deserves a special thanks for organizing everything in the department and making our lives much simpler.

I also want to mention my gratitude to Tabldot for serving hot meals daily even during the emptiest days of summer when all the other places are closed. With its perfect diet, we have carried out our brain development and pursued our research.

In this limited space, I may have forgotten to utter some of my friends' and colleagues' names however this does not mean that they are less valuable to me. Thanks to all of them.

The research that we present in this research is funded by TUBITAK with project number 111E057. I would like to thank them for their support.

Contents

List of Figures

List of Tables

List of Abbreviations

Abbreviation	Description
AWGN	Additive White Gaussian Noise
ATC	Adapt and Combine
CS	Compressive Sensing
CSM	Compressive Sensing Microarrays
CTA	Combine and Adapt
DCT	Discrete Cosine Transform
DFT	Discrete Fourier Transform
DHT	Discrete Hartley Transform
DMD	Digital Micromirror Device
DTFT	Discrete Time Fourier Transform
EMSE	Excess Mean-Square Error
FFT	Fast Fourier Transform
FIR	Finite Impulse Response
FV	Filtered Variation
HPF	High Pass Filter
LATV	Locally Adaptive Total Variation
LTV	Local Total Variation
MRI	Magnetic Resonance Imaging
NRMSE	Normalized Root Mean-Square Error
POCS	Projection onto Convex Sets
TV	Total Variation

Chapter 1

INTRODUCTION

In many signal processing applications, it may not be possible to have a direct access to the original signal. Instead, we can only access to measurements, which are noisy, irregularly taken, or sometimes below the sampling rate limit determined by Shannon-Nyquist theorem [5]. The inverse problem of reconstructing or estimating the original signal from this incomplete or defective set of measurements has always drawn the attention of the researchers. Recently, with the introduction of the Compressive Sensing (CS) [6] framework, research on sparsity has reached to a peak. Most signals such as speech, sound, image, and video signals are sparse in some transform domain such as DCT, and DFT. CS takes advantage of this fact and researchers developed methods for reconstructing the original signal from randomized measurements. Concept of sparsity has already been used in other inverse problems including deconvolution, image restoration from noisy and blurred measurements [7–10].

In this thesis, new signal processing algorithms for inverse problems are developed. These algorithms are based on sparsity [11] and interval convex programming [12]. Bregman's D-Projection [13], convex programming [12, 14, 15] and Total Variation (TV) [16] concepts from the literature are utilized to develop these algorithms. New CS signal reconstruction, signal denoising, and adaptive filtering methods are developed using these fundamental concepts.

The rest of the thesis is organized as follows. In the succeeding parts of Chapter 1, related algorithms in the literature are reviewed. In Section 1.2, the CS framework and some of the CS reconstruction algorithms are presented. The notation that is used throughout this thesis is also introduced in this section. In Section 1.3, the TV concept and its signal processing applications are briefly presented.

In Chapter 2, the modified entropy functional is defined. This functional approximates the ℓ_1 norm, which is the preferred cost function in sparse signal processing. Then, Bregman's D-Projection [13] operator is linked to the modified entropy functional, and entropy projection operator is introduced. This projection operator allows us to solve sparse signal processing problems as interval convex programming problems. Using row-action methods, large problems can be divided into smaller subproblems, and solved in an iterative manner through local D-projections. The proposed iterative algorithm is globally convergent, if certain starting point conditions are satisfied [13].

In Chapter 3, first the Filtered Variation (FV) concept is linked to the well known Total Variation (TV) function. Instead of using a single differencing operator as in TV, it is possible to use "high-pass filters" in FV. High-pass filter design is a well-established field in signal processing. As a result, the FV approach allowed high-pass filters to be incorporated into the TV framework. In Section 3.1, six different FV constraints, which impose bounds on the signal in different transform domains (e.g. spatial, Fourier, DCT) are introduced. These FV constraints will be used for signal reconstruction, and denosing purposes in Sections 4.1 and 5.2.

Starting from Chapter 4, signal reconstruction (Chapter 4), and signal denoising (Chapter 5) problems are discussed respectively, and new signal processing algorithms based on interval convex programming, modified entropy functional, and FV concepts are introduced. In Section 4.1, FV method is used for reconstructing signals from irregularly sampled data. Typically, low-pass filtering based interpolation algorithms are used for this purpose. In this thesis, an iterative approach, in which alternating time and frequency domain constraint are applied on the irregularly sampled data to estimate its regularly sampled version. Reconstruction results using different amount of samples, as well as the performance of the algorithm in noisy scenarios are presented.

In Section 4.2, a novel CS reconstruction algorithm, that uses modified entropy function based D-projections and row action methods is presented. The proposed algorithm divides the large problem into smaller subproblems defined by the rows of the measurement matrix. Each linear measurement defined by the rows of the measurement matrix defines a hyperplane constraint. The proposed algorithm individually solves these smaller subproblems in an iterative manner by taking D-projections onto these hyperplanes. The iterative algorithm converges to the solution of the large problem, in this way. Since the modified entropy functional is a convex cost function, projection on convex sets (POCS) theorem guarantees the convergence of the proposed iterative approach [17]. Simulation results on 1D and 2D signals, as well as a comparison with a well known algorithm from the literature called CoSaMP [18] are presented.

Signal denoising is another application area that we covered in this thesis. Both, a locally adaptive version of the TV denoising algorithm presented in [19] and FV based novel denoising algorithm are developed in this thesis. In Section 5.1, a locally adaptive TV denoising algorithm for signal denoising is presented. The TV denoising algorithms in the literature tries to minimize the same TV cost function on the entire image at once. This approach has two main drawbacks. All portions of a signal may not have similar edge content or may not have the same texture. Therefore, using the same TV minimization parameters on the entire image may oversmooth the edges or can not clean the noise at smooth regions effectively. Moreover, as the signal gets larger, the TV minimization approach may become computationally too complex to solve.

The developed locallly adaptive total variation (LATV) approach overcomes these drawbacks by block processing the image, and solving the TV minimization problem locally in each block. This block based approach also enables us to vary the TV denosing parameters according to the edge content of the blocks. The advantages of the proposed LATV approach over the TV denoising method are illustrated through image denoising examples.

In Section 5.2, a FV constraints based image denoising algorithm is presented. The proposed algorithm applies a set of FV constraints on the noisy image in a cascaded and cyclic manner. Through this cascaded and cyclic approach, the denoised signal that lies in the intersection of the FV constraints set is obtained. The proposed algorithm is compared with the results of the denoising method in [3].

In Chapter 6, entropy projection and FV constraints are used on a multi-node network for adaptation and learning purposes [20]. First the multi-node network framework by Sayed et al. [4] is introduced. Then, in Section 6.2, an entropy projection based adaptation scheme is presented. Since the modified entropy functional estimated the ℓ_1 norm much better than the ℓ_2 norm, it has much better adaptation performance under heavy-tailed noise such as ε-contaminated Gaussian noise. The adaptation algorithm presented in [4] and the proposed algorithm are compared against different noise scenarios.

In Section 6.3 new diffusion adaptation algorithms that uses the Total Variation (TV) and Filtered Variation (FV) frameworks are introduced. The TV and FV based schemes combine the information based on both spatially neighboring nodes and the last temporal state of the node of interest in the network. Experimental results indicate that the proposed algorithms lead to more robust systems, which provide improvements compared to the reference approach under heavy tailed noise such as ε-contaminated Gaussian noise.

1.2 Compressive Sensing

In discrete time signal processing applications, sampling is the first processing step. In this process, samples from a continuous time signal are collected by making equidistant measurements from the signal. Nyquist-Shannon sampling theorem [5] defines the necessary perfect reconstruction conditions that should be considered while discretizing a continuous time signal. When a bandlimited continuous time signal is sampled with a sampling frequency that is at least two times larger than its bandwidth, perfect reconstruction is possible using simple low pass filtering (sinc interpolation). The sampling rate offered by Nyquist-Shannon sampling theorem constitutes a lower bound for perfect reconstruction in time/spatial domain.

In most of the signal processing applications, first the signal is sampled according to the Nyquist-Shannon sampling criteria, and then transformed into another domain (e.g., Fourier, wavelet, discrete cosine transform domains), in which it has a simple representation. This simple representation can be obtained by getting rid of the negligibly small coefficients in the transform domain. This is an ineffective way of sampling a signal, because the information that will be thrown away after the signal transformation stage is also measured through the sampling process. However, sampling process is carried out by analog electronic circuits in many practical systems and it is very difficult to impose intelligence on analog systems. Therefore, we have to sample signals and images in a uniform manner in practice.

The sampling procedure would be more effective if it would be possible to sample the signal directly at the sparsifying transform domain, and just measure those few non-zero entries of the transformed signal. However, there are two problems with this approach: (i) the user may not have a prior knowledge about which transform domain to use, (ii) the user may not apriori know which transform domain coefficients are non-zero.

Let's assume that we have a mixture of two pure sinusoidal signals, whose frequencies are f_1, and f_2 respectively. According to Nyquist-Shannon sampling theorem, this signal should be sampled at least at rate of $2|f_1 - f_2|$ Hz (two times its bandwidth). On the other hand, the same signal can be represented using just four impulses in frequency domain. Therefore, it has a 4-sparse representation in frequency domain. If the sampling is done in the frequency domain, making only four measurements at the location of the impulses would be enough for perfect reconstruction.

However, in a typical signal processing application, the locations of those four non-zero coefficients cannot be known beforehand. Therefore, one needs to sample the signal at the Nyquist sampling rate and after that he/she can find the location of those impulses.

The CS framework [6, 11, 21] tries to provide a solution to this problem by making compressed measurements over the signal of interest. Assume that we have a signal $x[n]$, and a transformation matrix ψ that can transform the signal into another domain. The transformation procedure is simply finding the inner product of the signal $x[n]$ with the rows ψ_i of the transformation matrix ψ as follows

$$s_i = < \mathbf{x}, \psi_i >, \; i = 1, 2, ..., N, \tag{1.1}$$

where $\mathbf{x}$ is a column vector, whose entries are samples of the signal $x[n]$. The original signal $x[n]$ can be reconstructed using the inverse transformation operation in a similar fashion as

$$\mathbf{x} = \sum_{i=1}^{N} s_i.\psi_i \tag{1.2}$$

or in vector form as

$$\mathbf{x} = \psi.\mathbf{s} \tag{1.3}$$

where $\mathbf{s}$ is a vector containing the transform domain coefficients, s_i. The basic idea in digital waveform coding is that the signal should be approximately reconstructed from only a few of its non-zero transform coefficients. In most cases including JPEG image coding standard, the transform matrix ψ is chosen such that the new signal $\mathbf{s}$ is easily representable in the transform domain with a small number of coefficients. A signal $\mathbf{x}$ is compressible, if it has a few large valued s_i coefficients in the transform domain and the rest of the coefficients are either zeros or very small valued.

In compressive sensing framework, the signal is assumed to be a K-Sparse signal in a transformation domain such as DFT domain, DCT domain, or wavelet domain. A signal with length N is K-Sparse, if it has K non-zero and $(N - K)$ zero coefficients in a transform domain. The case of interest in CS problems is when $K << N$ i.e., sparse in the transform domain.

The CS theory introduced in [11, 21–23] tries to provides answers to the question of reconstructing a signal from its compressed measurements $\mathbf{y}$, which is defined as follows;

$$\mathbf{y} = \phi.\mathbf{x} = \phi.\psi.\mathbf{s} = \theta.\mathbf{s} \tag{1.4}$$

where ϕ, and θ are the $M \times N$ measurement matrices in signal and transform domains respectively, and $M << N$. Applying simple matrix inversion or inverse transformation techniques on compressed measurements $\mathbf{y}$ does not results in a sparse solution. A sparse solution can be obtained by solving the following optimization problem

$$\mathbf{s}_p = \text{argmin } ||\mathbf{s}||_0 \quad \text{such that} \quad \theta.\mathbf{s} = \mathbf{y}. \tag{1.5}$$

However this problem is a NP-complete optimization problem, therefore its solution can not be found easily. If certain conditions such as Restricted Isometry Property (RIP) [5,6] hold for the measurement matrix ϕ , then the ℓ_0 norm minimization problem (1.5) can be approximated by the ℓ_1 norm minimization as follows

$$\mathbf{s}_p = \text{argmin } ||\mathbf{s}||_1 \quad \text{such that} \quad \theta.\mathbf{s} = \mathbf{y}. \tag{1.6}$$

It is shown in [21, 22] that constructing ϕ matrix from random numbers, which are i.i.d Gaussian random variables, and choosing the number of measurements as $cKlog(N/K) < M \ll N$ satisfies the RIP conditions. This lower boundary for the number of the measurements can be decreased, if more constraints can be imposed on the signal model as in Model based Compressed Sensing approach in [24]

1.2.1 Compressed Sensing Reconstructions Algorithms

In the following parts of the thesis, a brief summary of the CS reconstruction algorithms is presented. The algorithms are categorized into 3 main groups as: ℓ_1 minimization, greedy, and combinatorial algorithms.

1.2.1.1 ℓ_1 Minimization Algorithms

As mentioned in Section 1.2, the CS reconstruction algorithm can be formulated as an ℓ_1 regularized optimization problem and can be solved accurately if certain conditions such as RIP are satisfied. On the other hand, through some modification the basis problem can be relaxed and converted to a convex optimization problem, which can be accurately and efficiently solved using numerical solvers. The equality constraint

$$\begin{aligned} &\underset{\mathbf{s}}{\text{argmin}} && ||\mathbf{s}||_1 \\ &\text{subject to} && \theta.\mathbf{s} = \mathbf{y} \end{aligned} \tag{1.7}$$

version of the CS problem can be solved using linear programming methods. If the measurements are contaminated by noise then the CS problem can be relaxed as

$$\begin{aligned} &\underset{\mathbf{s}}{\text{argmin}} && ||\mathbf{s}||_1 \\ &\text{subject to} && ||\theta.\mathbf{s} - \mathbf{y}||_2^2 < \varepsilon \end{aligned} \tag{1.8}$$

where $\varepsilon > 0$ constant depends on the noise power. This version of the problem can be solved using a conic constraint techniques respectively.

Basis Pursuit [25, 26] is one of the most famous algorithm of this type. It is a variant of linear programming that can be solved using standard convex optimization methods. Several researchers also developed and adapted other convex optimization techniques to solve the CS recovery problem. They convert the ℓ_1 minimization based CS reconstruction algorithms in unconstrained

$$x = \text{argmin}\frac{1}{2}||\theta\mathbf{s} - \mathbf{y}||_2^2 + \lambda||\mathbf{s}||_1 \tag{1.9}$$

or the constrained

$$\begin{aligned} &\underset{\mathbf{s}}{\text{argmin}} && ||\mathbf{s}||_1 \\ &\text{subject to} && ||\theta\mathbf{s} - \mathbf{y}||_2^2 < \epsilon \end{aligned} \tag{1.10}$$

minimization problems, which can be solved efficiently using convex optimization techniques [27–30]. For each ϵ in (1.10), there exits a conjugate λ value in (1.9), using which both of the formulations will lead to the same results.

1.2.1.2 Greedy Algorithms

Greedy algorithms aim to find the best or optimal solution for a subset of the large CS problem at each stage. It then aims to achieve the global optimum as the subset is extended to the entire problem. Some of the most well-known greedy CS reconstruction algorithms in the literature are Iterative Hard Thresholding (IHT) [31], Orthogonal Matching Pursuit (OMP) [32], and Compressive Sampling Matching Pursuit (CoSaMP) [18].

Iterative hard thresholding algorithm starts with an initial estimate of the $k-$sparse signal $\mathbf{s}_0$ as a length-N zero vector. Then the algorithm iterates a gradient descent step with respect to the measurements matrix and obtains $\mathbf{s}_1$. The hard thresholded version $\mathbf{s}_{1H}$ of the current iterate $\mathbf{s}_1$ is then obtained through the hard thresholding operator

$$s_{1H}[n] = \begin{cases} s_1[n] & , \quad |s_1[n]| > T \\ 0 & , \quad |s_1[n]| < T \end{cases} , \; n = 1, 2, ..., N. \tag{1.11}$$

which keeps k largest coefficients of iterate and sets the rest to zero. Then, the algorithm do another gradient descent opreation and proceeds with the same algorithmic steps until a stopping criterion is met. This stopping criteria can either be running for a certain amount of iterations or when the distance between to consecutive iterates become smaller than a certain threshold.

The OMP algorithm also starts with an initial estimate of the sparse signal $\mathbf{s}_0$ as a vector of zeros. Then it finds the column $\theta^*_{\mathbf{i}}$ of the measurement matrix θ that is most correlated with the measurement vector $\mathbf{y}$. Lets assume that j^{th} column of the measurement matrix θ^*_j results in the highest correlation with the measurement vector $\mathbf{y}$. Then the inner product of the measurement vector with j^{th} column of the measurement matrix is taken as

$$s_j =< \mathbf{y}, \theta^*_{\mathbf{j}} > \tag{1.12}$$

where s_j is the j^{th} coefficient of the sparse vector. At the end of the first step, the residual of the measurement vector $\mathbf{y}_1$ after the first iteration is calculated as

$$\mathbf{y}_1 = \mathbf{y} - \tilde{s}_j \theta^*_{\mathbf{j}} \tag{1.13}$$

Then, the algorithm reiterates using the residual vector $\mathbf{y}_1$, updated signal $\tilde{\mathbf{s}}_1$ and the rest of the measurement matrix θ^1

$$\theta^1 = \theta^*_{\mathbf{k}}, \quad k = 1, 2, 3, ..., M, \; k \neq j \tag{1.14}$$

The algorithm terminates if the iteration count reaches to a limit or the error $||\mathbf{y} - \theta \mathbf{s}_n||$ decreases under a certain predefined threshold at the n^{th} iteration. The OMP algorithm is so popular that variants of the algorithm such as: Stagewise OMP (StOMP) [33], regularized OMP (ROMP) [34], and Expectation Maximization based Matching Pursuit (EMMP) [35] are also developed by researchers.

CoSaMP [18] is another frequently used iterative CS reconstruction algorithm. Besides the measurement matrix and the measurement vector, CoSaMP algorithm also needs the exact sparsity level of the signal as a parameter to reconstruct the original signal from the CS measurements. The algorithm is composed five stages: (i) identification, (ii) support merger, (iii) estimation, (iv) pruning, and (v) sample update. CoSaMP iterations starts with an initial estimate for the residuals $\mathbf{r}_0 = \mathbf{y}$. In the identification stage, the algorithm estimates the signal proxy $\mathbf{p}_1$ from the current residual estimate as

$$\mathbf{p}_1 = \theta^* \mathbf{r}_0 \tag{1.15}$$

where θ^* is the conjugate transpose of the measurement matrix.

In the second step, the support of the current estimate is merged with the support from the last step. Then the projection of the observations $\mathbf{y}$ on the determined signal support is taken using pseudo inverse of the measurement matrix as

$$\mathbf{s}_1 = (\theta^* \theta)^{-1} \theta^* y \tag{1.16}$$

In the pruning step, the largest k components of the projection vector $\tilde{s}^1$ are kept and the rest of the entries are set to zero. In last stage, the residual vector is updated using the current signal estimate as

$$\mathbf{r}_1 = \mathbf{y} - \theta \; H_T(\mathbf{s_1}) \tag{1.17}$$

where $H_T(.)$ is the hard thresholding operator. Details, as well as the pseudo code of the algorithm is given in [18]. The proposed CS reconstruction algorithms will be compared with the CoSaMP algorithm in Section 4.2.

1.2.1.3 Combinatorial Algorithms

Combinatorial CS algorithms are originated from combinatorial group testing methods from theoretical computer science community [36]. This type of algorithms rely on designing the measurement or test matrices in such a way that the original signal can be reconstructed from minimum number of tests. The measurement matrix that is used in these type of approaches consists of two main parts. The first part locates the large components of the signal and the second part estimates those large components. Building a measurement matrix with such structure requires the user to freely play with the coefficients of the measurement matrix. This is in contrast with the RIP property, which puts restrictions on the measurement matrix to guarantee the convergence of the CS problem.

If such an effective matrix that satisfies the the RIP conditions can be designed, combinatorial methods work extremely fast.This is the main advantage of the combinatorial algorithms. Moreover, contrary to other CS recovery algorithms, the computational complexity of combinatorial algorithms increase linearly proportional to the sparsity level of the signal, not the signal length. Therefore they are independent of the problem size. However, their structural requirements on the measurement matrix limits their use in practice. Among the several algorithms, Heavy hitters on steroids (HHS) pursuit [37] and sub-linear Fourier transform [38] are the most well-known ones.

1.2.2 Applications of Compressed Sensing

CS sampling framework, has drawn attention from several fields such as electrical and electronics engineering, computer engineering, physics, etc... Resarchers have applied ideas from CS framework to a diverse set of research topics. One of the earliest application that CS framework made debut is the Single Pixel Camera [21, 39, 40]. Single pixel camera is composed of a lens, a DMD, and a single pixel sensor. The sensor takes compressed measurements of the captures scene, using the random sampling pattern on the DMD array. The system is actually working like a camera and takes several measurements for a certain amount of time with different sampling patterns on the DMD array. Then the picture of the captured scene is reconstructed from the compressed measurement using any of the methods that were described in this section. Video processing, coding [41], background subtraction [42] can be named as some of the other famous CS applications in the field of imaging.

Medical imaging is another field that CS framework is frequently applied to. Especially in Magnetic Resonance Imaging (MRI) field, CS has extensively been used. MRI data is implicitly sparse in spatial difference or in wavelet domains [43, 44]. In fact, angiograms are sparse in pixel representations [45, 46]. Due to the sparse nature of the captured images, CS framework has been frequently used for MRI applications. Other medical imaging fields that CS found field of applications are photo-acoustic tomography [47] and computerized tomography [48]. Another imaging field that CS frameworks is used is hyperspectral imaging. In [49], the authors developed a method for taking compressed measurements using a modified hyperspectral camera. They also developed the corresponding reconstruction framework.

Other than imaging, CS based algorithms are developed also for optics applications. In [50], the authors developed an algorithm for the reconstructing sub-wavelength information from the far-field of an optical image using CS reconstructions methods. In [51], authors developed a novel measurement matrix (pseudo-random phase-shifting mask) for sampling an optical field and related CS based reconstruction algorithm. Holography is another field in optics,in which several CS based algorithms are developed [52–54].

As another medical application, in [55], the authors presented a novel DNA microarray called compressive sensing arrays (CSM), which can take compressed measurement from the target DNA. They developed several methods for probe design and CS recovery, based on the new measuring procedure that they developed.

Audio coding [56], Radar signal processing [57–59], Remote Sensing [60, 61], Communications [62–64], and Physics [65,66] are some of the other research fields that CS framework found application ares.

1.3 Total Variational Methods in Signal Processing

The ℓ_p norm based regularized optimization problems take the signal as a whole and uses the ℓ_p-norm based energy of the signal of interest as the cost metric. However, most of the signals that are addressed in signal processing applications are low-pass in nature, which means that the neighboring samples are highly correlated with each other in general. Instead of considering the $p-$norm energy of the signal samples, the TV norm considers the ℓ_1 energy of the derivatives around each sample. So, it uses the relation between the samples rather than considering them individually. In this way, the TV norm based solutions preserve the edges and boundaries in an image more accurately, and result in sharper image reconstruction results. Therefore, the TV norm is more appropriate for image processing applications [67, 68].

Total Variation (TV) functional was introduced to signal and image processing problems by Rudin et al. in 1990's [3, 16, 69–74]. For a 1-D signal $\mathbf{x}$ of length N, the TV of $\mathbf{x}$ is defined as,

$$||\mathbf{x}||_{TV} = \sum_{n=1}^{N-1} \sqrt{(x[n] - x[n+1])^2}. \tag{1.18}$$

or in N-Dimension,

$$||\mathbf{I}||_{TV} = \int_{\Omega} |\nabla \mathbf{I}| d\mathbf{I} \tag{1.19}$$

where I is an N-dimensional signal, ∇ is the gradient operator and $\Omega \subseteq R^N$ is the set of the samples of the signal. TV functional is utilized by several purposes in the signal, and image processing literature. In the forthcoming subsections of the thesis, only the ones that are related to compressive sensing, and denoising applications are covered.

1.3.1 The Total Variation based Denoising

In this section, signal denoising problems in literature and their formulations are reviewed. Formulations regarding the two-dimensional case (e.g. image denoising) are used through the review, however extending the ideas to $\mathbb{R}^N$ is straightforward. Let the observed signal $\mathbf{y}$ be a corrupted version of the original signal $\mathbf{x}$ by some noise $\mathbf{u}$ as follows

$$y_{i,j} = x_{i,j} + u_{i,j}. \tag{1.20}$$

where $[i, j] \in \Omega$, and $y_{i,j}, x_{j,j}, u_{j,j}$ are the pixels at the $[i, j]^{th}$ location of the observed, original, and noise signals respectively. The aim of the denoising algorithms are to estimate the original signal $\mathbf{x}$ from the noisy observations with highest possible SNR. The initial attempts to achieve variational denoising involves least squares ℓ_2 fit, because it leads to linear equations [75–77]. These type of methods try to solve the following minimization problem

$$\begin{aligned} &\min && \int_\Omega \left(\frac{d^2\mathbf{x}}{di^2} + \frac{d^2\mathbf{x}}{dj^2}\right)^2 \\ &\text{subject to} && \int_\Omega \mathbf{y} = \int_\Omega \mathbf{x} \quad and \quad \int_\Omega (\mathbf{x} - \mathbf{y})^2 = \sigma^2. \end{aligned} \tag{1.21}$$

where $\mathbf{x}$ is the estimated image, and $\frac{d^2\mathbf{x}}{di^2} + \frac{d^2\mathbf{x}}{dj^2}$ are the second derivatives in horizontal and vertical directions of the image respectively. The system given in (1.21) is easy to solve using numerical linear algebraic methods. However the results are not satisfactory [16].

Using the ℓ_1 norm based regularizations in (1.21) is avoided because they can not be handled by purely algebraic frameworks [16]. However, when the solutions of the two norms are compared, the ℓ_1 norm based estimations are visually much better than the ℓ_2 norms based approximations [69]. In [67], the authors introduced the concept of shock filters to the image denoising literature. In [67], the shock filtered version of an image $\mathbf{I}_{SF}$ is defined as follows

$$\mathbf{I}_{SF} = -\nabla(\mathbf{I})F(\nabla^2(\mathbf{I})) \tag{1.22}$$

where F is a function that satisfies $F(0) = 0, \; sign(s)F(s) \geq 0$. The shock filter is iteratively applied to an image as

$$\mathbf{I}^{n+1} = \mathbf{I}^n - \mathbf{I}^n_{SF} \tag{1.23}$$

where $\mathbf{I}^n$ and $\mathbf{I}^{n+1}$ are the image after n^{th} and $n+1^{st}$ iterations. The authors showed in [67] that, shock filters can deblur images for noiseless scenarios. However, as shown in Figure 1.1, shock filters given in [67] do not change the TV of the signal that it operates on. Therefore, they can work on noisy and blurred images. Recently in [78], the authors developed shock filters based algorithms that can also deblur noisy images. In [68], the authors investigate the TV preserving enhancements on images. They developed finite difference schemes for deblurring images, without distorting the variation in the original image.

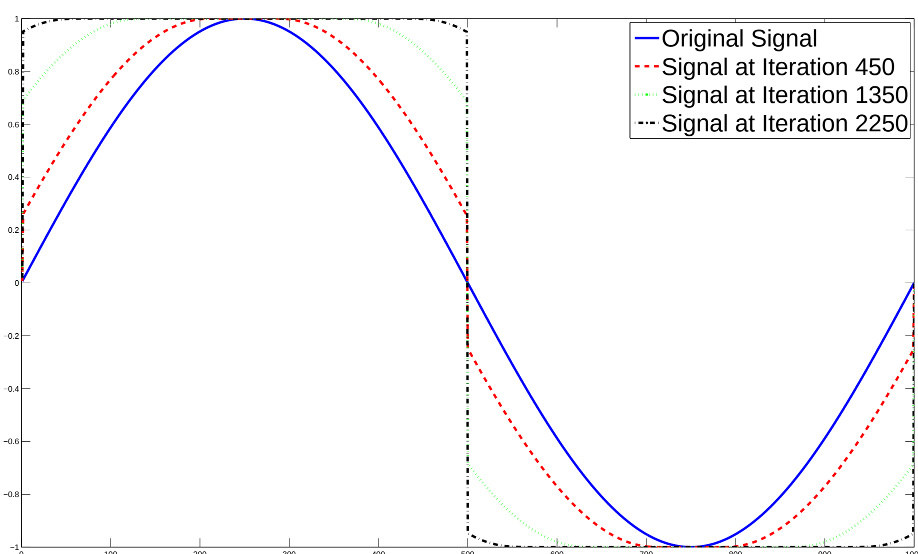

Figure 1.1: Shock filtered version of a sinusoidal signal after 450, 1340, and 2250 shock filtering iterations. To generate this figure, the code in [1] is used.

In [16], a TV constrained minimization algorithm for image denoising is proposed. This article is one of the first article that introduced the TV functional to the signal processing society. The algorithm solves the denoising problem through the following constrained minimization formulation

$$\begin{aligned} \min \quad & \int_\Omega \sqrt{(x_{i+1,j} - x_{i,j})^2 + (x_{i,j+1} - x_{i,j})^2} = ||\mathbf{x}||_{TV} \\ \text{subject to} \quad & \int_\Omega \mathbf{y} = \int_\Omega \mathbf{x} \\ & \int_\Omega \frac{1}{2}(\mathbf{y} - \mathbf{x})^2 = \sigma^2, \end{aligned} \tag{1.24}$$

where $\sigma > 0$ is a constant, which heavily depends on noise and $||\mathbf{x}||_{TV}$ is the TV norm. The authors used Euler-Lagrange method to solve (1.24).

Another formulation for the image denoising problem is proposed by Chambolle in [19] as follows

$$\begin{aligned} \min_{\mathbf{x}} \quad & ||\mathbf{x}||_{TV} \\ \text{subject to} \quad & ||\mathbf{y} - \mathbf{x}|| \leq \varepsilon. \end{aligned} \tag{1.25}$$

or in Lagrangian formulation

$$\min_{\mathbf{x}} ||\mathbf{y} - \mathbf{x}||^2 + \lambda ||\mathbf{x}||_{TV} \tag{1.26}$$

where ε is the error tolerance, and λ is the Lagrange multiplier. For each ε parameter in (1.25), there exists a conjugate λ parameter in (1.26), using which the solution of both formulations attain the same results. It is important to note that both (1.25), and (1.26) try to bound the variation between the pixels on the entire image. Therefore, some of the high-frequency details in the image may be over-smoothed or some the noise at low-frequency regions cannot be cleaned effectively.

In the Section 5.1 of this thesis, the formulation of Chambolle's image denoising algorithm [19] is revisited and a locally adaptive version of the this algorithm is presented.

1.3.2 The TV based Compressed Sensing

Most of the CS reconstruction algorithms in literature use the ℓ_p norm based regularization schemes where $p \in [0, 1]$. A brief review of such algorithms was given in Section 1.2. However, as mentioned in Section 1.3, the TV norm is more appropriate for image processing applications [67, 68]. The reason why the TV norm is more appropriate for CS reconstruction is as follows. The transitions between the pixels of a natural image are smooth, therefore the underlying gradient of an image should be sparse. As the ℓ_p norm based regularization results in sparse signal reconstruction, the TV norm based regularization results in signals with sparse gradients. This observation lead the researchers to develop new CS reconstruction algorithms, by replacing the ℓ_p norm based regularization with the TV regularization steps as follows

$$\begin{aligned} \underset{\mathbf{x}}{\text{argmin}} \quad & ||\mathbf{x}||_{TV} \\ \text{subject to} \quad & \theta.\mathbf{s} = \mathbf{y} \end{aligned} \tag{1.27}$$

where $||\mathbf{x}||_{TV}$ is defined as in (1.24) and the relation between $\mathbf{s}$ and $\mathbf{x}$ is defined as in (1.3). However, the model in (1.27) is hard to solve, since the TV norm term is non-linear and non-differentiable. Some of the most well-known CS reconstruction algorithms that solves the TV regularized CS problem are: Total Variation minimization by Augmented Lagrangian and Alternating Direction Minimization (TVAL3) [79], Second Order Cone Programming (SOCP) [80], ℓ_1-Magic [11, 22, 81], and Nesterov's Algorithm (NESTA) [82].

In [79] Li introduced TVAL3 algorithm that efficiently solves the TV minimization problem in (1.27) using a combination of Augmented Lagrangian Model and Alternating Minimization schemes. In the thesis, the author also introduces some measurement matrices with special structures that accelerates the TVAL3 algorithm.

The SOCP algorithm given in [80] reformulated the TV minimization problem as a second-order cone program, and solves it using interior point algorithms. SOCP is very slow since it uses interior-point algorithm and solves a large linear system at each iteration.

The ℓ_1-Magic algorithm also reformulated the TV regularized CS problem as a second-order cone problem. But instead of using interior-point method, it uses log-barrier method to solve the problem. The ℓ_1-Magic algorithm is more efficient than SOCP in terms of computational complexity, because it solves the linear system in an iterative manner. However, it is not effective in large-scale problems, since it uses Newton's method at each iteration to approximate the intermediate solution.

The NESTA [82] algorithm is a first order method of solving Basis Pursuit problems. The developers used Nesterov's smoothing techniques [83] to speed up the algorithm. It is possible to use the NESTA algorithm for the TV regularization based CS recovery, by modifying the smooth approximation of the objective function [79].

1.4 Motivation

Inverse problems cover a wide range of applications in signal processing. An algorithm developed for a specific problem can easily be adapted to several other type of inverse problems. For example TV functional is first introduced to the signal processing literature as a method for denoising in [16]. Then it found wide range of applications in signal reconstruction problems such as compressive sensing. Actually compressive sensing itself is example for this situation.

CS was first introduced as an alternative sampling scheme. During recent years, both sampling and reconstruction parts of the CS algorithms became a subject of research. Several scientists developed new methods for constructing more efficient measurement matrices for finding more effective ways of taking compressed measurements, whereas some other scientists developed new reconstruction methods. Moreover, the efforts to apply the CS framework to different applications can not be underestimated.

Besides developing novel tools, researchers also took several other algorithms and methods from literature and adapted/applied them to inverse problems. TV functional and interval convex programming are two of the several algorithm of this kind. Especially from optimization literature countlessly many algorithms are migrated to the signal processing field and used succesfully.

In this thesis, our motivation is to develop novel methods that can be used in several different type of inverse problems. In that sense, our aim is not only developing a specific algorithm but also a generic tool that can be widely used. Inspired from Bregman's D-Projection operation and related row-action methods, two new tools are developed for sparse signal processing applications. First the D-Projection concept is integrated with a convex cost functional called modified entropy functional, which is a shifted and even-symmetric version of the original entropy function. The proposed functional well estimates the ℓ_1 norm; therefore, it is well suited for obtaining sparse solutions from convex integer programming problems. Moreover, due the convex nature of its cost function, entropic projection is suitable for row-iteration type of operations, in which smaller and independent subproblems in the entire problem are solved individually in an iterative and cyclic manner and yet the solution converges the solution of the large problem.

Then, the well-known TV functional based methods are improved through a high-pass filtering based variation regularization scheme called Filtered variation (FV). FV framework enables the user to integrate various types of filtering schemes into the signal processing problems that can be formulated as variation regularization based optimization problems.

As mentioned earlier, the applicability of the new tools are not limited to a specific inverse problem. In this thesis, the efficacy of the new tools are illustrated on three different problems. However, the applicability of the proposed methods to other signal processing examples is also possible. Starting from next chapter, first these new tools are defined, then they are applied to three different type of inverse problems namely as signal reconstruction, signal denoising and adaptation and learning in multi node networks.

Chapter 2

ENTROPY FUNCTIONAL AND ENTROPIC PROJECTION

In this section, the modified entropy functional is introduced as an alternative cost function against the ℓ_1 and the ℓ_0 norms, and entropic projection operator is defined. Bregman's D-Projection operator introduced in [13] is utilized for this purpose. Bregman developed D-Projection, and related convex optimization algorithms in 1960's and his algorithms are widely used in many signal reconstruction and inverse problems [3, 12, 15, 17, 70, 84–90].

The ℓ_p norm of a signal $\mathbf{x} \in \mathbb{R}^N$ is defined as follows

$$||\mathbf{x}||_p = \left(\sum_i x_i^p \right)^{\frac{1}{p}}, \ i = 1...N. \tag{2.1}$$

The ℓ_p norm is frequently used as a cost function in optimization problems such as the ones in [4, 21, 22]. Assume that M measurements y_i are taken from a length-N signal $\mathbf{x}$ as

$$\theta_i.\mathbf{s} = y_i \quad \text{for} \quad i = 1, 2, ..., M, \tag{2.2}$$

where θ_i is the i^{th} row of the measurement matrix θ and $\mathbf{s}$ is the k-sparse transform domain representation of the signal $\mathbf{x}$. Each equation in (2.2) represents a hyperplane $H_i \in \mathbb{R}^N$, which are closed and convex sets in $\mathbb{R}^N$. In many inverse problem, the main aim is to estimate the original signal vector $\mathbf{x}$ or its transform domain representation $\mathbf{s}$ using the measurement vector $\mathbf{y}$. If $M = N$ and the columns of the measurement matrix are uncorrelated (hyperplanes are orthogonal to each other), then the solution can be found through inversion of the measurement matrix θ.

However, in most of the signal processing applications, we either have less number of measurements ($M < N$), e.g. CS, or the measurements are noisy, e.g. denoising. In this case, the best we can do is to find the solution that lies at the intersection of the hyperplanes or hyperslabs defined by the rows of the measurement matrix. This problem can be converted to an optimization problem as follows

$$\begin{aligned} &\min && g(\mathbf{s}) \\ &\text{subject to} && \theta_i.\mathbf{s} = y_i,\ i = 1, 2, ..., M. \end{aligned} \tag{2.3}$$

where $g(\mathbf{s})$ is the cost function, and it can be chosen as any ℓ_p norm. When $p > 1$ the ℓ_p norm cost function is convex. Therefore, convex optimization tools can be utilized. However, when $p \in [0, 1]$, e.g. CS problems defined in (1.5) and (1.6), the cost function is neither convex, nor differentiable everywhere. Due to this reason, convex optimization tool cannot be used directly.

Several researcher replaced the ℓ_0 norm in (1.5) with the ℓ_p norm, where $p \in (0, 1)$ [91] for solving the CS problems. Even if the resulting optimization problem is not convex, several studies in the literature have addressed these ℓ_p norm based non-convex optimization problems and apply their results to the sparse signal reconstruction example [92, 93]. In this thesis, an entropy functional based cost function is used to find approximate solutions to the inverse problems defined in (2.3), which will lead us to the entropic projection operator.

The entropy functional

$$g(v) = -v \log v \tag{2.4}$$

has already been used to approximate the solution of ℓ_1 optimization and linear programming problems in signal and image reconstruction by Bregman [13], and others [12, 84, 87, 89, 94]. However, the original entropy function $-vlog(v)$ is not valid for negative values of v. In signal processing applications, entries of the signal vector may take both positive and negative values. Therefore, the entropy function in (2.4) is modified and extended to negative real numbers as follows

$$g_e(v) = \left(|v| + \frac{1}{e}\right) \ln \left(|v| + \frac{1}{e}\right) + \frac{1}{e}, \tag{2.5}$$

and the multi-dimensional version of (2.5) is given by

$$g_e(\mathbf{v}) = \sum_{i=1}^{N} \left(|v_i| + \frac{1}{e}\right) \ln \left(|v_i| + \frac{1}{e}\right) + \frac{1}{e}, \tag{2.6}$$

where $\mathbf{v}$ is a length-N vector with v_i as its entries and e is the base of natural logarithm or the Euler's number. Actually, by changing the base of the logarithm, a family of cost functions can be defined. For any base b, the modified entropy function can be defined as

$$g_b(v) = \left(|v| + \frac{1}{b^{ln(b)}}\right) \log_b \left(|v| + \frac{1}{b^{ln(b)}}\right) + \frac{1}{b^{\ln(b)} \ln(b)}, \tag{2.7}$$

Through out the thesis we will use ln and log interchangeably, and if we would like to use logarithm with another base we will write the base of the logarithm explicitly.

The modified entropy function is a new cost function that is used as an alternative way to approximate the CS problem. In Figure 2.1, plots of the different cost functions including the modified entropy function with base e as well as the absolute value $g(v) = |v|$ and $g(v) = v^2$ are shown. The modified entropy functional (2.5) is convex, and continuously differentiable, and it slowly increases compared to $g(v) = v^2$, because $\ln(v)$ is much smaller than v for high v values as seen in Figure 2.1. Moreover, it well approximates ℓ_1 norm, which is frequently used in sparse signal processing applications such as compressed sensing and denoising.

Bregman provides globally convergent iterative algorithms for problems with convex, continuous and differentiable cost functionals. His iterative reconstruction algorithm starts with an initial estimate $\mathbf{s}_0 = \mathbf{0} = [0, 0, ...0]^T$. In each step of the iterative algorithm, successive D-projections are performed onto the hyperplanes H_i, $i = 1, 2, ..., M$ with respect to a cost function $g(\mathbf{s})$, that are defined as in (2.3).

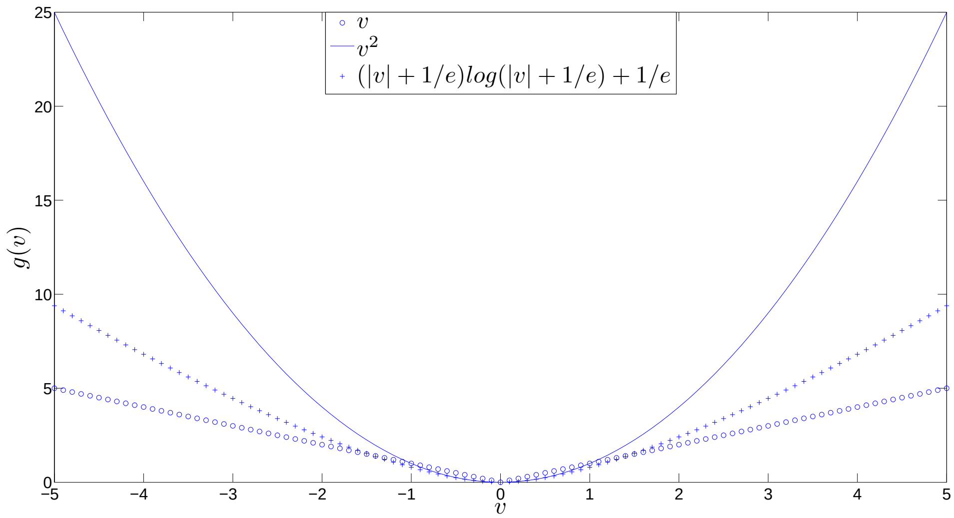

Figure 2.1: Modified entropy functional $g(v)$ $(+)$, $|v|$ $(\circ)$ that is used in the ℓ_1 norm, and the Euclidean cost function v^2 $(-)$ that is used in the ℓ_2 norm

.

The D-projection onto a closed and convex set is a generalized version of the orthogonal projection onto a convex set [13]. Let $\mathbf{s}_o$ be arbitrary vector in $\mathbb{R}^N$. Its' D-projection $\mathbf{s}_p$ onto a closed convex set C with respect to a cost functional $g(\mathbf{s})$ is defined as follows

$$\mathbf{s}_p = \arg\min_{\mathbf{s}\in C} D(\mathbf{s},\mathbf{s}_o) \quad \text{such that} \quad \theta.\mathbf{s} = \mathbf{y} \tag{2.8}$$

where

$$D(\mathbf{s},\mathbf{s}_o) = g(\mathbf{s}) - g(\mathbf{s_o}) - < \bigtriangledown g(\mathbf{s_o}), \mathbf{s} - \mathbf{s_o}) > \tag{2.9}$$

and D is the distance function related with the convex cost function $g(.)$, and $\bigtriangledown$ is the gradient operator. In CS problems, we have M hyperplanes $H_i : \theta_i.\mathbf{s} = y_i$ for $\quad i = 1, 2, ..., M$. For each hyperplane H_i, the D-projection (2.8) is equivalent to

$$\bigtriangledown g(\mathbf{s}_p) = \bigtriangledown g(\mathbf{s_o}) + \lambda\theta_i \tag{2.10}$$

$$\theta_i.\mathbf{s}_p = y_i \tag{2.11}$$

where λ is the Lagrange multiplier. As pointed out above, the D-projection is a generalization of the orthogonal projection. When the cost functional is the

Euclidean cost functional $g(\mathbf{s}) = \sum_n s[n]^2$ the distance $D(\mathbf{s_1}, \mathbf{s_2})$ becomes the ℓ_2 norm of difference vector $(\mathbf{s_1} - \mathbf{s_2})$, and the D-projection simply becomes the well-known orthogonal projection onto a hyperplane.

The orthogonal projection of an arbitrary vector $\mathbf{s}_o = [s_o[1], s_o[2], ..., s_o[N]]$ onto the hyperplane H_i is given by

$$s_p[n] = s_o[n] + \lambda\theta_i[n], n = 1, 2, ..., N \tag{2.12}$$

where $\theta_i(n)$ is the n-th entry of the vector θ_i and the Lagrange multiplier λ is given by,

$$\lambda = \frac{y_i - \sum_{n=1}^{N} s_o[n]\theta_i[n]}{\sum_{n=1}^{N} {\theta_i}^2[n]}. \tag{2.13}$$

When the cost functional is the entropy functional $g(\mathbf{s}) = \sum_n s(n)\ln(s(n))$, the D-projection onto the hyperplane H_i leads to the following equations

$$s_p[n] = s_o[n].e^{(\lambda.\theta_i[n])},\ n = 1, 2, ..., N \tag{2.14}$$

where the Lagrange multiplier λ is obtained by inserting (2.14) into the hyperplane equation given in (2.2); therefore, the D-projection $\mathbf{s}_p$ must be on the hyperplane H_i. The previous set of equations are used in signal reconstruction from Fourier Transform samples [89] and the tomographic reconstruction problem [84]. However, the entropy functional is defined only for positive real numbers. As mentioned earlier, the original entropy function can be extended to negative real numbers by modifying the original entropy function as in (2.5), and (2.6).

The modified entropy functional $g_e(\mathbf{s})$ based version of the optimization problem given in (2.3) can be defined as

$$\begin{aligned} \min_{\mathbf{s}} \quad & g_e(\mathbf{s}), \\ \text{subject to} \quad & \theta.\mathbf{s} = y\ . \end{aligned} \tag{2.15}$$

The continuous cost functional $g_e(\mathbf{s})$ satisfies the following conditions,

(i) $\frac{\partial g_e(0)}{\partial s_i} = 0$, $i = 1, 2, ..., N$ and

(ii) g_e is strictly convex everywhere and continuously differentiable.

On the other hand, the ℓ_1 norm is not a continuously differentiable function; therefore, non-differentiable minimization techniques such as sub-gradient methods [95] should be used for solving ℓ_1 based optimization problems. On the other hand, the ℓ_1 norm can be well approximated by the modified entropy functional as shown in Figure 2.1. Another way of approximating the ℓ_1 penalty function using an entropic functional is available in [96].

To obtain the D-projection of $\mathbf{s}_o$ onto a hyperplane H_i with respect to the entropic cost functional (2.6), we need to minimize the generalized distance $D(\mathbf{s}, \mathbf{s}_o)$ between $\mathbf{s_0}$ and the hyperplane H_i:

$$D(\mathbf{s}, \mathbf{s}_o) = \mathbf{g_e}(\mathbf{s}) - \mathbf{g_e}(\mathbf{s_o}) - < \bigtriangledown \mathbf{g_e}(\mathbf{s_o}), \mathbf{s} - \mathbf{s_o} > \tag{2.16}$$

with the condition that $\theta_i \mathbf{s} = y_i$. Using (2.10), entries of the projection vector $\mathbf{s}_p$ can be obtained as follows

$$sgn(\mathbf{s}_p(n)).\left[\ln(|\mathbf{s}_p(n)| + \frac{1}{e})\right] = sgn(\mathbf{s}_o(n)).\left[\ln(|\mathbf{s}_o(n)| + \frac{1}{e})\right] + \lambda\theta_i[n], n = 1, \ldots, N \tag{2.17}$$

where λ is the Lagrange multiplier, which can be obtained from $\theta_i \mathbf{s} = y_i$. The D-projection vector $\mathbf{s_p}$ satisfies the set of equations (2.17), and the hyperplane equation $H_i : \theta_i.\mathbf{s} = y_i$.

In Section 4.2, the entropic projection operator based iterative algorithm is utilized in CS reconstruction problem. First the ℓ_1 norm in (1.6) is replaced by the modified entropy function based norm. Using a convex function such as the modified entropy function, enables us to solve CS problem using the D-projection based iterative algorithms. The CS problem can be divided into M subproblems defined by the rows of the measurement matrix as given in (2.3). Interval convex programming techniques enables us to solve the large CS problem by solving the subproblems using the row-iteration methods [12]. The details, as well as numerical results of the modified entropy functional based iterative CS reconstruction method are presented in Section 4.2.

In Chapter 6, an entropic projection based adaptive filtering algorithm for multi-node networks is presented. The multi-node network estimation problem defined in [4] is composed of two main parts namely as; adaptation and combination. Typically ℓ_2 cost function based projection (orthogonal projection) operator is used in the adaptation stage of this algorithm. In this thesis, the adaptation stage is replaced with the entropy projection. As the modified entropy functional estimates the ℓ_1 norm, it results in sparse projections. Therefore, the resulting projection is more robust than the orthogonal projection against heavy-tailed noise such as ε-contaminated Gaussian noise. In Section 6.2, details of the proposed algorithm as well as experimental results are presented. In Section 6.3, this time the combination stage is replaced by a TV or FV based scheme. The new scheme uses high-pass filtering based constraints while combining the information from neighboring nodes. It is also possible to use the new combination scheme together with new adaptation scheme introduced in Section 6.2. The proposed adaptation and combination constraints are closed and convex sets, therefore, the new diffusion adaptation algorithm can be solved in an iterative manner. The details of the new diffusion adaptation algorithm as well as the simulations results with different node topologies under white Gaussian and ε-contaminated Gaussian noise models are given in Section 6.3.

Chapter 3

FILTERED VARIATION

Total Variation (TV) based solutions are quite popular for inverse problems such as denoising and signal reconstruction [3, 16, 69, 71–74, 97]. In discrete TV functional, the difference between neighboring samples are computed and the ℓ_1 or ℓ_2-norm of the difference vector is minimized. Hence, the TV method inherently assumes that the signal (or image) is a low-pass signal and tries to minimize the high-pass energy. Instead of computing just the one-neighborhood difference between the samples, it can be possible to filter the signal using an appropriate high-pass filter and minimize the ℓ_1 or ℓ_2 energy of the output signal. Furthermore, it is also possible to use diagonal or even custom designed directional high-pass filters in image and video processing applications according to the needs of the user or the characteristics of the signal.

As pointed out in Chapter 1, for a 1-D signal $\mathbf{x}$ of length N, the discretized TV functional of $\mathbf{x}$ is defined as,

$$||\mathbf{x}||_{TV} = \sum_{n=1}^{N} \sqrt{(x[n] - x[n+1])^2} \tag{3.1}$$

where a discrete-gradient of the signal is the key component of the TV functional. We note that the discrete gradient operation $v[n] = x[n] - x[n+1]$ in (3.1) is a rough high-pass filtered version of $\mathbf{x}$. This filter is the high-pass filter used in Haar wavelet transform. Therefore, the relation between the signals $\mathbf{x}$ and $\mathbf{v}$ can be represented via convolution denoted by the operator $*$ as follows:

$$v[n] = h[n] * x[n] \tag{3.2}$$

where $h[n] = \{-1, 1\}$ is the impulse response of the Haar high-pass filter. In the DFT domain the same relationship can be represented by a multiplication operation as follows:

$$V[k] = H[k]X[k], \quad k = 1, 2, ..., N. \tag{3.3}$$

provided that the DFT size N is larger than the length of convolution.

In (3.3), $X[k], H[k], V[k]$ are the N-point DFT of the desired signal $x[n]$, high-pass filter $h[n]$ and the output $v[n]$, respectively. The TV cost function is equivalent to filtering the signal with a Haar high-pass filter and computing the ℓ_1 or ℓ_2 energy of the filtered output signal corresponding to anisotropic or isotropic cases, respectively.

The Haar filter has an ideal normalized angular cut-off frequency of $\frac{\pi}{2}$. It is possible to apply other high-pass filters and compute the output energy or it is possible to use the Parseval's relation and other Fourier domain relations to impose sparsity conditions on the desired signal. It is well-known [98] that:

$$\sqrt{\sum_n |v[n]|^2} = \sqrt{\sum_k \frac{1}{N}|V[k]|^2} \leq \max_k |V[k]| \leq \sum_n |v[n]| \quad . \tag{3.4}$$

for an arbitrary discrete-time signal $v[n]$. In Section 3.1, based on the above relations, both time (space) and frequency domain FV constraints, which correspond to closed and convex sets for the CS problem are defined.

FV framework has two major advantages over the TV framework. First of all, if the user has prior knowledge about the frequency content of the signal, it becomes possible to design custom filters for that specific band. In some application areas such as biomedical, satellite, forensics etc . . . image processing applications, a pool of similar images exists. From this pool, one can find a model of the high frequency information or, more generally, the structure of the signal. Using this information, one can design custom FV constraints appropriate for the structure of the signal. For example, if a set of images contain specific texture characteristics, e.g.the fingerprint image in Figure 3.1, FV constraints that preserve this texture information can be designed. Or for practical signals, one can design a high-pass filter in Fourier domain with exponentially decaying coefficients in the transition band of the filter as given in Figure 3.2. Many practical signals typically have exponentially decaying Fourier domain responses. It is possible to obtain good reconstruction/denoising results by restricting the signal with such FV constraint. Another FV strategy that can be used, if the user does not have any information about the signal content, is as follows. The user may individually apply high-pass-filters (HPF) from a set of filters with different pass-bands and directionalities. Then, according to the output of the flters, he/she can choose a subset of these HPFs and use them as a FV constraints. By this way FV based approach may adapt itself better to the signal content.

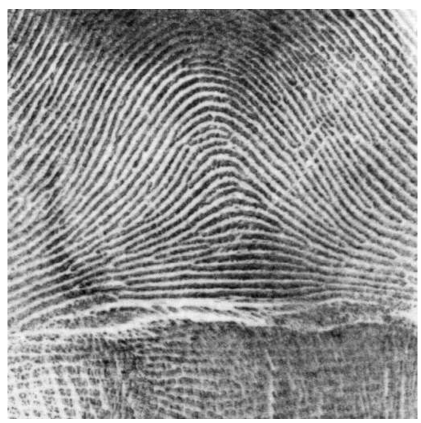

Figure 3.1: It is possible to design special high-pass filters according to the structure of the data. The black and white stripes (texture) in the fingerprint image corresponds to a specific band in the Fourier domain. A high pass filter that corresponds to this band can be designed and used as a FV constraint.

.

The filtered output in transform domain $V[k] = H[k]X[k]$ is basically specified by the filter $\mathbf{H}$, which can be selected according to a given bandwidth specified by the user. In 2-D or higher dimensions, one is not restricted to horizontal or vertical high-pass filters. It is also possible to use directional high-pass filters. Moreover, the user is not restricted with just filtering type of constraints but, any type of convex constraint set becomes applicable to the signal through the FV scheme. The FV constraints are iteratively applied to the signal of interest in a cyclic manner. The convergence of the iterative algorithm is guaranteed by

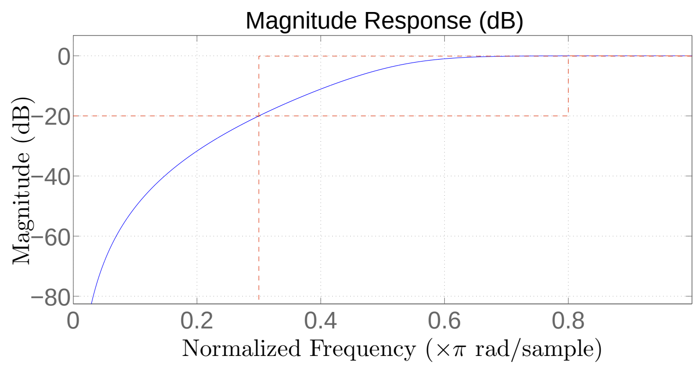

Figure 3.2: An example high pass filter with exponentially decaying transition band.

.

the POCS theorem because, our constraints are convex [17].

As mentioned before, it is also possible to define constraint sets on other transform domain representations, such as wavelets, but in this thesis, we focus on DFT and DCT domain.

3.1 Filtered Variation Algorithm and Transform Domain Constraints

In this section, we list seven possible closed and convex constraints that can be used in inverse problems. Each constraint qualifies different properties of the estimated signal such as; ℓ_1 or ℓ_2 energy of the high frequency band of the signal, local variations in the signal, the mean of the signal, the bit depth of the sample, and the sample value locality. All the constraints can be used at the same time, or any combination of these can be used together depending on the nature of the signal (or image) and problem type. The constraints defined below will be used for signal reconstruction in Section 4.1 and for denoising in Section 5.2.

3.1.1 Constraint-I: ℓ_1 FV Bound

The first constraint is based on the ℓ_1 energy of high frequency coefficients

$$C_1 = \left\{ \mathbf{x} : \sum_{k=0}^{N-1} |H[k]X[k]| \leq \varepsilon_1 \right\}. \tag{3.5}$$

It is possible to perform orthogonal projections onto this set in Discrete Time domain as described in [87]. Since, the DFT is a complex transform, it is easier to work with a real transform such as DCT or DHT. In this case the boundary hyperplanes of the region specified by the constraint set are real. The projection operation is essentially equivalent to making orthogonal projections onto hyperplanes forming the boundary, and it is similar to projection onto an ℓ_1 ball but it is on the transform domain and only high-frequency coefficients are updated. Since we perform projections onto an ℓ_1 ball type region, the solution turns out to be sparse.

3.1.2 Constraint-II: Time and Space Domain Local Variational Bounds

The second constraint is based on the change in intensity between the consecutive samples of a signal (pixels of the image). In real-life, there is strong correlations between the samples of discrete-time signals (or images), and there is very little correlation between different parts of the signals (or images). Therefore, it is possible to remove the summation operator in the TV or the FV and consider regional TV or FV constraints on the signal. This leads to a high-pass constraint set for each sample of the signal (or pixel of the image)

$$C_{2,n} = \left\{ \mathbf{x} : \left| \sum_{i=-l}^{l} h[i]x[n-i] \right| \leq P \right\}, \tag{3.6}$$

where $h[i]$ is a high-pass filter with support length $2l+1$ and P is a user defined bound. Selecting the P value, effects the smoothness level of the target signal significantly. Projection onto hyperslabs $C_{2,n}$ do not correspond to low-pass filtering, because projections are essentially non-linear operations. If the current iterate does not satisfy the bound, it is projected onto the hyperslab given in (3.6).

If the user does not have a clear knowledge about the signal content, a very large bound ($P = 128$) for the high-pass filter $\mathbf{h} = \{\frac{-1}{4}, \frac{1}{2}, \frac{-1}{4}\}$ is selected to avoid distorting the high frequency parts of the signal. When there is an impulse within the analysis window of the filter, the filter output will be high and the samples within that window are modified by the projection. For example, the $C_{2,n}$ family of sets turn out to be useful for Laplacian noise. In image processing applications, it is also possible to apply filters in vertical and diagonal directions depending of the nature of the original image.

3.1.3 Constraint-III: Bound on High Frequency Energy

The following anisotropic constraint on high-frequency energy of the signal $\mathbf{x}$ is a closed and convex set:

$$C_{3a} = \left\{ \mathbf{x} : \sum_{k=k_0}^{N-k_0} |X[k]|^2 \leq \varepsilon_{3a} \right\} \tag{3.7}$$

where ε_{3a} is an upper bound. This corresponds to filtering the signal $\mathbf{x}$ with a high-pass filter whose cut-off frequency index is k_0 in the DFT domain

$$H[k] = \begin{cases} 0, & \text{for} \quad k < k_0 \text{ or } k > N - k_0 \\ 1, & \text{for} \quad k_0 \leq k \leq N - k_0 \end{cases} \tag{3.8}$$

where N is the size of the DFT. Although this filter suffers from the Gibbs phenomenon in time-domain, it is possible to use it in signal processing applications such as denoising. The index k_0 is equal to $\frac{N}{4}$ for the normalized angular cut-off frequency of $\frac{\pi}{2}$, but any $0 < k_0 < \frac{N}{2}$ can be selected for a desired smoothness level. The set given in Eq. (3.7) is a convex set and it is easy to perform orthogonal projections onto this set. Let $s_o[n]$ be an arbitrary signal and $S_0[k]$ be its DFT.

$S_p[k]$ of the projection $s_p[n]$ is given by

$$S_p[k]=\begin{cases}\sqrt{\frac{\varepsilon}{\varepsilon_o}}S_0[k] & \text{, if } \sum_{k=k_0}^{N-k_0}|S_0[k]|^2 \geq \varepsilon,\ k_o \leq k \leq N-k_o \\ \\ S_0[k], & \text{otherwise,}\end{cases} \tag{3.9}$$

where $\sum_{k=k_0}^{N-k_0}|S_o[k]|^2 = \varepsilon_o$.

We can also use a DCT domain high-pass energy constraint on the desired signal using the following set

$$C_{3b} = \left\{\mathbf{x} : \sum_{k=k_0}^{N-1}(X_{DCT}[k])^2 \leq \varepsilon_{3b}\right\}, \tag{3.10}$$

which is also a convex set. In (3.10), $\mathbf{X}_{DCT}$ represents the DCT of the signal $\mathbf{x}$. It is straightforward to make orthogonal projections onto the DCT domain set C_{3b} as in Equation (3.9).

3.1.4 Constraint-IV: User Designed High-pass Filter

In this case, instead of using a specific cut-off frequency, the frequency response of a given high-pass filter is used as

$$C_4 = \left\{\mathbf{x} : \sum_{k=0}^{N-1}|H[k]X[k]|^2 \leq \varepsilon_4\right\}. \tag{3.11}$$

The set C_4 is also a closed and convex set. Orthogonal projection onto this set is not as easy as Condition-I, because the set is a closed ellipsoid. It can be implemented using numerical methods, [99, 100].

3.1.5 Constraint-V: The Mean Constraint

The fifth constraint is actually proposed in [3]. It is based on the desired mean of the target signal. Typically this information can be estimated from a pool of similar types of images (e.g. satellite images, images of hand-writing, faces etc.) A constraint based on the mean information can be defined as follows

$$C_5 = \left\{ \mathbf{x} : \sum_{n=1}^{N} \frac{x[n]}{N} = \mu_x \right\} \tag{3.12}$$

where N is the number of the pixels in the image and μ_x is the mean of the original image.

3.1.6 Constraint-VI: Image bit-depth constraint

In general, the users know the color (bit) depth of the original image. Due to this fact, it is possible to define a constraint on the bit depth of the reconstructed image as follows:

$$C_6 \left\{ \mathbf{x} : \ 0 \leq x[i,j] \leq (2^M - 1) \right\} \tag{3.13}$$

where M is the number of the bit planes used in the original representation. This constraint is also proposed in [3]. This constraint is not restricted to image processing applications. The user may know the signal bit-depth for any other type of signal. Therefore, the extension of this constraint to other type of signals is trivial. The projection onto this set is simple thresholding operation, where the upper and lower thresholds are determined by the upper and lower bounds given in 3.13. A signal sample exceeding the thresholds is limited to the closest bounding values.

3.1.7 Constraint-VI: Sample Value Locality Constraint

The following constraint originates from the regularization term in the optimization type formulations of both the denoising and the compressed sensing problems. In both the compressed sensing and the signal denoising problems, the samples that are taken from the signal are reliable to some extend. Therefore, the solution should be sought in the proximity of the samples. The coverage of this proximity heavily depends on the noise of the samples. In the original signal domain, this constraint can be defined as

$$C_7 \left\{ \mathbf{x} : |\tilde{x}[n] - y[n]| < \delta_n \right\}, \tag{3.14}$$

where $x[n]$ and $y[n]$ are the samples of the signal $\mathbf{x}$, and the noisy measurements $\mathbf{y}$ from the signal, respectively. This formulation is convenient for denoising problems. In the compressed sensing applications, the proposed constraint can be applied on the compressed measurements as

$$C_{7,CS} \left\{ \mathbf{x} : |\mathbf{A}\mathbf{x}[n] - y[n]| < \delta_n \right\}, \tag{3.15}$$

where $\mathbf{A}$ is the measurement matrix and $\mathbf{y}$ are the compressed measurements, that are taken from the original signal $\mathbf{x}$. The parameter δ_n heavily depends on the noise model, e.g. if the signal is contaminated by white Gaussian noise with variance σ, then choosing $\delta_n \in [\sigma, 2\sigma]$ is a reasonable assumption.

In Section 4.1, an algorithm for estimating regularly sampled version of a signal from its irregularly sampled version is presented. Most typically, sinc interpolation is used for solving this problem. Here in this thesis, a filtered variation based approach is presented. The irregularly sampled signal is projected onto alternating convex FV constraints iteratively and the regularly sampled version of the signal is estimated. As another FV application, in Section 5.2, an FV based signal denoising algorithm that uses constraints C_1-C_6 is presented.

Chapter 4

SIGNAL RECONSTRUCTION

The problem of reconstructing a signal from its uniform samples has been well studied in the literature. However, there is a variety of scenarios in the literature, where uniforms samples from a signal can not be collected. For examples, in CT and MRI, only non-uniform frequency domain samples are available [101]. If the average sampling rate is above twice the bandwidth of the signal, the signal can be reconstructed from its nonuniform samples [101]. The theory on nonuniform sampling and reconstruction was well studied by Yao and Thomas in [102], and Yen [103]. Yen considered to spread the samples taken from a signal in an arbitrarily nonuniform manner, as well as taking groups of uniform samples from a signal in a periodic manner. In [104], Jerri presented a review of nonuniform sampling schemes in the Literature, as well as the related reconstruction algorithms.

However, none of the above papers introduces a practical reconstruction method that can be implemented on a computer [101]. In [105], and [106] Finite-impulse filtering (FIR) based approaches are introduced for non-periodic and periodic signals, respectively. In [107], and [108], iterative reconstruction methods for reconstructing band-limited signals from their nonuniform samples have been presented. In [109], a non-iterative block based method is proposed. However, these methods are computationally complex and works only for a special set of nonuniform samples. Recently, in [101], Margolis and Eldar derived closed form algorithms for reconstructing periodic band-limited signals from nonuniform samples. Another recent research direction in nonuniform sampling is compressive sensing.

In this chapter, two different signal reconstruction algorithms are presented. In the first algorithm, a signal is reconstructed from its irregularly sampled version through low-pass filtering. The proposed method works like Filtered Variation constraints in the sense that the high frequency part of the signal spectrum is bounded during the reconstruction process. In the second algorithm, a CS reconstruction method that utilizes entropy projection and row-action methods is presented.

4.1 Signal Reconstruction from Irregular Samples

Let us assume that samples $x_c(t_i)$, $i = 0, 1, 2, ..., L-1$, of a continuous time-domain signal $x_c(t)$ are available. These samples may not be on an uniform sampling grid. Let us define $x_d[n] = x_c(nT_s)$ as the uniformly sampled version of this signal. The sampling period T_s is assumed to be sufficiently small (below the Nyquist period) for the signal $x_c(t)$. In a typical discrete-time filtering problem, one do have $x_d[n]$ or its noisy version and apply a discrete-time low-pass filter to the uniformly sampled signal $x_d[n]$. However, $x_d[n]$ is not available in this problem. Only nonuniformly sampled data $x_c(t_i)$, $i = 0, 1, 2, ...L-1$ are available in this problem.

Our goal is to low-pass filter the nonuniformly sampled data $x_c(t_i)$ according to a given cut-off frequency. One can try to interpolate available samples to the regular grid and apply a discrete-time filter to the data. However, this will amplify the noise because the available samples may be corrupted by noise [110]. In fact, only noisy samples are available in some problems [111]

The proposed filtering algorithm is essentially a variant of the well-known

Papoulis - Gerchberg interpolation method [17,70,85,112–115] and the FIR filter design method presented in [116]. The proposed solution is based on Projections onto Convex Sets framework (POCS). In this approach, specifications in time and frequency domain are formulated as convex sets and a signal in the intersection of constraint sets is defined as the solution, which can be obtained in an iterative manner. In each iteration, the fast Fourier Transform algorithm (FFT) is used to go back and forth between the time and frequency domains.

In many signal reconstruction and band-limited interpolation problems [17,70, 112,114] Fourier domain information is represented using a set, which is defined as follows

$$C_p = \{\mathbf{x} : X(e^{jw}) = 0 \quad \text{for} \quad w_c \le w \le \pi\}, \tag{4.1}$$

where $X(e^{jw})$ is the discrete-time Fourier Transform (DTFT) of the discrete-time signal $x[n]$ and w_c is the band-limitedness boundary or the desired normalized angular low-pass cut-off frequency [17,112,114]. This constraint is similar to the "C_1" filtered variation constraint defined in (3.5), which uses an ideal high-pass filter with a specific cut-off frequency and $\varepsilon_1 = 0$. As in the filtered variation method, this condition is imposed on a given signal $x_o[n]$ by orthogonal projection onto the set C_p. The projection $x_p[n]$ is obtained by simply imposing the frequency domain constraint on the signals

$$X_p(e^{jw}) = \begin{cases} X_o(e^{jw}) & \text{for } 0 \le w \le w_c \\ 0 & \text{for } w > w_c \end{cases}, \tag{4.2}$$

where $X_o(e^{jw})$ and $X_p(e^{jw})$ are the DTFTs of $\mathbf{x}_o$ and $\mathbf{x}_p$, respectively. Members of the set C_p are infinite extent signals so the FFT size should be large during the implementation of the projection onto the set C_p. However, strict band-limitedness constraints as in C_p may induce ringing artifacts due to Gibbs phenomenon.

The band-limitedness constraint can be relaxed by allowing the signal to have some high-frequency components according to the tolerance parameter δ_s. The use of the stop-band and the transition regions eliminates ringing artifacts due to Gibbs phenomenon. In this respect, the proposed approach is different from the Papoulis-Gerchberg type method, which uses strict band-limitedness condition.

This new constraint corresponding to the stop-band condition in Fourier domain is defined as follows

$$C_s = \{\mathbf{x} : |X(e^{jw})| \leq \delta_s \quad \text{for} \quad w_s \leq w \leq \pi\} \tag{4.3}$$

where the stop-band frequency $w_s > w_c$. The set C_s is also a convex set [17,117] and this condition can be imposed on iterates during iterative filtering. A member $\mathbf{x}_g$ of the set C_s corresponding to a given signal $x_o[n]$ can be defined as follows

$$X_g(e^{jw}) = \begin{cases} X_o(e^{jw}) & \text{for } 0 < w < w_s \\ X_o(e^{jw}) & \text{for } |X_o(e^{jw})| \leq \delta_s,\ w \geq w_s \\ \delta_s e^{j\phi_o(w)} & \text{for } \ |X_o(e^{jw})| \geq \delta_s,\ w \geq w_s \end{cases} \tag{4.4}$$

where $\phi_o(w)$ is the phase of $X_o(e^{jw})$. Clearly, $X_g(e^{jw})$ is in the set C_s. In our implementation the set C_s plays the key role rather than the set C_p because almost all signals that we encounter in practice are not perfect band-limited signals. Most signals have high-frequency content. The frequency band (w_c, w_s) corresponds to the transition band used in ordinary discrete-time filter design.

This relaxed version of the band-limitedness constraint in (4.4) also works like an FV constraints in the sense that it controls the behavior of the reconstructed signal in a specific band (e.g. high pass frequencies).

This constraint is also a variant of the set C_1 defined in (3.5). Instead of putting a bound on the ℓ_1 energy of the highpass filtered version of the signal as in C_1, the C_s limits the behavior of the transform domain coefficients in the high-pass band individually. On the other hand, it is also possible to replace C_s with C_1. As C_1 corresponds to projection onto ℓ_1 ball, it results in sparse projections with few non-zero transform domain coefficients in the high-pass band. The corresponding C_1 type constraint can be defined as

$$\tilde{C}_1 = \left\{ \mathbf{x} : \sum_{k=0}^{N-1} |H[k]X[k]| \leq \varepsilon_1 \right\}, \tag{4.5}$$

$$H[k] = \begin{cases} 1, & k < k_c \text{ or } k > N - k_c \\ 0, & k_c \leq k \leq N - k_c \end{cases}, \tag{4.6}$$

where $k_c = \frac{N w_c}{2\pi}$ and $\varepsilon_1 = (N - k_c)\delta_s$ in our experiments. It is possible to use any $\varepsilon_1 > 0$ depending on the desired smoothness level of the regularly sampled signal.

Since, ℓ_1 projection is used while implementing this constraint, it is named as ℓ_1 projection based interpolation throughout the experiments.

It is also possible to use C_{3a} defined in (3.7), which represents bound on high frequency energy constraint defined in (3.7) to restrict the high-pass components of the restored signal. In this case, the stop band energy parameter is choosen as $\varepsilon_{3a} = (N - k_c)\delta_s$. This constraints cornensponds finding the ℓ_2 projection of the high frequency components of the signal onto the set defined in (3.7). Therefore, it is refered as ℓ_2 based interpolation throughout the experiments.

It is also possible to replace the ℓ_2 projection operation with entropic projection operator. ℓ_1, and entropic projection based constraints results in sparse reconstructions [21,36]. Therefore, they may induce ringing artifacts due to Gibbs phenomenon. Since the ℓ_2 projection based constraints, limits all the stop-band coefficients in an evenly manner, it produces much smooth reconstructions. On the other hand, ℓ_1, and entropic projection based algorithms are more robust against noise, since they produce sparse projections. In the experimental results section of this chapter, these claims will be illustrated through numerical examples.

Besides the frequency domain constraints defined by sets (4.1), and (4.3), another set of constraints should be defined in time domain, so that it would be possible to realize the aformentioned Papoulis-Gerchberg type of iterations. As pointed out above a sampling period, which is smaller than the Nyquist period is used. Let's assume that $0, T_s, 2T_s, ..., (N-1)T_s$ is a dense grid covering $t_i, i = 0, 1, 2, ..., L-1$ and let's also assume that all $t_i < t_{i+1}$ and $t_i \geq 0$ and $t_{L-1} \leq (N-1)T_s$ without loss of generality.

The set describing the time-domain information is defined using the regular sampling grid $0, T_s, 2T_s, ..., (N-1)T_s$. The sample at $t = t_i$ is assumed to be close to nT_s. The upper and lower bounds that are imposed on $x[n]$ as follows:

$$x_c(t_i) - \varepsilon_i \leq x[n] \leq x_c(t_i) + \varepsilon_i, \tag{4.7}$$

and the corresponding time-domain set is defined as

$$C_i = \{x : x_c(t_i) - \varepsilon_i \leq x[n] \leq x_c(t_i) + \varepsilon_i\}, \tag{4.8}$$

where the time-domain bound parameter e_i can be either selected as a constant value or as an α-percent of $x_c(t_i)$ in a practical implementation. Although the signal value at nT_s on the regular grid is not known, it should be close to the sample value $x_c(t_i)$ due to the low-pass nature of the desired signal. Therefore, this information is modelled by imposing upper and lower bounds on the discrete-time signal in sets $C_i, i = 0, 1, 2, ..., L-1$. Furthermore samples may be corrupted by noise and upper and lower bounds on sample values provide robustness against noise. If there are two signal samples close to $x[n]$ the grid size can be increased, i.e., the sampling period can be reduced so that there is one $x[n]$ corresponding to each $x_c(t_i)$. C_i can also be defined as

$$C_i = \{\mathbf{x} : |x_c(t_i) - x[n]| \leq \varepsilon_i\}\,. \tag{4.9}$$

This formulation of C_i constraint is actually very similar to the FV constraint "C_2: Time Domain Local Variational Bound" given in Section (3.1.2).

Other time-domain constraints that can be used in an iterative algorithm include the positivity constraint $x[n] \geq 0$ (similar to "C_6: Bit Depth Constraint" in (3.13)), if the signal is nonnegative, and the finite energy set

$$C_E = \{\mathbf{x} : ||x||^2 \leq E\}, \tag{4.10}$$

which is introduced in [17] for band-limited interpolation problems to provide robustness against noise. C_E is a C_3 type of constraint defined as in (3.7), and (3.10) but in time domain instead of transform domain. Projection on C_E can be calculated as in (3.9).

The iterative filtering algorithm consists of going back and forth between time and frequency domains and imposing the time and frequency constraints on iterates. The algorithm starts with an arbitrary initial signal $x_o[n]$. Then it is projected onto sets C_i by using the time domain constraints defined in (4.7) and obtain the first iterate $x_1[n]$. Next, the DTFT X_1 of time domain signal $x_1[n]$ is computed and the frequency domain constraint defined in Eq. (4.4) are imposed on X_1 to obtain X_2.

Then compute the inverse-DTFT of X_2 is computed to obtain x_2. At this stage other time domain constrains such as positivity and finite energy can be also imposed on x_2, if the signal is known to be a nonnegative signal. Once x_2 is obtained it probably violates the time domain constraints defined by inequalities (4.7). Therefore x_3 is obtained by imposing the constraints on x_2. The iterates defined in this manner converge to a signal in the intersection of the time-domain set C_i and the frequency domain set C_s, if they intersect. Eventually a low-pass filtered version of the signal $x_c(t)$ on the regular grid defined by $0, T_s, 2T_s, ..., (N-1)T_s$ is found. If the intersection of the sets C_i and C_s is empty then either the bounds e_i should be increased or the the cut-off frequency w_s should be increased.

The iterative algorithm is globally convergent regardless of the initial starting signal, $x_o[n]$. The proof of convergence is due to the projections onto convex sets (POCS) theorem [17], [70], because the sets C_s, C_i, C_E are all convex sets in l_2. Successive orthogonal projections onto these sets lead to a solution, which is in the intersection of C_s, C_i, and C_E. Papoulis-Gerchberg type iterations jumping back and forth between time and frequency domains converge in a relatively slow manner. Convergence speed can be increased using the nonorthogonal projection methods such as the ones described in [17, 70, 118].

The original signal that we would like to reconstruct from its irregular samples may not be covered by the time and Fourier domain constraint sets that we defined in 4.1-4.10. Obviously, in this case the perfect reconstruction of the original signal by our algorithm is not possible. However, if sufficiently many informative samples are taken from the signal, it is possible for the algorithm to approximate the signal effectively. Here, informative samples refers to critical points in the signal such as the peaks and the sharp edge point of the HeaviSine signal. This condition needs to be satisfied even if the original signal is included in the Fourier and time domain constraint sets. The algorithm tries to fit a smooth model with some high frequency components to the irregular samples. Therefore, it aims to find the smoothest signal that fits to the Fourier and time domain constraints.

4.1.1 Experimental Results

The proposed frequency and time domain constraints are tested with an irregularly sampled version of the length-1024 noiseless Heavisine signal in Figures 4.3, 4.4, and 4.6 and its noisy version in Figures 4.1, 4.2, 4.5, and 4.7. Due to the edges, the original Heavisine signal has high-frequency content. Therefore, the strict band-limited interpolation employing the set C_p will not produce satisfactory results for this signal as demonstrated in [110]. Moreover, when the irregularly samples signal is noisy, spline interpolation based algorithms will not produce good results either [110].

In all the experiments that are conducted, the time domain constraint C_i that is defined in (4.9) with different ε_i parameters is used as the time domain constraint. The values of the time domain parameters ε_i that are used in the different experiments can be found in Table 4.1. As the frequency domain constraints, 6 different constraints that are introduced in Section 4.1 are used. The parameters related to these constraints are also given in Table 4.1. These different interpolation schemes are also compared against each other in this section.

The experiments can be divided into two main groups: noiseless (Simulations 3,4,6) and noisy (Simulations 1,2,5,7). For the noiseless case, four different frequency domain constraints that corresponds to four different interpolation schemes are used. These interpolation schemes and related constraints are (i) strict band-limited interpolation (SBL), which uses C_p in (4.1), (ii) relaxed band-limited interpolation, which uses C_s in (4.3), (iii) ℓ_1 based interpolation, which uses $\tilde{C_1}$ in (4.6), and (iv) ℓ_2 based interpolation, which uses C_{3a} in (3.7). In case of restoration from noisy samples, two more interpolation methods are added to the comparisons. These methods are entropic projection based recovery in (4.6), and cubic spline interpolation. These interpolation schemes are compared against each other using the SNR metric, which is defined as

$$20log_{10}\left(\frac{||\mathbf{x}||_2}{||\mathbf{x}-\mathbf{x}_{rec}||_2}\right), \tag{4.11}$$

where $\mathbf{x}$ is the original signal and $\mathbf{x}_{rec}$ is the signal reconstructed from irregular samples.

In the first set of experiments, the original noiseless Heavisine signal is irregularly sampled at a given number of sampling points and the underlying continuous-time signal at 1024 uniformly selected instances, i.e., $x[n]$, $n = 0, 1, 2, ..., 1023$ is estimated. The simulation parameters used in these experiments are given in respective columns of Table 4.1. In this case, the time domain constraint parameter is fixed to $\varepsilon_i = 0$, because all the samples are known to be taken from the original signal, hence, they are correct. According to the results of Simulations 3, and 6, which are presented in Figures 4.3, and 4.6, respectively, it is possible to say that increasing the number of samples taken from the original signal also increases the reconstruction quality.

As mentioned before, if the high-pass band is suppressed too much, oscillatory behavior around the edge locations in the signal occurs. Therefore, strict band-limited (SBL) interpolation gives the worst results among the all the other interpolations methods used in the simulations. ℓ_2 based, and filtered interpolations achieved the best results for different stop-band parameters δ_s. However, as shown in Figures 4.3, and 4.4, C_s based interpolation seems to be more sensitive to changes in stop-band parameter. Contrary to ℓ_2 based, and filtered interpolations, ℓ_1 based interpolation produces sparse results. It keeps few large high-frequency components and sets the rest of the coefficients to zero. It works similar to strict band-limited interpolation and provides average performance. Spline interpolation results are not shown in noiseless test. However it is important to note that for the reconstruction of the Heavisine signal, spline interpolation achieves slightly better results than ℓ_2 based interpolation. Entropy projection based interpolation also produces sparse solutions in frequency domain as the ℓ_1 projection based interpolation method. Therefore, its performance is similar to ℓ_1 based interpolation.

It is important to note that, the signals that are restored using the ℓ_2 based, and filtered interpolation methods are similar to the signal obtained using the wavelet domain methods described in [110].

As a last remark, the Fourier domain coefficients corresponding to the high frequency part of the original Heavisine signal are larger than the δ_c values in

Table 4.1. Moreover, the high frequency energy of the Heavisine signal exceeds the levels defined by ε_1 parameters. In other words, the original Heavisine signal is not in any of the sets that are defined by the parameters in Table 4.1. Therefore the perfect reconstruction of the original signal by these parameter sets is not possible. As another test we increased the frequency domain bounds δ_c such that the constraints sets covered the Heavisine signal and then execute the reconstruction algorithm. In this case the outcome of the algorithm contains unwanted oscillations.

In the second set of experiments, 32, 128, and 256 sample points from the noisy HeaviSine signal are randomly picked and the underlying discrete-time signal at 1024 uniformly selected instances, i.e., $x[n]$, $n = 0, 1, 2, ..., 1023$ is estimated. The available signal samples are corrupted by white Gaussian noise with a standard deviation of either $\sigma = 0.2$ or $\sigma = 0.5$ as in [110]. The reconstruction results obtained using the proposed interpolation schemes are comparable to the wavelet domain interpolation method described in [110]. As in the noiseless case, it is also possible to restore the main features of Donoho's HeaviSine signal.

The time domain constraint parameter ε_i is selected according to the signal noise content. Since measurement error has a standard deviation of σ, the ε_i parameter is set to the same value. So the restored signal values at the sampling locations has the flexibility to move around the sampled signal value. This type of a constraint corresponds to thresholding.

Another set of experiments is conducted with the signals in Figure 4.8. In this experiment 64 or 128 random samples are taken from the noisy version signals and the signal is reconstructed from these irregular measurements. The standard deviation of the noise on the signal is given at the third column of Table 4.2. The results obtained by using different constraints are presented in Table 4.2.

As in the case of noiseless experiments, when the number of samples taken from the signal increases, the SNR between the restored and the original signal also increases. Different from the noiseless case, this time the best restoration results are achieved either by ℓ_1 or entropy projection based interpolation methods. It is well known in signal literature that, ℓ_1 projection has better denoising

Table 4.1: Simulation parameters used in the tests.

Simulation	1	2	3	4	5	6	7
Figure	4.1	4.2	4.3	4.4	4.5	4.6	4.7
σ	0.2	0.5	0	0	0.2	0	0.2
ε_i	0.2	0.5	0	0	0.2	0	0.2
δ_s	0.5	0.5	0.5	0.3	0.3	0.3	0.2
k_c	31	31	31	31	31	31	21
Number of Samples	32	32	32	32	128	128	256

performance than the ℓ_2 projection [119–121]. As mentioned before, ℓ_1 norm promotes sparsity, and it cleans the noise component at the high pass band of the restored signal more effectively. Likewise, since entropy functional based projection estimates ℓ_1 projection, it also results in sparse solutions, it is also robust against noise.

As mentioned in [110], spline interpolation is very sensitive to noise. Therefore, it turns out the worst reconstruction results among all the interpolation schemes we used.

Convergence of the iterative algorithm can be proved using the projections onto convex sets theorem [17, 70], because the set C_s and sets C_i are closed and convex sets. In Figure 4.9, restored signals after 1, 10, 20 and 58 iteration rounds are shown.

A two-dimensional (2D) example is also provided in Figures 4.10, 4.11 and 4.12. The original terrain model given in Figure 4.10 consists of 225×425 sample points. As a first example, one-fourth of the samples of the original signal are available in a random manner. The 2D signal shown in Figure 4.11 is reconstructed using the cut-off frequency $w_c = \frac{\pi}{4}$, $\delta_s = 0.03$, and $e_i = 0.01$. In the second example, one-eighth of the samples of the original signal are available in a random manner. The reconstructed signal using the parameters $w_c = \frac{\pi}{8}$, $\delta_s = 0.03$, and $e_i = 0.01$ are shown in Figure 4.12. Reconstruction results, which are given in Figures 4.11 and 4.12 are like low-pass filtered versions of the original 2D signal in a dense 2D grid.

Table 4.2: Reconstruction results for signals in Figure 4.8. All the SNR results are given in dB.

Signal No	Number of Samples	Noise standard deviation (σ)	Relaxed band-limited interpolation (in dB)	ℓ_1 Projection reconstruction (in dB)	ℓ_2 Projection reconstruction (in dB)	Strict band-limited interpolation (in dB)	Spline interpolation (in dB)
1	64	0.01	25.61	25.27	22.16	24.02	13.21
1	128	0.01	27.43	27.49	27.36	24.77	17.63
1	64	0.1	14.31	14.14	13.2	13	2.11
1	128	0.1	16.16	14.28	14.02	11.53	2.41
2	64	0.01	13.45	12.53	12.93	12.31	11.83
2	128	0.01	18.34	18.24	18.54	17.19	17.53
2	64	0.1	12.25	12.44	11.8	11.51	4.37
2	128	0.1	15.82	15.51	13.96	11.63	4.74
3	64	0.01	14.97	15.29	15.03	14.54	15.45
3	128	0.01	16.23	15.68	14.88	14.2	16.26
3	64	0.1	11.46	11.65	9.19	5.53	1.61
3	128	0.1	12.74	12.24	10.82	8.87	4.06
4	64	0.01	20.58	20.85	20.32	19.78	16.07
4	128	0.01	22.48	22.77	22.45	21.25	15.97
4	64	0.1	12.64	12.88	11.33	11.86	2.52
4	128	0.1	14.79	14.18	12.99	11.15	4.63

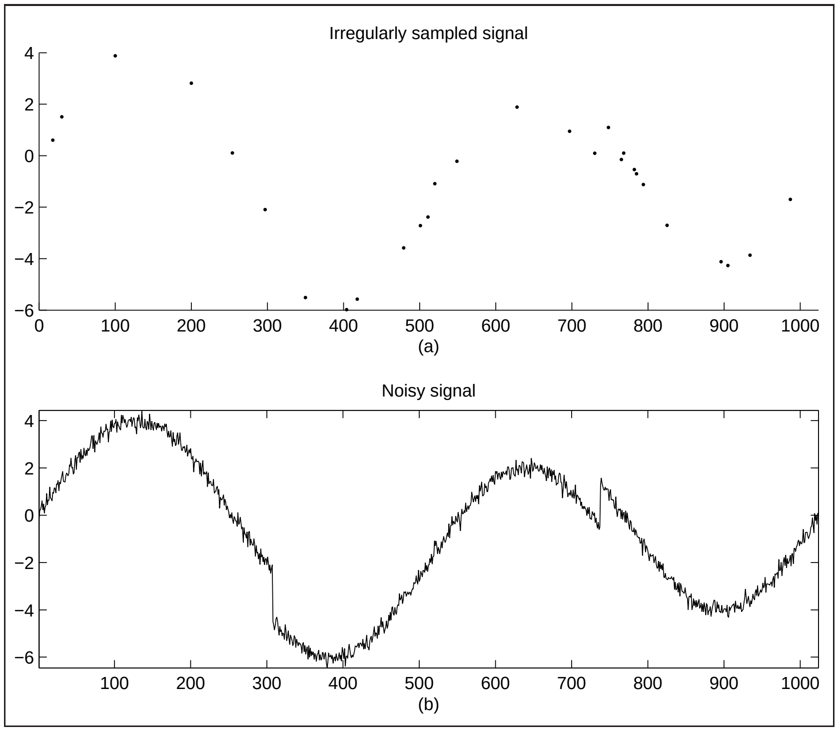

(i)

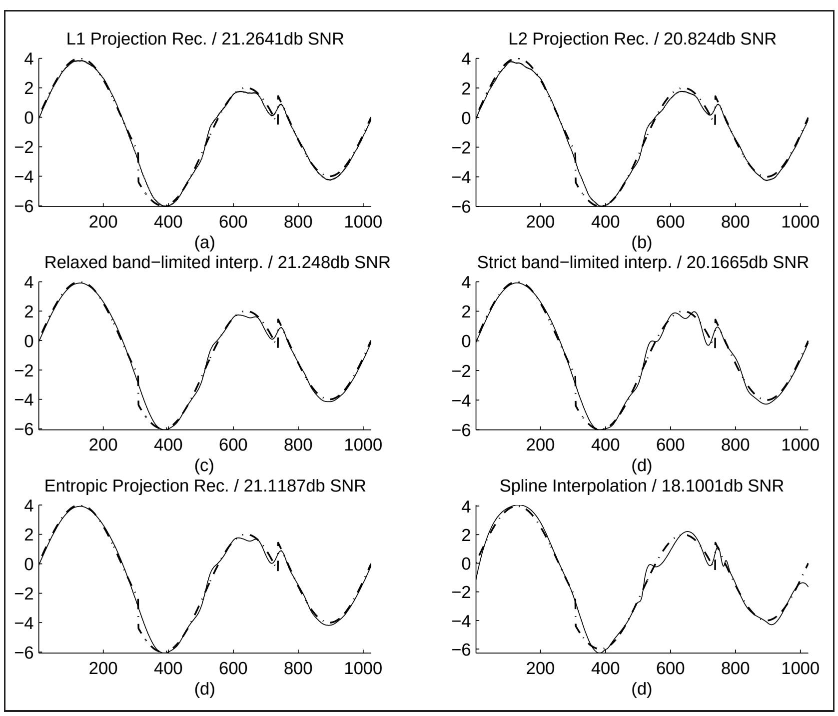

(ii)

Figure 4.1: (i) 32 point irregularly sampled version of the Heavisine function and the original noisy signal ($\sigma = 0.2$). (ii) The 1024 point interpolated versions of the function given at (i) using different interpolation methods.

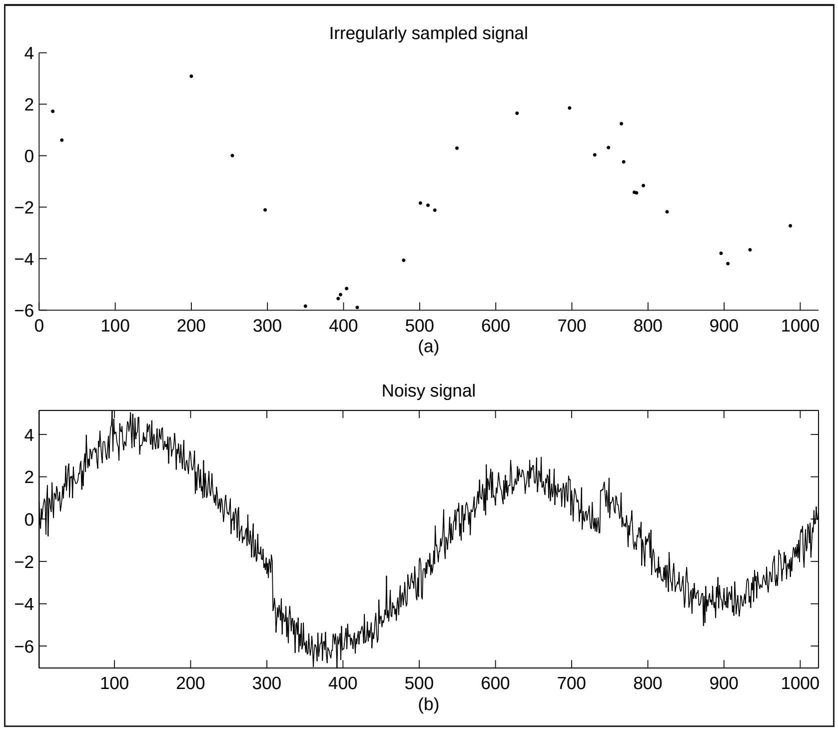

(i)

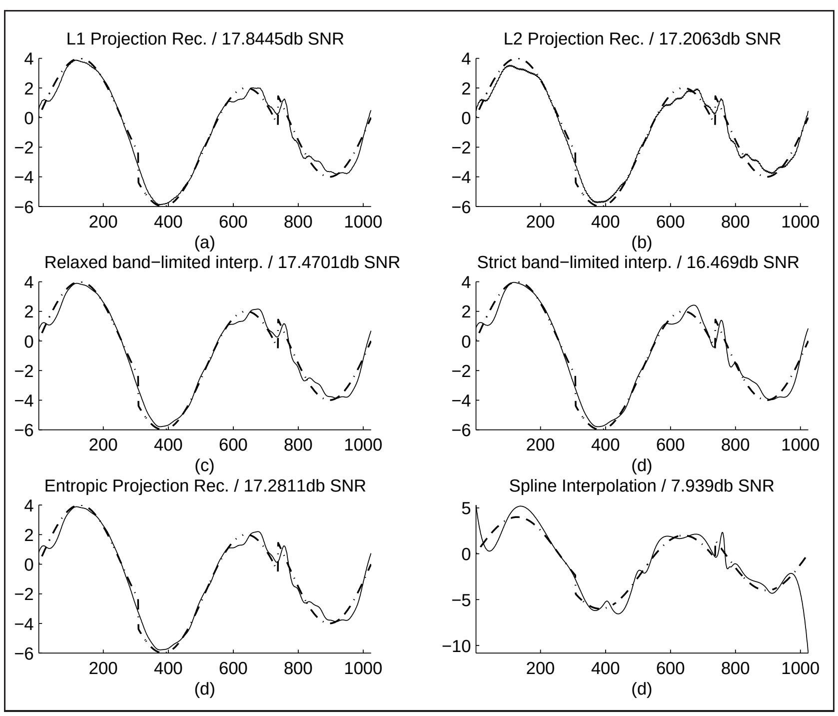

(ii)

Figure 4.2: (i) 32 point irregularly sampled version of the Heavisine function and the original noisy signal ($\sigma = 0.5$). (ii) The 1024 point interpolated versions of the function given at (i) using different interpolation methods.

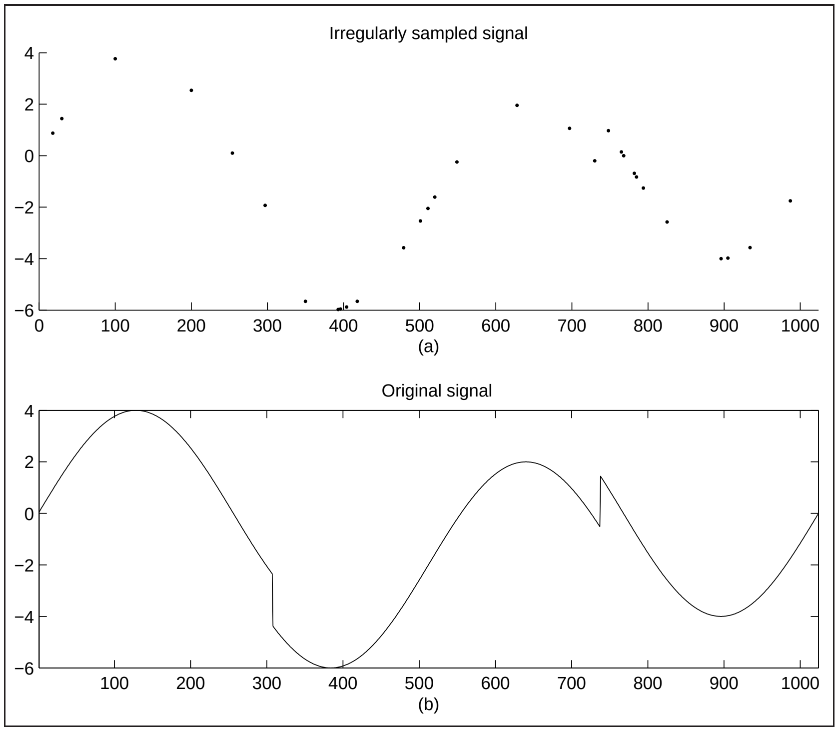

(i)

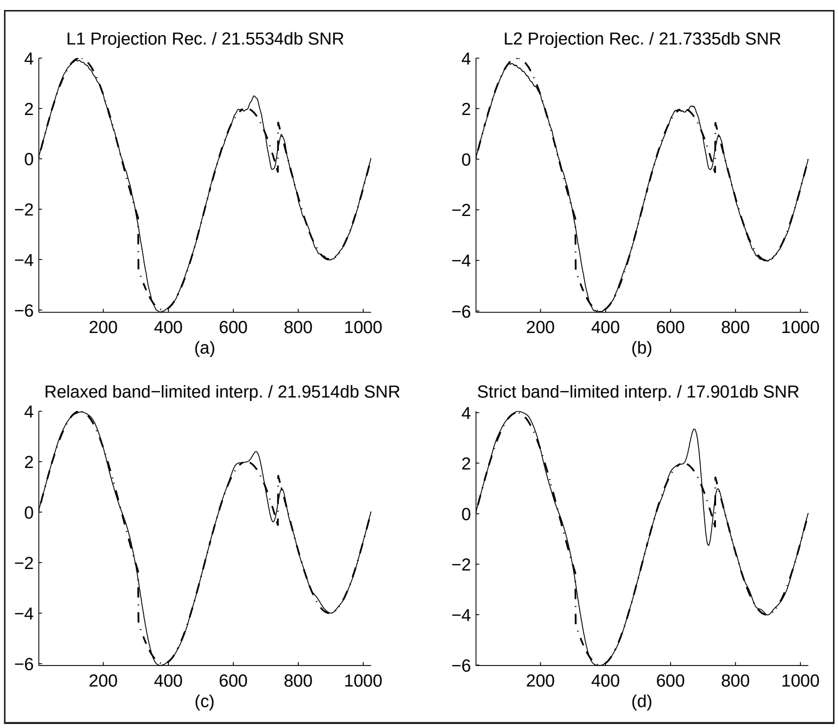

(ii)

Figure 4.3: (i) 32 point irregularly sampled version of the Heavisine function and the original noiseless signal. (ii) The 1024 point interpolated versions of the function given at (i) using different interpolation methods.

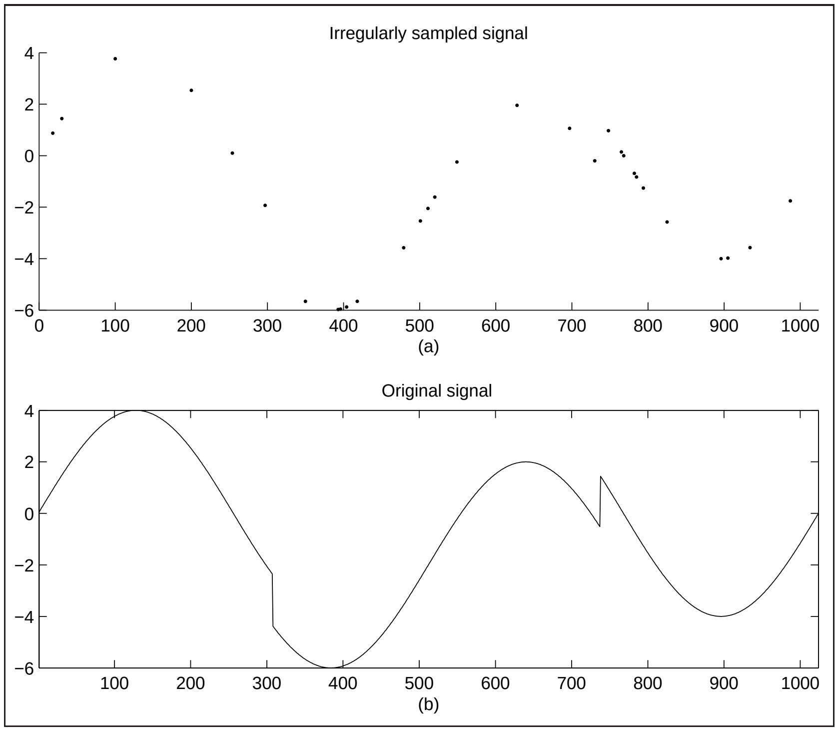

(i)

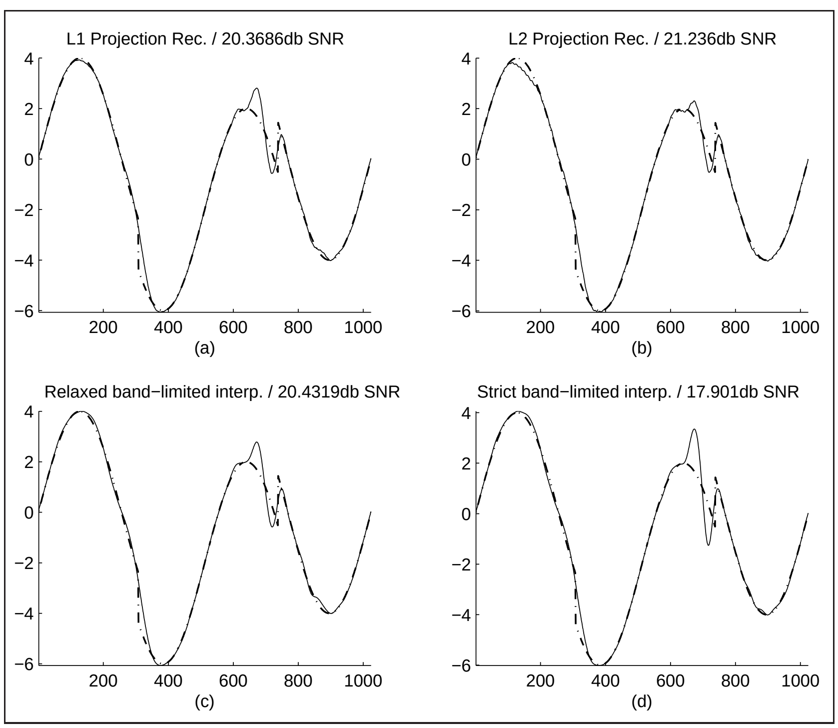

(ii)

Figure 4.4: (i) 32 point irregularly sampled version of the Heavisine function and the original noiseless signal. (ii) The 1024 point interpolated versions of the function given at (i) using different interpolation methods.

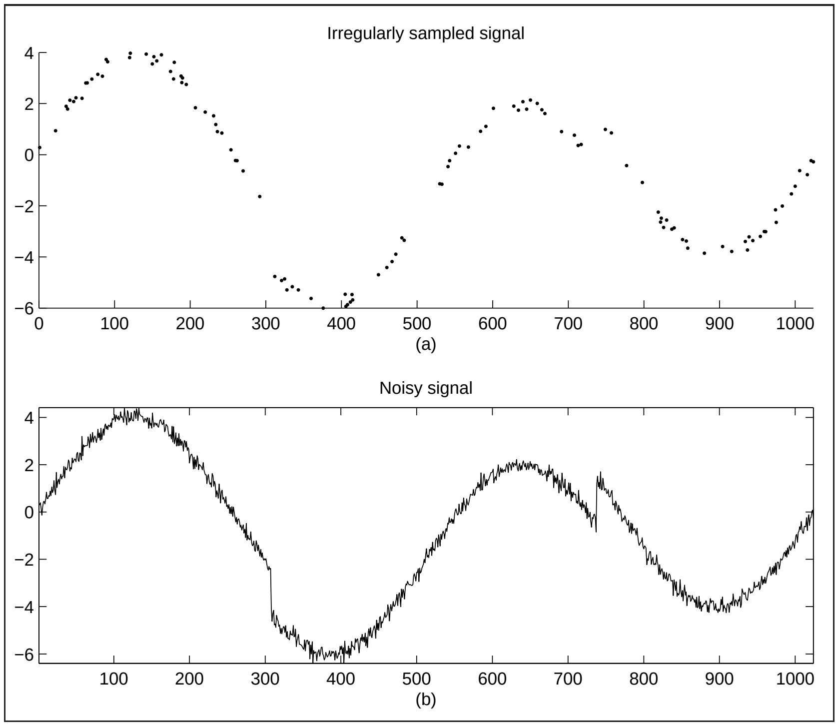

(i)

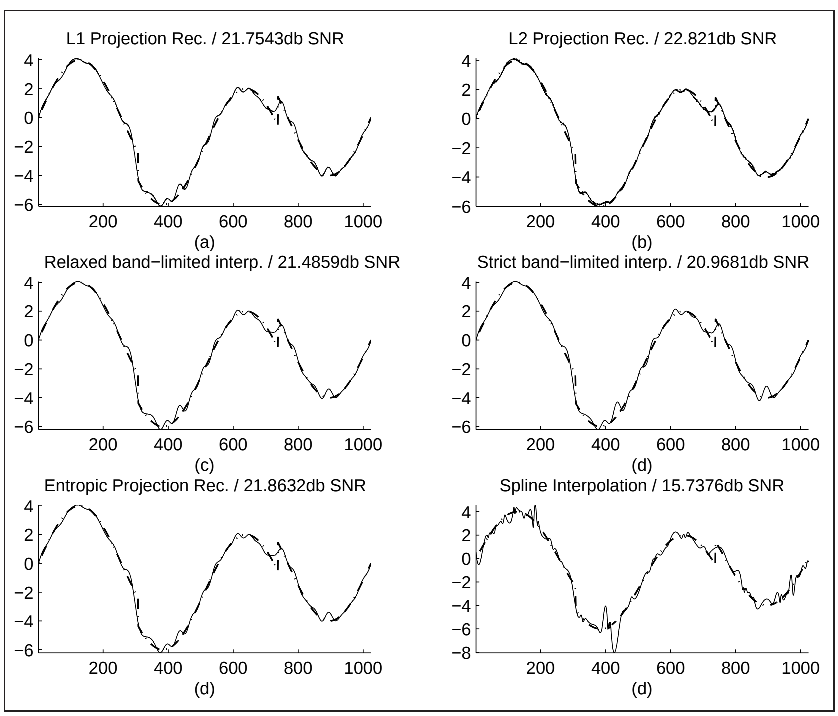

(ii)

Figure 4.5: (i) 128 point irregularly sampled version of the Heavisine function and the original noisy signal ($\sigma = 0.2$). (ii) The 1024 point interpolated versions of the function given at (i) using different interpolation methods.

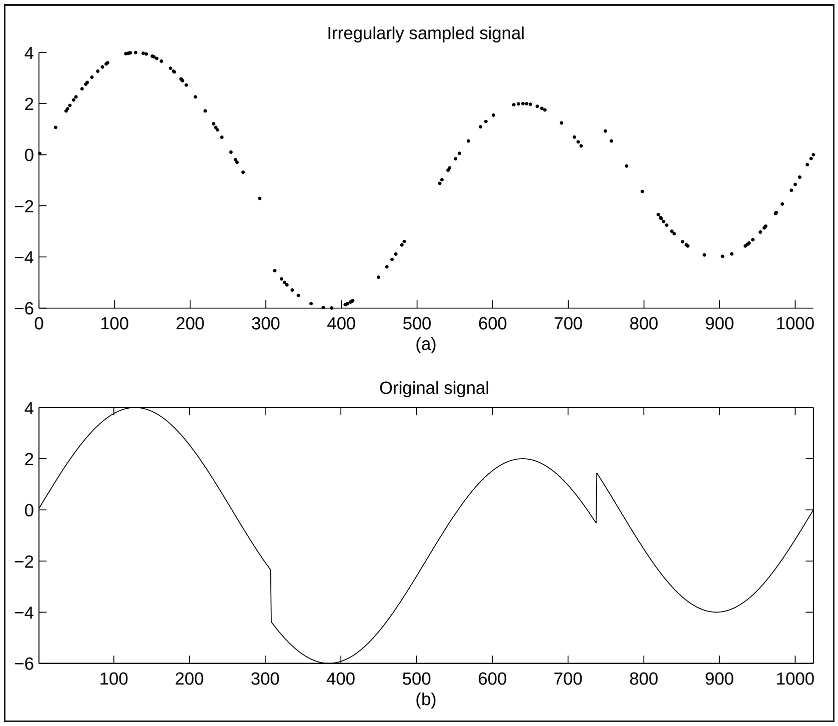

(i)

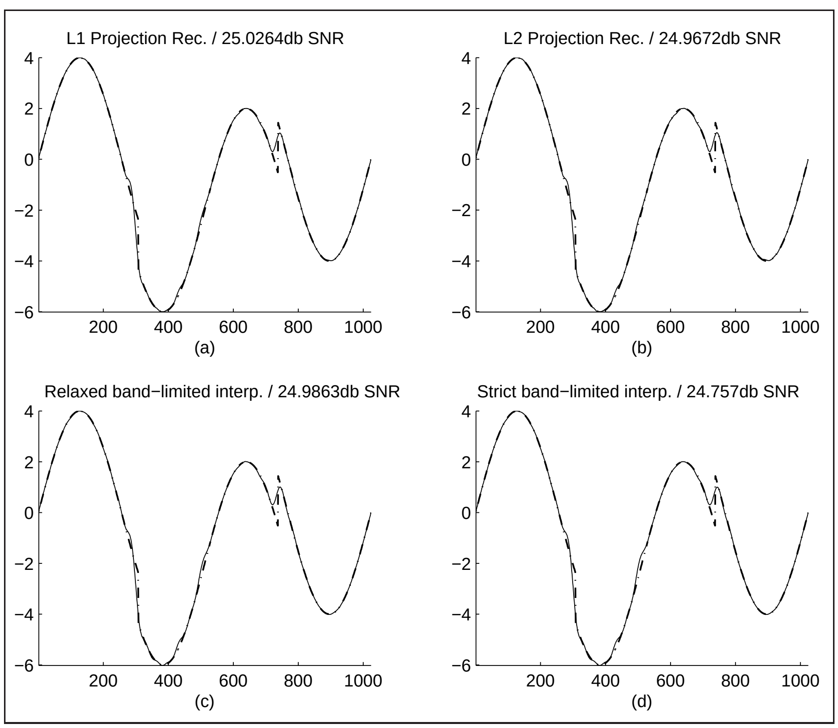

(ii)

Figure 4.6: (i) 128 point irregularly sampled version of the Heavisine function and the original noiseless signal. (ii) The 1024 point interpolated versions of the function given at (i) using different interpolation methods.

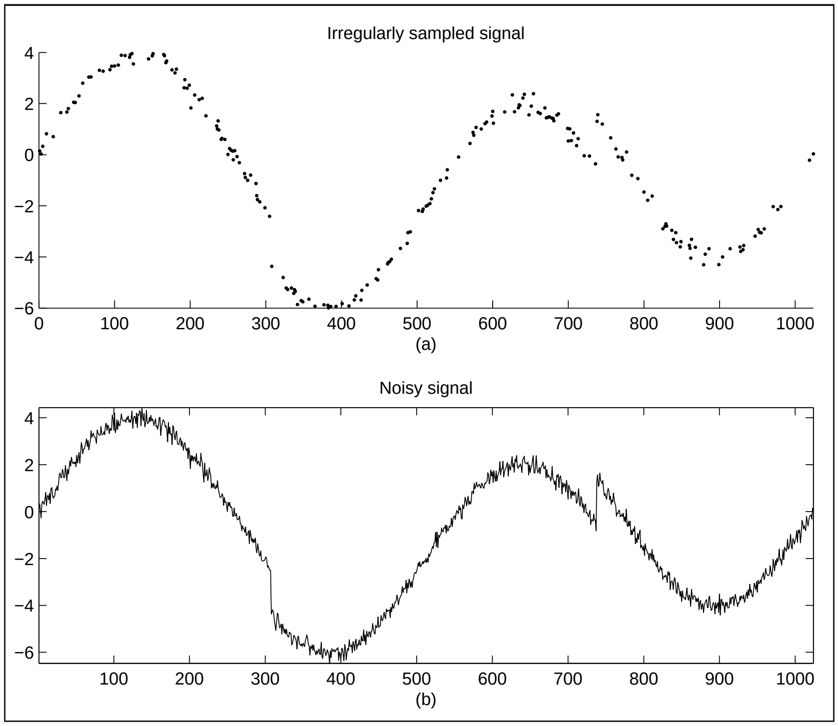

(i)

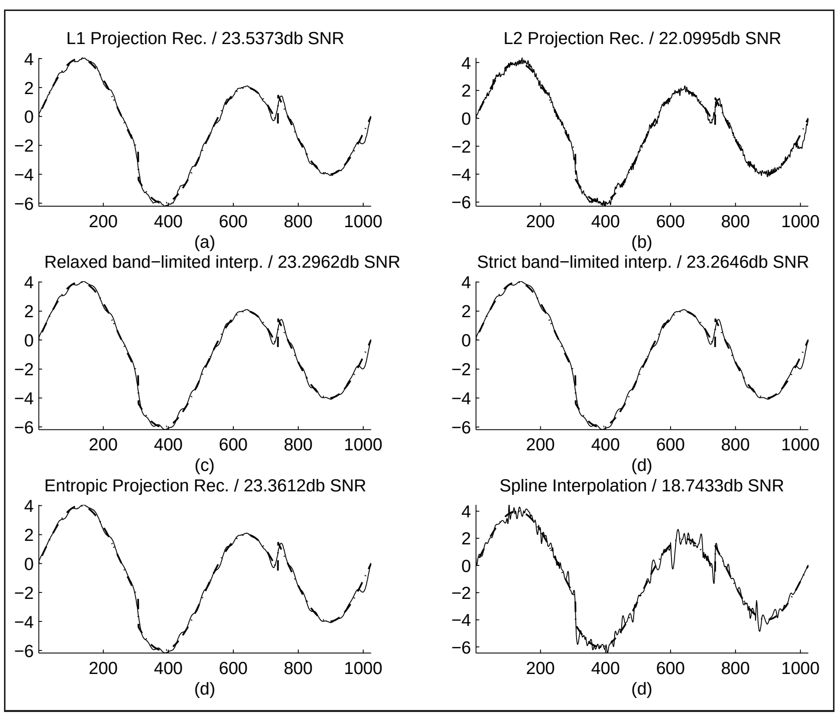

(ii)

Figure 4.7: (i) 256 point irregularly sampled version of the Heavisine function and the original noisy signal ($\sigma = 0.2$). (ii) The 1024 point interpolated versions of the function given at (i) using different interpolation methods.

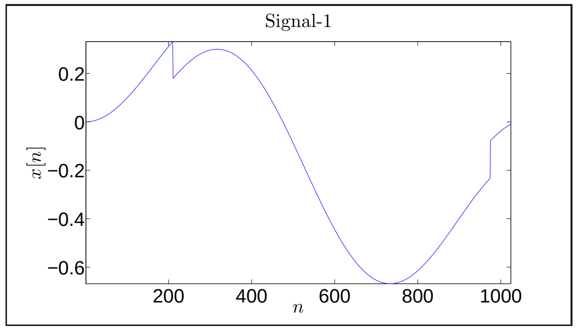

(a)

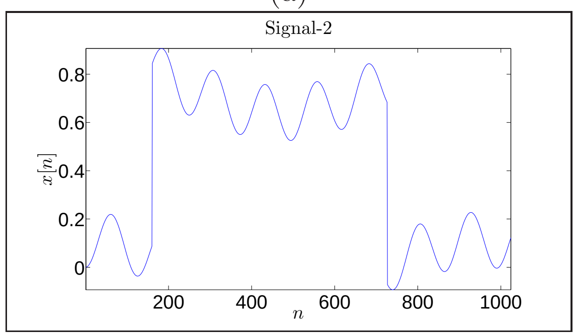

(b)

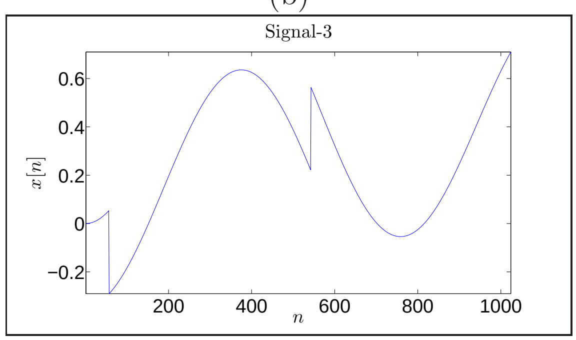

(c)

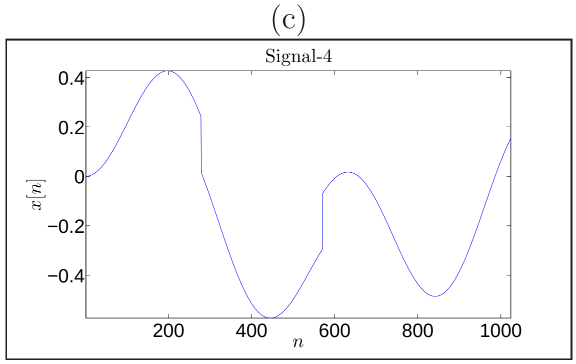

(d)

Figure 4.8: 4 of the other test signals that we used in our experiments. The related reconstruction results are presented in Table 4.2

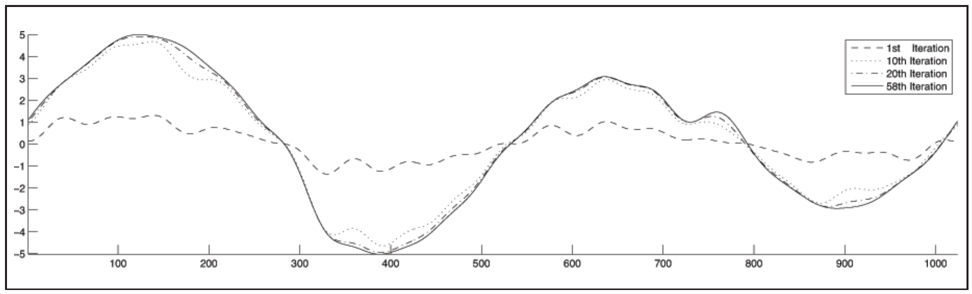

(a)

Figure 4.9: Restored Heavisine signal after 1, 10, 20 and 58 iteration rounds.

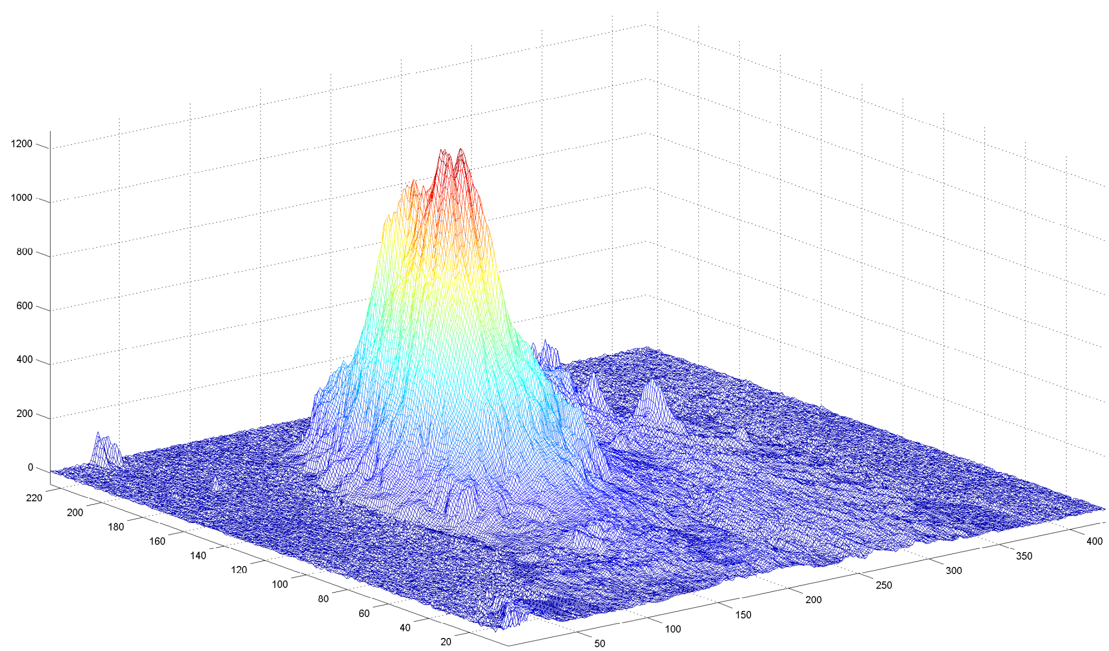

Figure 4.10: The original terrain model. The original model consists of 225×425 samples

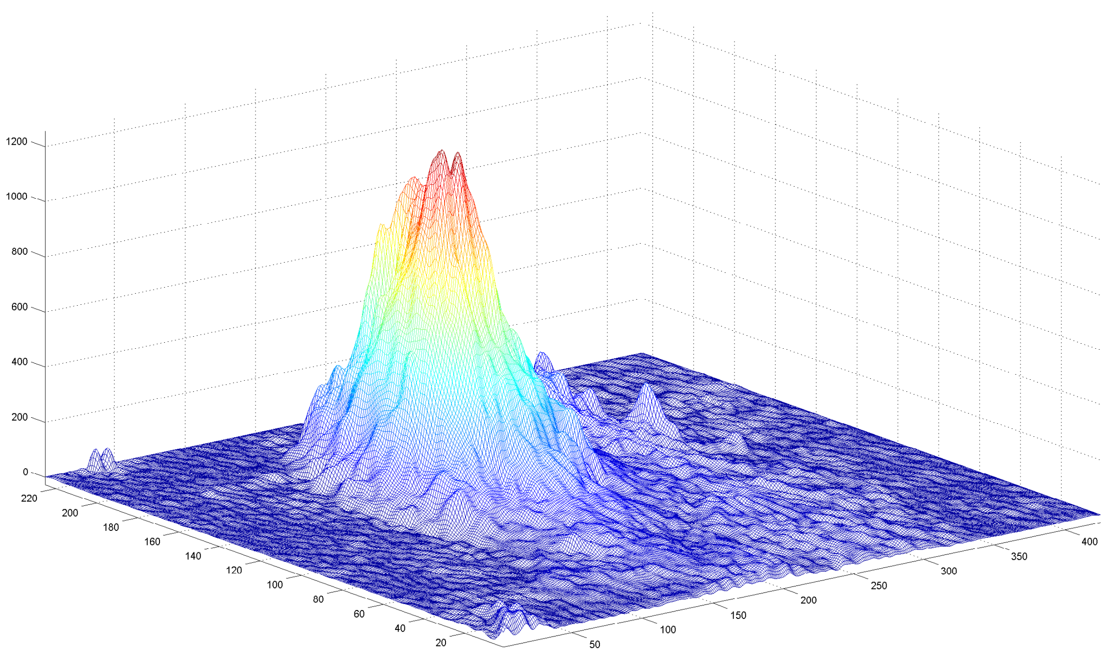

Figure 4.11: The terrain model in Figure4.10 reconstructed using one-fourth of the randomly chosen samples of the original model. The reconstruction parameters are $w_c = \frac{\pi}{4}$, $\delta_s = 0.03$, and $e_i = 0.01$.

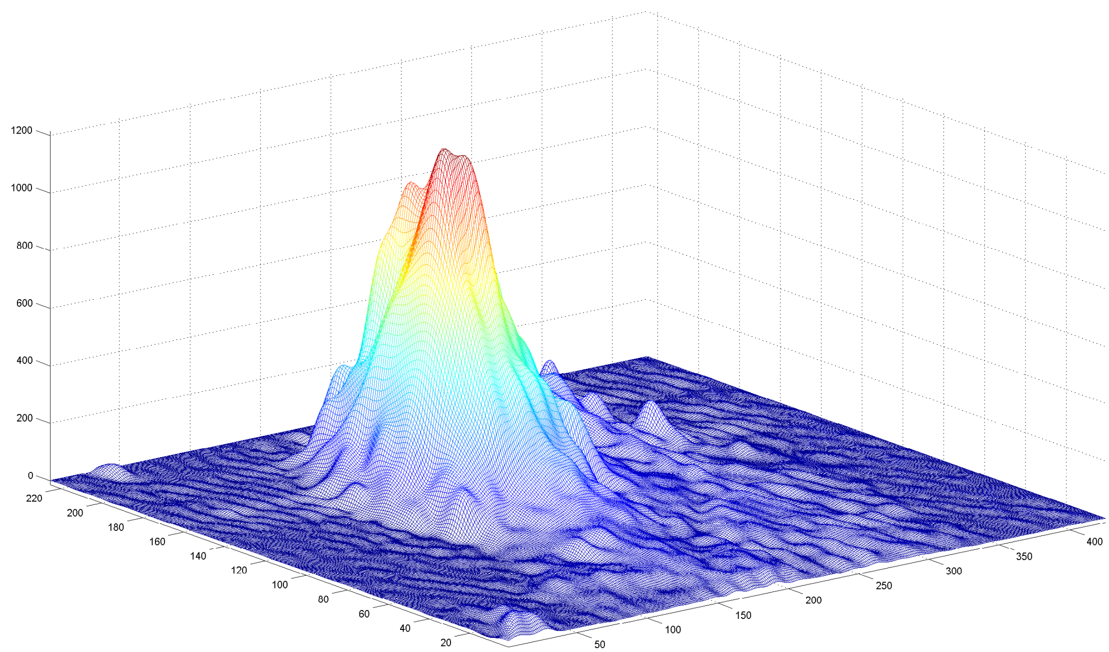

Figure 4.12: The terrain model in Figure 4.10 reconstructed using $\frac{1}{8}$ of the randomly chose samples of the original model. The reconstruction parameters are $w_c = \frac{\pi}{8}$, $\delta_s = 0.03$, and $e_i = 0.01$.

4.2 Signal Reconstruction from Random Samples

As presented in Section 1.2, CS framework defines a set of rules for taking compressed measurements from a signal, and reconstructing the original signal from those compressed measurements. In this section, the sampling part of the CS framework is used as it is (c.f. Section 1.2). On the other hand, a new signal reconstruction algorithm, which utilizes both row-iteration method from interval convex programming, and entropic projection operator, is defined.

Assume that, a length-N signal $\mathbf{x}$ has a K-sparse transform domain representation $\mathbf{s}$. The relation between $\mathbf{x}$ and $\mathbf{s}$ can be defined as in the following two equations

$$s_i =< \mathbf{x}, \psi_i >, \; i = 1, 2, ..., N, \tag{4.12}$$

$$\mathbf{x} = \sum_{i=1}^{N} s_i.\psi_i, \quad \text{or} \quad \mathbf{x} = \psi.\mathbf{s}, \tag{4.13}$$

where ψ is the transformation matrix and ψ_i is i^{th} row of the transformation matrix. According to CS theory, compressed measurements $\mathbf{y}$ can be taken from signal $\mathbf{x}$ as

$$\mathbf{y} = \phi.\mathbf{x} = \phi.\psi.\mathbf{s} = \theta.\mathbf{s} \tag{4.14}$$

where ϕ is the $M \times N$ measurement matrix, and $M << N$. The K-sparse signal $\mathbf{s}$ can be reconstructed from compressed measurement by solving following the ℓ_o norm optimization problem

$$\begin{aligned} \min_{\mathbf{s}} \quad & ||\mathbf{s}||_0 \\ \text{subject to} \quad & \theta.\mathbf{s} = y_i \;\; . \end{aligned} \tag{4.15}$$

As mentioned before (4.15) is an combinatorial problem. On the other hand, if RIP conditions [6, 21] are satisfied by the sampling procedure, then problem in (4.15) can be approximated by the ℓ_1 norm optimization as

$$\begin{aligned} \min_{\mathbf{s}} \quad & ||\mathbf{s}||_1 \\ \text{subject to} \quad & \theta.\mathbf{s} = y_i \;\; . \end{aligned} \tag{4.16}$$

In this thesis, the ℓ_0, and the ℓ_1 norms based cost functions are replaced by entropy functional in (2.15). Moreover, the CS reconstruction problem is divided into smaller subproblems so called row-iterations and solved through successive local D-projections. Bregman developed iterative row-action methods to solve the global convex optimization problem by successive local D-projections [13].

The global CS optimization problem can be divided into smaller optimization problems, and the i^{th} step of the problem can be defined as follows

$$\begin{aligned} \mathbf{s}_i = \arg\min \quad & D(\mathbf{s}, \mathbf{s}_{i-1}) \\ \text{subject to} \quad & \theta_i.\mathbf{s} = y_i, \; i = 1, 2, ..., M. \end{aligned} \tag{4.17}$$

where $D(\mathbf{s}, \mathbf{s}_{i-1})$ is the D-distance, which is defined as

$$D(\mathbf{s}, \mathbf{s}_{i-1}) = g(\mathbf{s}) - g(\mathbf{s}_{i-1}) - < \nabla g(\mathbf{s}_{i-1}), \mathbf{s} - \mathbf{s}_{i-1}) >, \tag{4.18}$$

$g(\mathbf{s})$ is a convex cost function, and θ_i is the i^{th} row of the constraint matrix. In each iteration step, a D-projection, which is a generalized version of the orthogonal projections, is performed onto a hyperplane represented by a row of the constraint matrix θ. In [13], Bregman proved that the proposed D-projection based iterative method is guaranteed to converge to global minimum if the algorithm starts from a proper choice of initial estimate (e.g. $\mathbf{s}_0 = \mathbf{0}$)

Since, neither the ℓ_0 norm nor the ℓ_1 norm are convex, the original CS reconstruction problems in (4.15), and (4.16) cannot be solved using row iteration methods. Therefore, they are replaced by the modified entropy functional $g_e(v) = (|v| + \frac{1}{e}) \log(|v| + \frac{1}{e}) + \frac{1}{e}$, which is a convex and continiously differentiable function as shown in Appendix A. In Chapter 2, it is shown that if the modified entropy functional is used in (4.17), this optimization problem can be solved using row action methods. Each row action step is actually an entropic projection onto the hyperplanes that are defined by the rows of the constraint matrix θ.

The proposed algorithm works as follows. The iterations start with an initial estimate $\mathbf{s}_o = \mathbf{0}$. In the first iteration cycle, this vector is D-projected onto the hyperplane H_1 and $\mathbf{s}_1$ is obtained. The iterate $\mathbf{s_1}$ is projected onto the next hyperplane H_2 (see Figure 4.13). This iterative process continues until the $N-1^{st}$

estimate $\mathbf{s}_{N-1}$ is D-projected onto H_N and $\mathbf{s}_N$ is obtained. In this way the first iteration cycle is completed. In the next cycle, the vector $\mathbf{s}_N$ is projected onto the hyperplane H_1 and $\mathbf{s}_{N+1}$ is obtained etc. Bregman proved that the iterates $\mathbf{s}_i$ converges to the solution of the optimization problem in (4.17). The geometric interpretation of the algorithm is given in Figure 4.13.

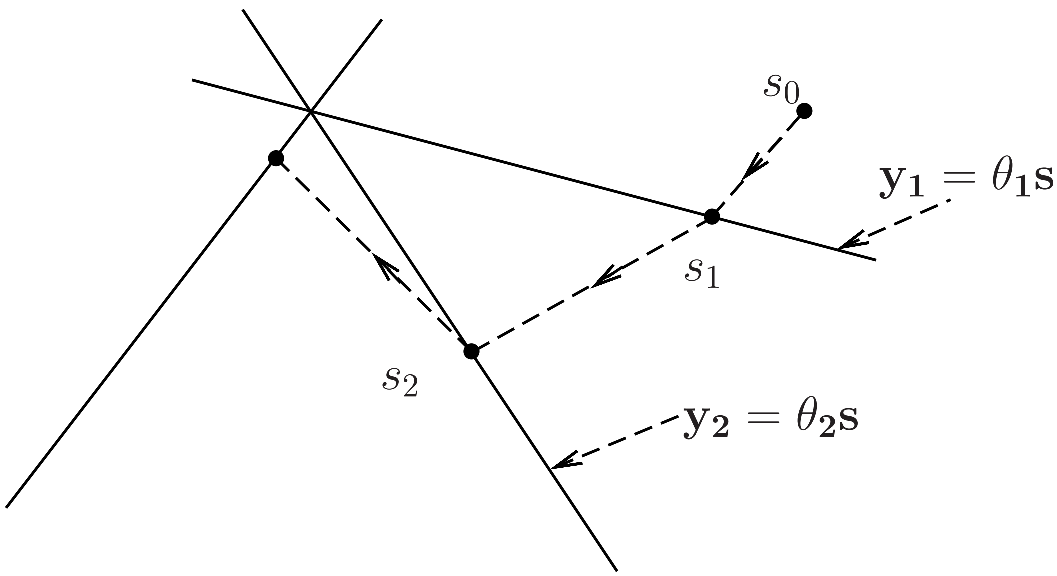

Figure 4.13: Geometric interpretation of the entropic projection method: Sparse representation $\mathbf{s_i}$ corresponding to decision functions at each iteration are updated so as to satisfy the hyperplane equations defined by the measurements y_i and the measurement vector θ_i. Lines in the figure represent hyperplanes in $\mathbb{R}^N$. Sparse representation vector s_i converges to the intersection of the hyperplanes. Notice that D-projections are not orthogonal projections.

Bregman's D-projection method can handle inequality constraints as well. The iterative algorithm is still globally convergent, when the equality constraints in (4.17) are relaxed by ϵ_i

$$y_i - \epsilon_i \leq \theta_i \mathbf{s} \leq y_i + \epsilon_i, \quad i = 1, 2, ..., N. \tag{4.19}$$

This is because hyperslabs defined by (4.19) are also closed and convex sets. In each step of the iterative algorithm the current iterate is projected onto the closest boundary hyperplane defined by one of the inequality signs in (4.19). If the iterate satisfies the current inequality, it is simply projected onto the next hyperslab.

The globally convergent row-action method described above can be easily extended to a block iterative version by combining the entropic D-projections to several rows of the θ matrix. However, we can not give a convergence proof of the block-iterative method at this point.

Instead of performing successive D-projections onto each hyperplane constraint, as in (4.17), it is also possible to perform groups of projections. In [122], a parallel version of the POCS algorithm called the block iterative approach is presented. In this version, one may project the current iterate s_{i-1} onto a set of hyperplanes defined by the rows of the measurement matrix θ. The selection of the rows of the measurement matrix onto which the current iterate will be projected onto can be selected either consecutively, randomly or according to a rule. The geometric interpretation of the parallel algorithm is illustrated in Figure 4.14 Typically, the parallel algorithm converges faster. However, the convergence of the algorithm for this problem cannot be proved at this stage.

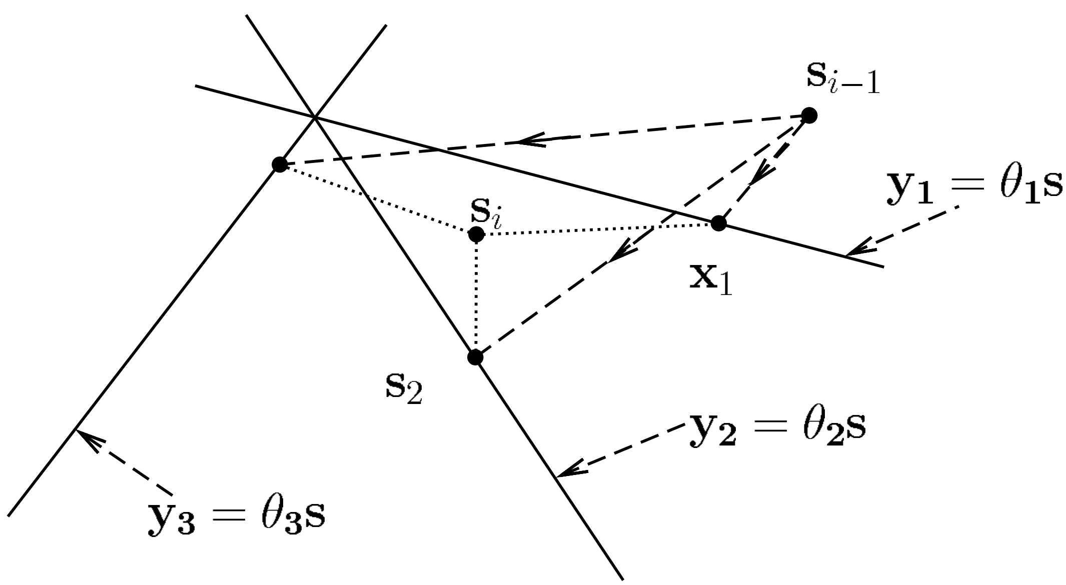

Figure 4.14: Geometric interpretation of the block iterative entropic projection method: Sparse representation $\mathbf{s_i}$ corresponding to decision functions at each iteration are updated by taking individual projections onto the hyperplanes defined by the lines in the figure and then combining these projections. Sparse representation vector s_i converges to the intersection of the hyperplanes. Notice that D-projections are not orthogonal projections.

4.2.1 Experimental Results

For the validation and testing of the entropic minimization method, experiments with 3 different one-dimensional (1D) signals, and 6 different images are carried out. The *cusp* signal, which consists of 1024 samples, and *hisine* signal, which consists of 256 samples are shown in Figures 4.15, 4.16, respectively. The cusp and the hisine signals can be sparsely approximated in DCT domain. The 4 random signal is composed of 128 samples and it consists of 4 randomly located non-zero samples. The measurement matrices ϕ are chosen as Gaussian random matrices.

In the first set of experiments $M = 204, 717$ measurements are taken from the cusp signal and $M = 24, 40$ measurements are taken from the $S = 5$ random signal. The original signals are reconstructed from those measurements. The reconstructed signals using the entropy based cost functional are shown in Figures 4.17(a), 4.17(b), 4.18(a), and 4.18(b). The cusp signal has 76 DCT coefficients, whose magnitudes are larger than 10^{-2}. Therefore, it can be approximated by a $S = 76$ sparse signal in DCT domain. 39 and 44 dB SNR are achieved by the reconstructing the original signal using the proposed method from $M = 204, 717$ measurements respectively. In case of the experiment with random signals, the proposed method missed one sample from the original signal using 30 measurement and perfectly reconstructed the original signal using 50 measurements.

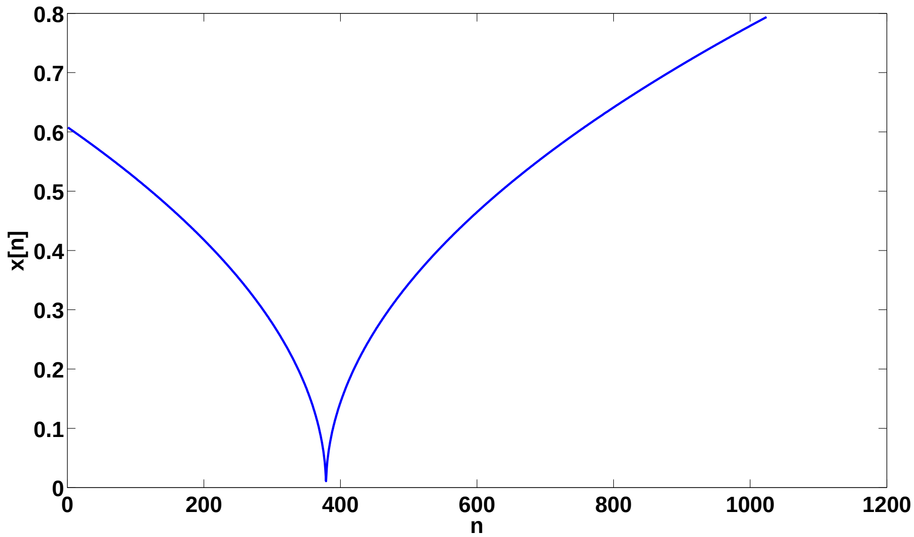

Figure 4.15: The cusp signal with $N = 1024$ samples

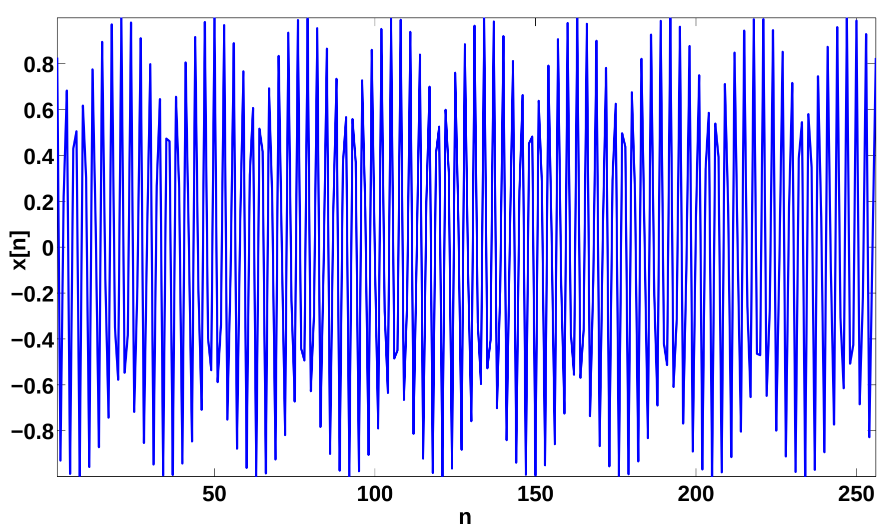

Figure 4.16: Hisine signal with $N = 256$ samples

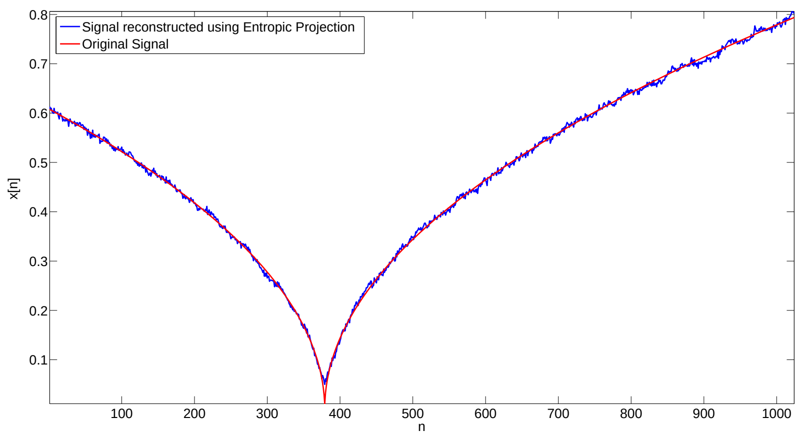

(a) $N = 1024$ length cusp signal reconstructed from 204 measurements

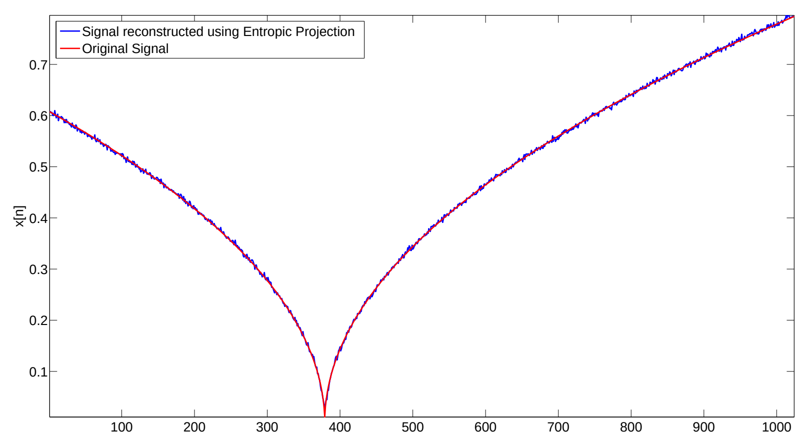

(b) $N = 1024$ length cusp signal reconstructed from 716 measurements

Figure 4.17: The cusp signal with 1024 samples reconstructed from $M = 204$ (a) and $M = 716$ (b) measurements using the iterative entropy functional based method.

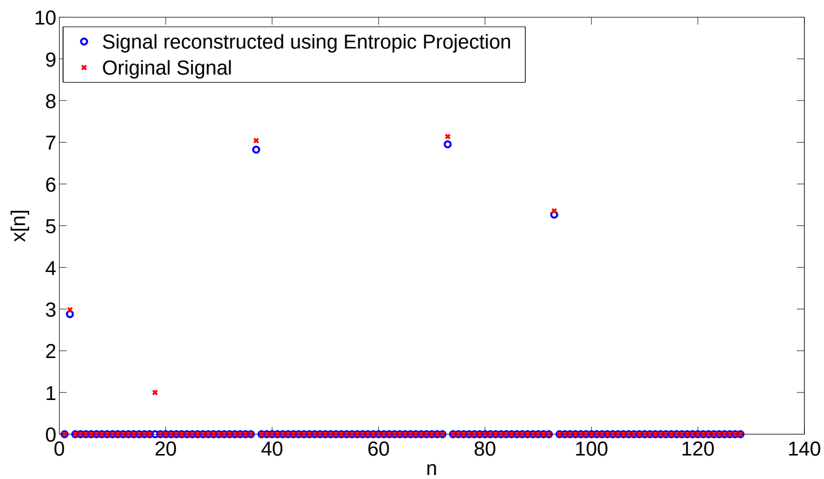

(a) $N = 128$ length random sparse signal reconstructed from $3S = 15$ measurements

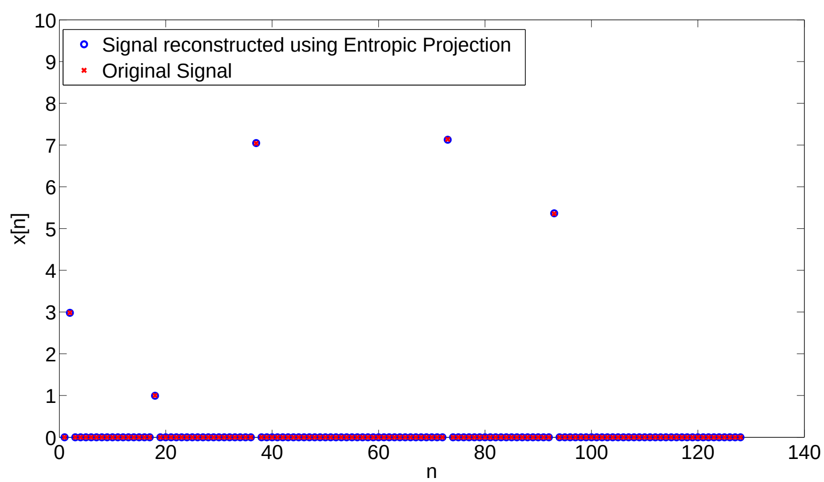

(b) $N = 128$ length random sparse signal reconstructed from $4S = 20$ measurements

Figure 4.18: Random sparse signal with 128 samples is reconstructed from (a) $M = 3S$ and (b) $M = 4S$ measurements using the iterative, entropy functional based method.

In the next set of experiments, the reconstruction results of the proposed algorithm is compared with the CoSaMP algorithm [18]. Different amount of measurements in the range of 10% to 80% of the total number of the samples of the 1D signal are taken and the original signal is estimated. Then the SNR between the original and the reconstructed image are measured. The SNR measure is defined as follows;

$$\text{SNR} = 20log_{10}\left(\frac{||\mathbf{x}||_2}{||\mathbf{x}-\mathbf{x}_{rec}||_2}\right), \tag{4.20}$$

where $\mathbf{x}$ is the original signal and $\mathbf{x}_{rec}$ is the reconstructed signal. As shown in Figures 4.19, 4.20, and 4.21, the proposed algorithm outperforms CoSaMP for the reconstruction of the cusp and hisine signals. For example, the proposed method achieves 15dB SNR at 103 measurements (10%), while CoSaMP achieves only 3dB SNR for the cusp signal.

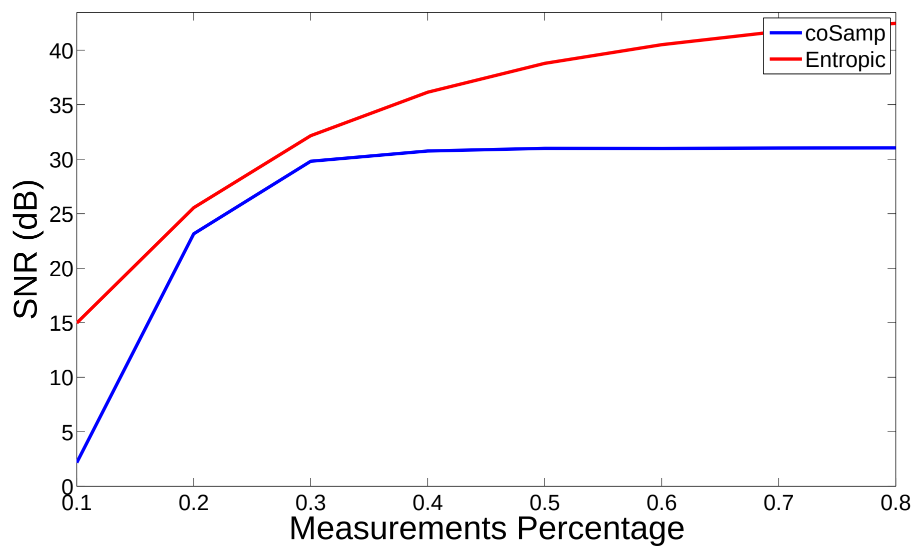

Figure 4.19: The reconstructed cusp signal with $N = 1024$ samples

It is important to note that, neither the cusp nor the hisine signals are sparse. They are compressible in the sense that most of their transform domain coefficients are not zero but negligibly small [123]. Therefore, their sparsity level can not be known exactly beforehand. On the other hand, the CoSaMP method outperformed the proposed algorithm for the 25 sparse random signal, which consists of randomly located 25 isolated impulses. In this case the sparsity level is exactly known beforehand. Both the proposed algorithm and the CoSaMP method

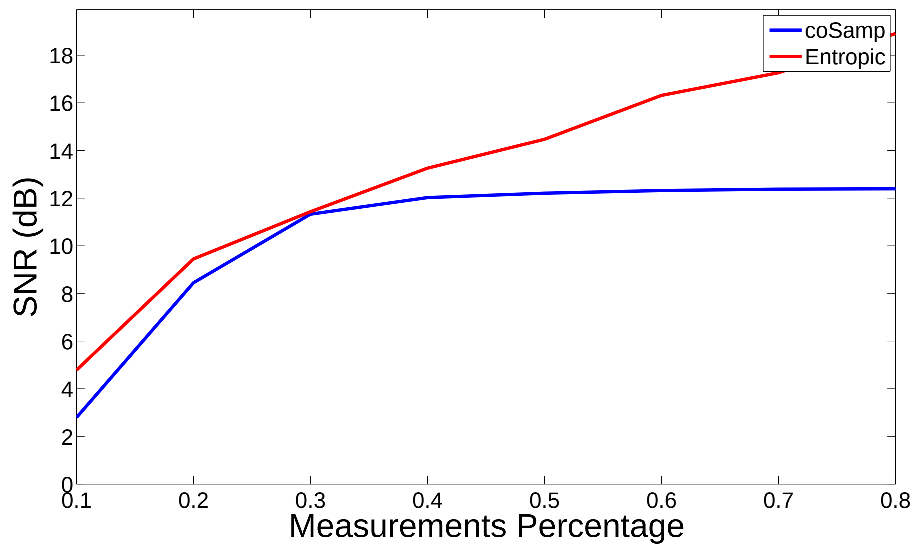

Figure 4.20: The reconstruction error for a hisine signal with $N = 256$ samples.

achieved higher than 50 dB SNR level, for the same number of measurement. Due to numerical imprecision in the calculation of the alternating entropic projections, the proposed algorithm achieves approximately 50 dB SNR. On the other hand the CoSaMP method achieved approximately 300 dB SNR. Above 40-50 dB of SNR, the signal reconstruction can be counted as perfect reconstruction. Therefore, it can be safely said that both algorithms achieved perfect reconstruction at the same measurement level.

In the last set of experiments, the proposed algorithm is implemented in 2-dimensional (2D) and applied to 26 different images. The results are compared with the block based compressed sensing algorithm given in [2]. As in [2] the image is divided into blocks and reconstructed from those block individually. The proposed and Fowler et.al's algorithms are tested using random measurements, that are as many as the %30 of total number of the pixels in the image.

In Figures 4.22, 4.23, and 4.24 details extracted from images reconstructed using (a) the proposed method, and (b) the method in [2]. Images reconstructed using Fowler's method are oversmoothed whereas the proposed reconstruction methods leads to more sharp images. For example, in the fingerprint image that is shown in Figure 4.22, the fingerprint lines seem to be slightly oversmoothed by

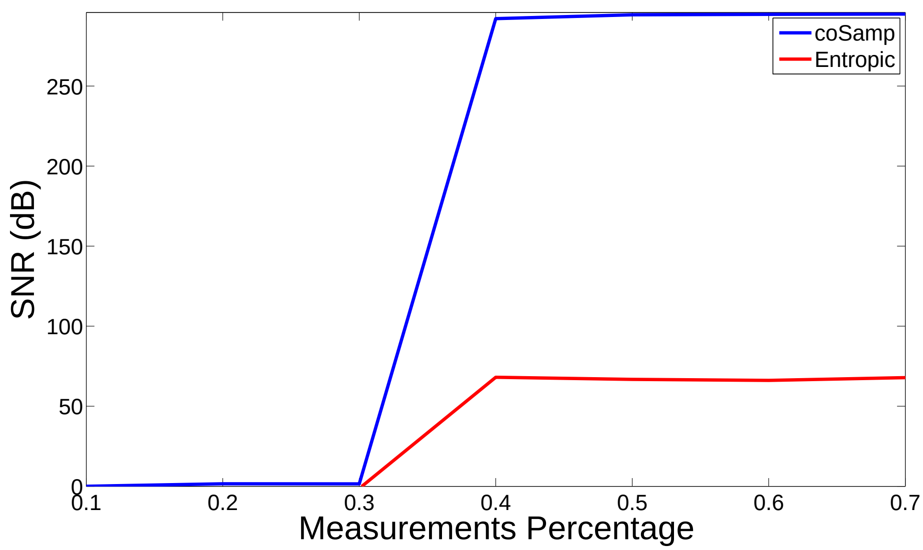

Figure 4.21: The impulse signal with $N = 256$ samples. The signal consists of 25 random amplitude impulses that are located at random locations in the signal.

Fowler's reconstruction shown in (b) compared to the entropy projection based reconstruction shown in (a). The difference can be seen much better in Figure 4.23. The hair detail around the eyes and the nose of the Mandrill is kept by the entropy projection based reconstruction whereas Fowler's method oversmoothed all the details. Same effect can be seen at the window detail of the house in Figure 4.24.

In all of the above examples, the entropic projection algorithm is implemented as follow. The algorithm starts with an initial estimate of the signal such as a zero amplitude signal. Then in the first iteration cycle the estimated signal is entropically projected on the hyperplanes defined by the measurements one after another. At the end of the iteration cycle, transform domain coefficients of the resulting estimate are rank ordered according to their magnitude values and only the significant coefficients are kept and the rest is set to zero. After each iteration cycle the number of retained transform domain coefficients that are kept is increased by one. The upper bound of the transform domain coefficients that are kept during the iterations can not exceed the number of the measurements. If the initial signal is known to be exactly K-sparse, then only K largest absolute valued transform domain coefficients kept.

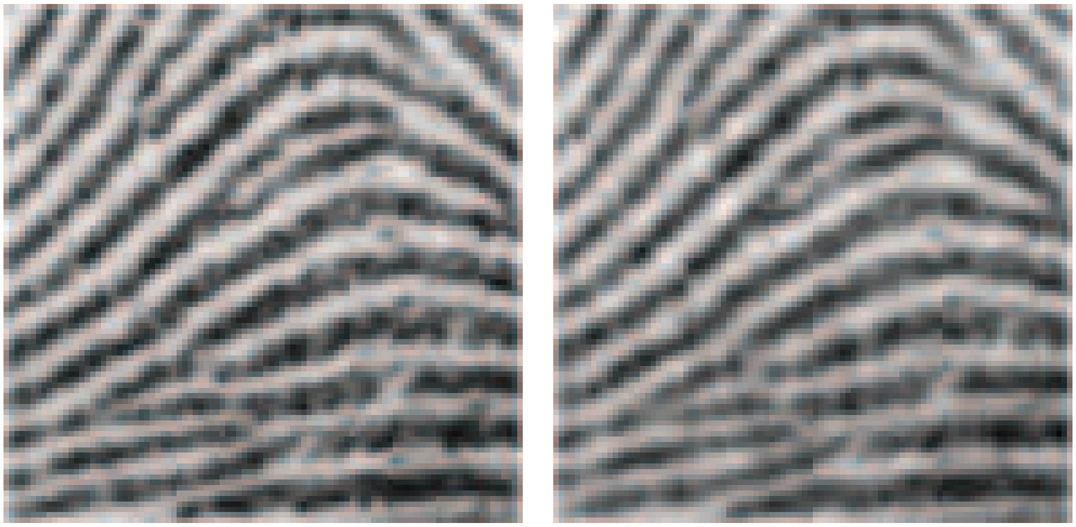

(a) Rec (b) FWL

Figure 4.22: Detail from resulting reconstruction of the Fingerprint image using (a) the proposed and (b) Fowler's [2] method.

It is important to note that, in both methods, the images are processed using a low-pass filter to smooth out the blocking artifacts caused due to block processing.

SNR values obtained through the experiments with different images can be found in Table 4.3. In most of the cases approximately 1dB higher SNR compared to the algorithm given in [2] is achieved by the proposed algorithm.

The experimental results given in this section indicate that it is possible to

Table 4.3: Image reconstruction results. The images are reconstructed using measurements that are 30 % of the total number of the pixels in the image.

	Fowler's Method [2]	Proposed Method
Images	SNR in dB	SNR in dB
Barbara	19.412	18.528
Mandrill	16.822	17.401
Lenna	26.516	26.806
Goldhill	22.473	23.857
Fingerprint	20.171	22.205
Peppers	26.831	25.854
Kodak(Average)	21.51	21.98
Average	21.63	21.90

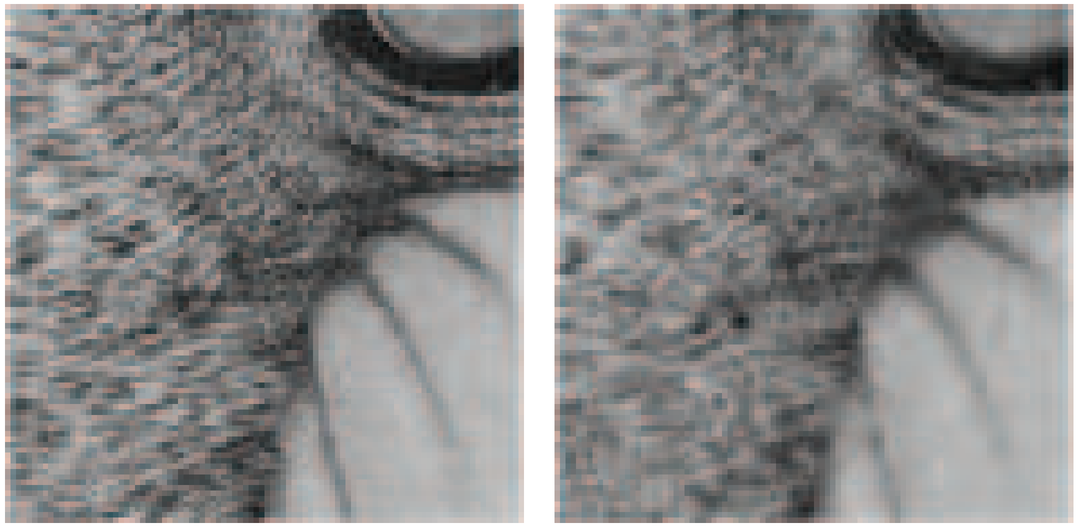

(a) Rec (b) FWL

Figure 4.23: Detail from resulting reconstruction of the Mandrill image using (a) the proposed and (b) Fowler's [2] method.

reformulate the CS reconstruction problem using the modified entropy based cost function based regularization. Since this function approximates the ℓ_1 norm and is continuous and differentiable everywhere, the proposed formulation of the reconstruction problem can be solved using interval convex optimization metods; such as iterative row-action methods. The proposed algorithm is globally convergent due to POCS theorem. It is experimentally observed that the entropy based cost function and the iterative row-action method can be used for reconstructing both sparse and compressible signals from their compressed measurements. Since most practical signals are not exactly sparse but compressible, the proposed algorithm is suitable for compressive sensing of practical signals.

It should also be noted that the row-action methods provide a solution to the on-line CS problem. The reconstruction result can be updated on-line according to the new measurements without solving the entire optimization problem again in real time.

(a) Rec

(b) FWL

Figure 4.24: Detail from resulting reconstruction of the Goldhill image using (a) the proposed and (b) Fowler's [2] method.

Chapter 5

SIGNAL DENOISING

This chapter comprises of two different signal denoising algorithms. In Section 5.1, an algorithm that makes use of block processing to solve the TV denoising problem. The algorithm adapts itself to the local content of the image blocks and adjusts the TV denoising parameters accordingly. In Section 5.2, an image denoising algorithm, which utilizes the filtered variations contraints defined in 3.1, is presented.

5.1 Locally Adaptive Total Variation

In this section, a local Total Variation (LTV), and a locally adaptive Total Variation (LATV) regularized denoising scheme are introduced. In the proposed approaches an N-by-M image $\mathbf{x}$ is reconstructed from its noisy observation $\mathbf{y}$ using LTV or LATV denoising algorithm. In ordinary TV approach, the TV cost function is minimized over the entire image. However, the correlation between the samples in a typical signal or an image decreases as the distance between two samples increases. Therefore, globally minimization of a cost function over the whole signal may not be necessary in denoising problems. Block processing is a commonly referred technique in image processing to take advantage of local processing and computational efficiency. On the other hand, the disadvantage of block processing techniques is that they may introduce artificial edges at the boundaries of the blocks in the restored image.

Both LTV and LATV methods are block based algorithms. They work like a nonlinear filter and produces a single output for each input block. Therefore, they do not suffer from blocking artifacts. Furthermore, LATV enables the possibility of adapting optimization parameters according to the block content and introduce adaptivity to the TV cost functional.

In image denoising problem, it is assumed that the original signal $\mathbf{x}$ is corrupted by additive noise $\mathbf{u}$ as follows

$$\mathbf{y} = \mathbf{x} + \mathbf{u}. \tag{5.1}$$

In TV regularization based denoising approach, the original signal is estimated by solving the following minimization problem:

$$\begin{aligned} \min_{\mathbf{x}} \quad & ||\mathbf{x}||_{TV} \\ \text{subject to} \quad & ||\mathbf{y} - \mathbf{x}|| \leq \varepsilon. \end{aligned} \tag{5.2}$$

or in Lagrangian formulation

$$\min_{\mathbf{x}} ||\mathbf{y} - \mathbf{x}||^2 + \lambda ||\mathbf{x}||_{TV} \tag{5.3}$$

where ε is the error tolerance, and λ is the Lagrange multiplier. There exists an ε corresponding to each λ such that both optimization problems result in the same solution [124, 125]. These parameters can also be used for adjusting the smoothness level of the solution. In [19], an iterative algorithm was proposed to solve the optimization problem given in (5.2) and (5.3). This algorithm solves the TV minimization optimization on the whole image; therefore, as the image size increases, the problem size also increases, and therefore the computational complexity of the algorithm increases.

In regular TV denoising only a single optimization problem is solved for the entire image. Due to this global approach, some of the high-frequency details of the image may be over-smoothed or the noise may not be cleaned effectively at smooth regions. To deal with this problem, a local adaptation strategy is developed. The proposed LTV and LATV methods overcome this problem through a block-based local adaptation strategy.

Let $w_{\mathbf{n}}$ be a window centered at the pixel $\mathbf{n} = (n_1, n_2)$. The window can be a rectangular window, or it can take any shape. Furthermore, one can apply decaying weights to the samples within each window. LTV algorithm solves the following problem for each pixel

$$\begin{aligned} &\min_{\mathbf{x}[\mathbf{n}]} && \sum_{\mathbf{k}\in w_{\mathbf{n}}} \nabla \mathbf{x}[\mathbf{k}] \\ &\text{subject to} && \sum_{\mathbf{k}\in w[\mathbf{n}]} (x[\mathbf{k}] - y[\mathbf{k}])^2 < \varepsilon \end{aligned} \tag{5.4}$$

where $\mathbf{k} = (k_1, k_2)$. Chambolle's algorithm [19] actually restores all the pixels in $w[\mathbf{n}]$, but only the center pixel is picked as the restored output. To restore the next pixel, the analysis window is moved one pixel to the left $(k_1, k_2 + 1)$, or down $(k_1 + 1, k_2)$, and the problem described in (5.4) is solved once again. The entire noisy image is processed pixel by pixel in this manner. The optimization problem described in (5.4) is solved in a small neighborhood unlike (5.3), which is solved for the entire image. Therefore, the computational complexity of the LTV method is low.

The optimization parameter ε in (5.4) can be used to set the smoothness level of the solution. As ε value increases, the minimization part will turn out more smooth regions. Ideally, it should be selected close to the standard deviation of the signal noise [19], which can be estimated from the flat regions of the image. In the first set of experiments that is summarized in the first two columns of Tables 5.1 and 5.2, we used the same optimization parameter (just scaled by the number of the pixels in the processing area) for both the ordinary TV and the proposed LTV methods.

We tested the proposed approach on 35 different images. We used 24 images from the *Kodak* dataset taken from http://r0k.us/graphics/kodak/ and some well known images from image processing literature. We selected the block size as 9×9. According to the results summarized in Table 5.1 and 5.2, the LTV approach provides slightly better results compared to Chambolle's global algorithm [19] even without varying the optimization parameters over the image.

Solving the TV problem in (5.2) and (5.3) using the same optimization parameters throughout the entire image does not produce the best denoising results. As pointed out before, this approach may cause over smoothing of the high-pass details, or may not effectively clean the noise at smooth blocks. In the LATV algorithm, an adaptivity stage is added to the LTV algorithm. The optimization parameter ε in (5.4) is varied according to the local content of the processed block of the image.

When there is an edge in the analysis block, the optimization parameter ε is decreased compared to the flat regions of the image. In order to determine edges in the analysis block, the local TV value of the block is used. In Figures 5.1.(a), 5.1.(b), and 5.1.(c), the TV images of the original, noisy and low-pass filtered noisy (simple 3-by-3 averaging filter) Cameraman images are shown, respectively. Images shown in Figure 5.1 are determined as follows: The TV value is computed in an $r \times r$ ($r = 3$) window for each pixel. In Figure 5.1.(c) the image is low-pass filtered first and the TV value of each pixel is computed afterwards.

As shown in Figure 5.1.(c), it is possible to use a threshold on the TV value of a block to determine blocks with high edge content. The threshold value can be determined in a heuristic manner or using the threshold $T_{TV} = \mu_{TV} + \alpha\sigma_{TV}$ where μ_{TV} and σ_{TV} are the mean and standard deviation value of the TV of the blocks in the image, respectively. The parameter α can be selected as any number between 2 and 3.

One can also use other edge detection methods, but we prefer to use the TV values of each block to reduce the computational cost of the denoising process because the TV value of each block is computed during the minimization of (5.4).

The locally adaptive method is not very sensitive to the threshold value because denoising is performed in all the blocks regardless of the nature of the block. An incorrect edge decision does not produce discontinuities in the image because whenever the nature of the block is incorrectly determined it is highly likely that the next block is also incorrectly decided.

In blocks containing edges, the optimization parameter ε is simply reduced to $\varepsilon_1 < \varepsilon$. The third columns of Table 5.1 and 5.2 are obtained with $\varepsilon_1 = 0.85\varepsilon$.

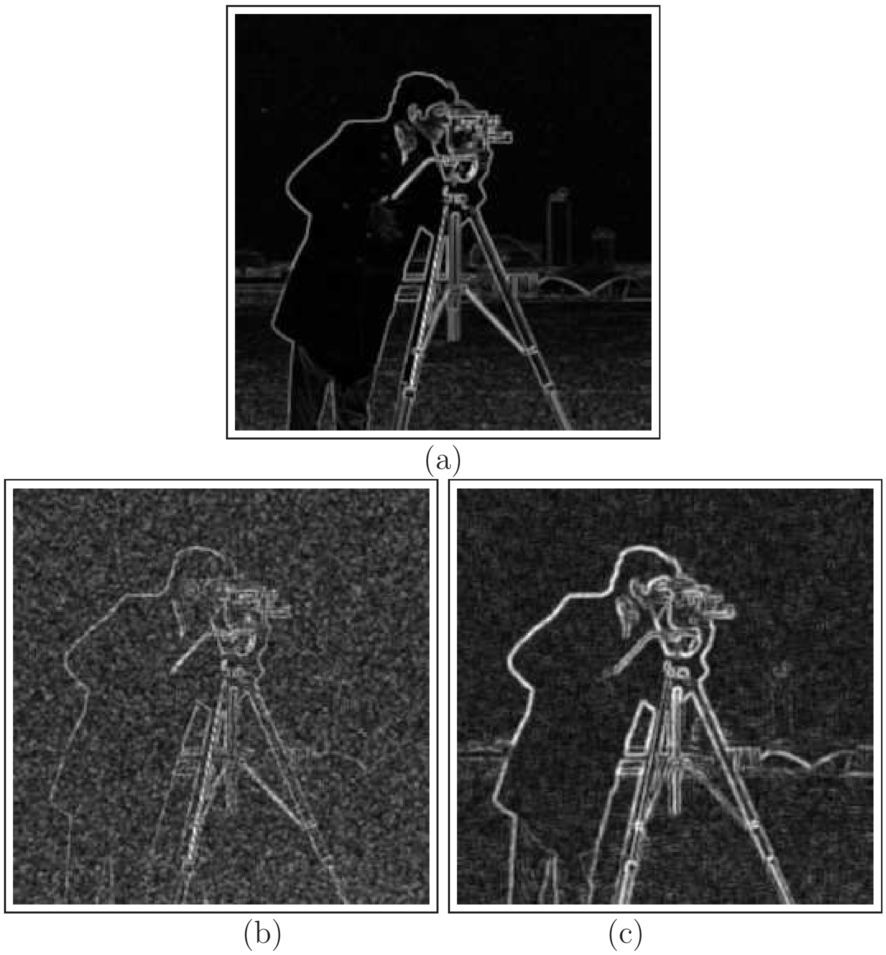

Figure 5.1: TV images of (a) original, (b) noisy, and (c) low-pass filtered noisy Cameraman images. All images are rescaled in $[0, 1]$ interval.

As summarized in Table 5.1 the LATV approach provides an 0.5 dB improvement over the standard TV approach in our dataset consisting of 35 images when the noise is Gaussian with standard deviation $\sigma = 0.1$. Original image pixel values are normalized to $[0, 1]$ range before adding the noise. In Table 5.2, the improvement is 0.3 dB when $\sigma = 0.2$.

In Figure 5.2.(a), an image from Kodak database is shown. Images restored using TV regularized denoising algorithm [19], LTV, and LATV are shown in

Figures 5.2.(b), 5.2.(c), and 5.2.(d), respectively. Details extracted from reconstructed images are also shown in the left column of the respective images. The eye of the parrot is over-smoothed by the ordinary TV algorithm as shown in Figure 5.2.(b). On the other hand, LTV and LATV methods preserve the details of the eye region. The performance of the LTV, and LATV methods are also slightly better or comparable in smooth edges as shown in right column of Figure 5.2.(b).

Table 5.1: The denoising results of the dataset images, which are corrupted by Gaussian noise with a standard deviation $\sigma = 0.1$.

	TV	LTV	LATV
lena	22.23574	22.19087	22.47191
peppers	21.57556	21.59862	21.86155
mandrill	18.04912	18.32569	18.4303
goldhill	20.67087	20.2761	20.58329
house	25.07268	24.77957	25.04167
phantom	19.43513	19.88716	20.22095
flintstones	19.72539	19.73119	19.96897
fingerprint	18.26503	18.13161	18.13784
barbara	18.87506	19.31177	19.48198
cameraman	21.95962	22.08064	22.41337
boat	21.04447	21.02014	21.31028
Kodak (Average)	19.79169	20.07921	20.32923
Average	20.05455	20.26384	20.50925

The experimental results indicate that the LATV scheme produces better SNR values compared to the TV regularized denoising scheme in our data set. The proposed LATV regularized denoising method acts like a nonlinear filter in each block of the input. Through the LATV approach, it is possible to adapt the optimization parameters for each block according to the content of the individual block. By this way, the LATV approach obtained better SNR results compared to the original TV denoising approach. Another advantage of the LATV is that it can restore very large images because it solves small sized TV optimization problems separately. It is also possible to implement the LATV algorithm using parallel computers because the optimization is performed locally.

Table 5.2: The denoising results of the dataset images, which are corrupted by Gaussian noise with a standard deviation $\sigma = 0.2$.

	TV	LTV	LATV
lena	19.24773	19.2451	19.00683
peppers	18.36458	18.48303	18.46
mandrill	15.36189	15.47109	15.63699
goldhill	18.19988	18.05389	18.06939
house	21.59912	21.66437	21.61823
phantom	14.26244	14.76556	14.89326
flintstones	15.73838	15.61027	15.97411
fingerprint	14.79675	14.4792	14.54405
barbara	16.45275	16.58397	16.5387
cameraman	18.4502	18.53198	18.7544
boat	18.06239	18.02803	18.18796
Kodak (Average)	16.91179	17.20234	17.34503
Average	17.04054	17.25065	17.37042

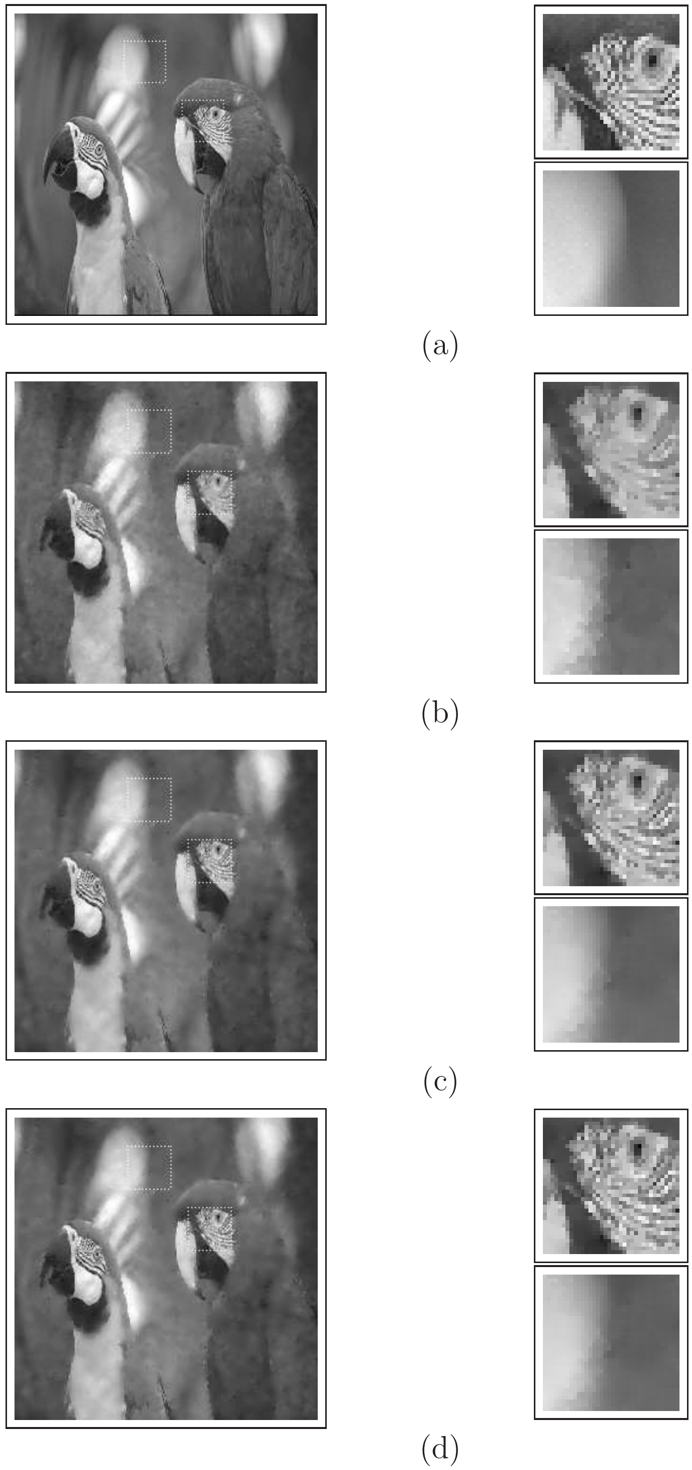

Figure 5.2: The denoising result for (a) 256-by-256 kodim23 image from Kodak dataset, using (b) TV regularized denoising, (c) LTV, and (d) LATV algorithms. Details that are extracted from the reconstruction results are also presented in the right column of the respective images. The original image is corrupted by Gaussian noise with a standard deviation $\sigma = 0.1$.

5.2 Filtered Variation based Signal Denoising

In this section, an algorithm that denoises the noisy signal $\mathbf{y}$ by putting bounds on the variation of the reconstructed signal is introduced. These bounds can be in spatial domain, as well as in a signal transform domain (e.g. DFT, DCT, DHT). The signal model is the same as in Section 5.1. The original signal $\mathbf{x}$ is corrupted by additive noise $\mathbf{u}$ as in (5.1).

In FV based denoising, the goal is to find a solution to the following optimization problem:

$$\min \ \mathrm{FV}_p(\mathbf{x}) \tag{5.5}$$

$$\text{s.t.} \ \ \|\mathbf{x} - \mathbf{y}\| \leq \delta \tag{5.6}$$

where FV stands for the filtered variation and it is defined as follows:

$$\mathrm{FV}_p(\mathbf{x}) = \|\mathbf{HDx}\|_p \, , \ p = 1, 2 \tag{5.7}$$

where $\mathbf{X}, \mathbf{D}$ and $\mathbf{H}$ represent the signal, the signal transform (e.g., DCT, DHT, DFT) and the discrete-time filter in the transform domain, respectively and p denotes which ℓ_p-norm is used. In (5.6) and (5.7) the norm can be selected as the ℓ_1 or ℓ_2 norms, which correspond to anisotropic and isotropic FV, respectively.

In the FV approach, denoising is achieved by minimizing the high-frequency energy of the observations, subject to the constraint given in (5.6). In (5.5)-(5.7) we posed the problem in frequency domain because for any given fixed transform, noise is typically in coherent with the transform, therefore it is spread out. By means of a proper filtering operation in the transform domain, one can exploit this fact to effectively denoise the signal. Besides, it is possible to solve the problem completely in time (or space) domain as well.

We solve this regularized signal denoising problem by applying several different time (space) and frequency domain constraints on filtered versions of the signal $\mathbf{x}$. This approach is similar to the methodology described in [85, 87, 126]. Since the FV cost function is convex it is also possible to solve FV based problems using convex programming. We provide a solution using the Projections onto Convex

Sets (POCS) method. The following FV based constraints correspond to a class of convex sets:

$$C_i^p = FV_p(\mathbf{x}) = \left\{ \|\mathbf{HDx}\|_p \leq \varepsilon \right\}, \; p = 1, 2 \text{ and } i = 1, \ldots, M. \tag{5.8}$$

where $p = 1, 2$ corresponds to the ℓ_1 and the ℓ_2-norms respectively. Other closed and convex sets, described in Section 5.2 can be also imposed on the desired signal $\mathbf{x}$. The solution of the denoising problem is assumed to lie in the intersection of M different constraint sets as follows:

$$\mathbf{x} \in C = \bigcap_{i=1}^{M} C_i, \tag{5.9}$$

where the constraint sets (C_i) are defined by the convex constraints as given at (5.8). Therefore, it is possible to reconstruct the original signal by performing successive orthogonal projections onto the closed and convex sets C_i [13, 17]. The POCS based iterative algorithm consists of making successive operations in time (or space) and transform domains, and it converges to a solution in the intersection of constraint sets C_i.

Extension to 2-D or higher dimensional signals is straightforward. Instead of a 1-D high-pass filter, 2-D or higher dimensional high-pass filters can be used in (5.9).

For image denoising applications, 6 different filtered variation constraints are designed in this thesis. These contraints are defined in Section 3.1. In each test, a subset of these constraints are applied on the noisy signal one-by-one, and the solution at the intersection the constraints in the set is obtained.

We first present a denoising example from [3]. Combettes and Pesquet used the image shown in Fig.5.3-(a) in [3], to test their TV based denoising algorithm. They added i.i.d. Laplacian noise to the original 128x128 grayscale image. The signal-to-noise ratio is 1dB. To compare the FV algorithm to the TV denoising, we cropped the original image (Fig. 5.3-(a)) from their paper and added Laplacian noise to the image. In [3] the pixel range was [-261,460]. In our case the pixel range turns out to be [-391,511].

As shown in Fig. 5.3, the characters in the image that are recovered by FV based denoising algorithm (Fig.5.3-(e)) are visually sharper compared to Fig.5.3-(c) and the impulsive noise is significantly reduced compared to ℓ_1 denoising.

In [3], the authors used Normalized Root Mean Square Error (NRMSE) as the error metric. They measure the error between the original signal $\mathbf{x}$ and reconstructed signal $\mathbf{x_o}$ as

$$||\mathbf{x} - \mathbf{x}_o||/||\mathbf{x}_o||. \tag{5.10}$$

The progress of the decrease in reconstruction error, is shown in Fig. 5.4. FV based denoising algorithm converges to an NRMSE level of -9 dB in 10-to-12 iterations. On the other hand, the time-domain TV algorithm takes around 100 iterations to converge as shown in Fig. 18 in [3].

ℓ_1 and ℓ_2 high-frequency energy bounds ε_1 and ε_3 can be estimated from the noisy image. In another set of experiments, the bounds are selected as 80% of ℓ_1 (ε_{1a}), 60% of ℓ_1 (ε_{1b}) and 80% of the ℓ_2 (ε_{3a}) energies of the noisy image, respectively. ε_{1o} corresponds to the ℓ_1 energy of the original image. Experimental results indicate that estimating ε_1 and ε_3 are possible from flat portions of the image and the FV algorithm is not sensitive to the ε_1 and ε_3 values. As shown in Fig. 5.4, in all cases NRMSE values for the restored images are very close to each other. Convergence graphs closely overlap with each other as shown in Fig.5.3

In another experiment the fingerprint shown in Fig.5.5-(a) is used. A noisy version of the image (Fig. 5.5-(b)) with SNR=4.9dB, is obtained by adding White Gaussian Noise to the original signal. Using FV constraints, lead to the reconstructed signal with SNR=12.75 dB (Fig. 5.5-(d)). On the other hand, TV constraint leads to an image with SNR=7.45dB (Fig. 5.5-(c)).

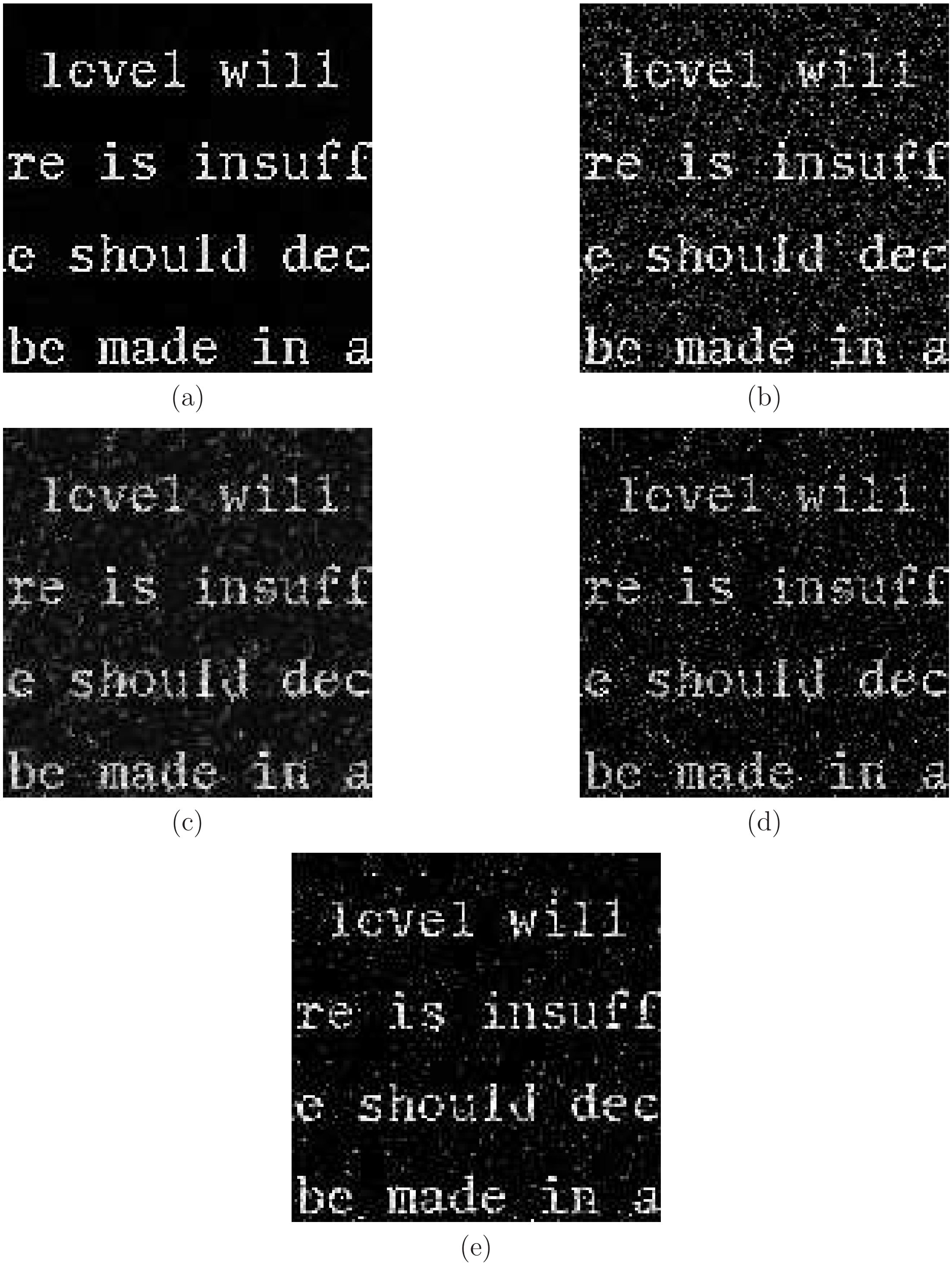

Figure 5.3: (a) Original image. (b) noisy image. (c) ℓ^p denoising with bounded total variation and additional constraints [3] (Fig. 15 from [3]) (p=1.1). (d) ℓ^p denoising without the total variation constraint [3] (Fig. 16 from [3]). (e) Denoised image using the FV method using C_2, C_4 and C_5.

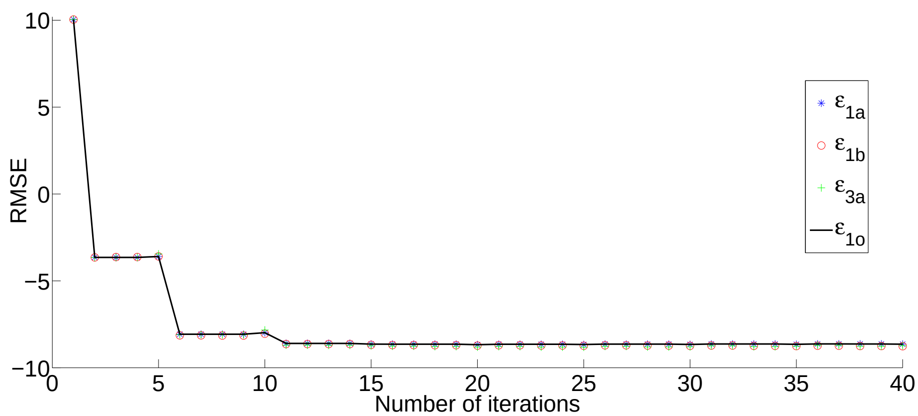

Figure 5.4: NRMSE vs. iteration curves for FV denoising the image shown in Fig. 5.3. ε_{1o} and ε_{3o} correspond to the ℓ_1 and ℓ_2 energy of the original image. Bounds are selected $\varepsilon_{1a} = 0.8\varepsilon_{1o}$, $\varepsilon_{1b} = 0.6\varepsilon_{1o}$, and $\varepsilon_{3a} = 0.8\varepsilon_{3o}$

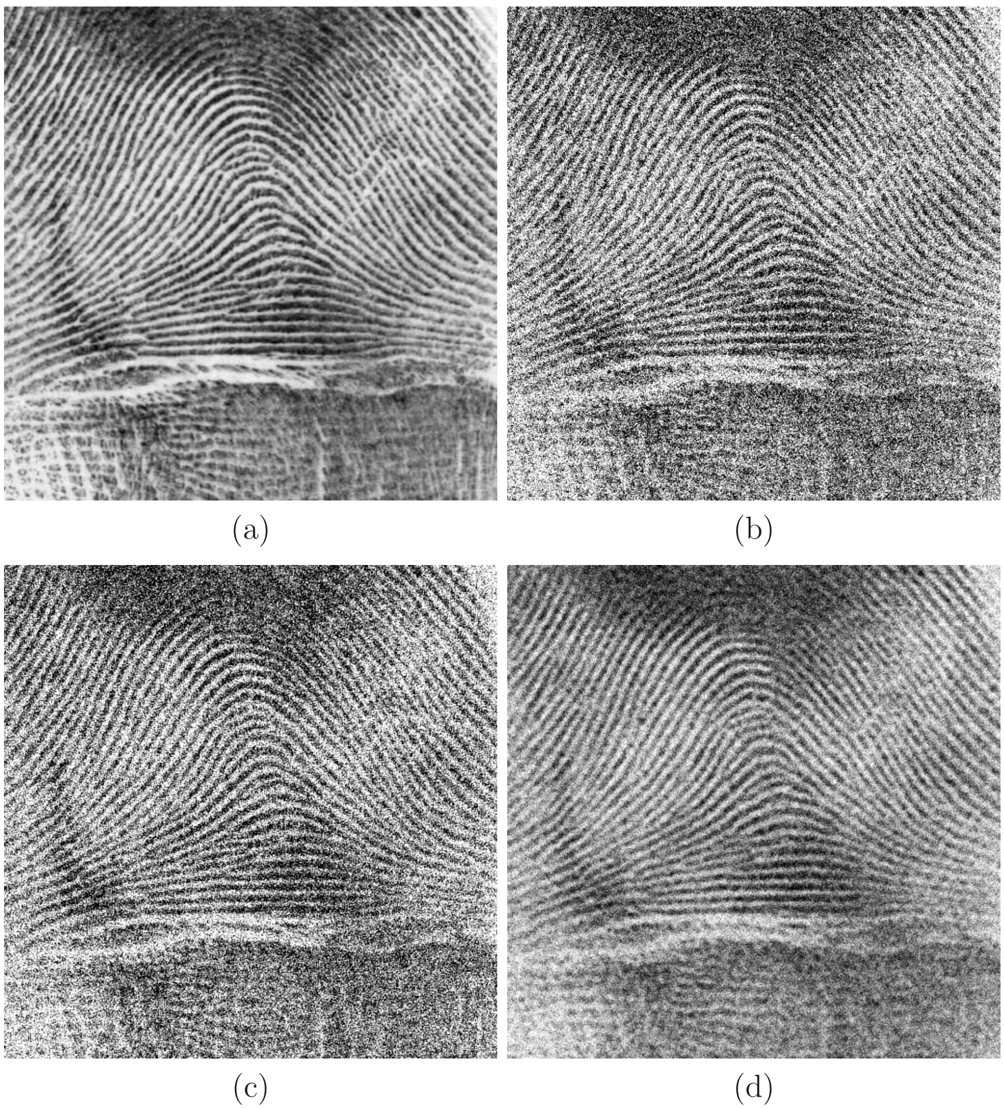

Figure 5.5: (a) Original fingerprint image, (b) fingerprint image with AWGN (SNR = 4.9 dB). (c) Image restored using the TV constraint (SNR=7.45dB). (d) Image restored using the proposed algorithm using C_2, C_4 and C_5 (SNR=12.75 dB)

In another set of experiments, the edge preserving characteristic of the proposed FV scheme is tested. The FV scheme, gives the user the possibility to use any type of high-pass filter that he/she desires to use. This feature of the proposed FV scheme is very useful, especially when the user has some prior knowledge about the signal. As a first step, the user may group the samples of the signal into two sets as low-pass and high pass samples using a set of high-pass filters. This aim can be achieved by determining samples, which gives high amplitude output to a high-pass filter. Even if the user does not have a prior knowledge about the signals high-pass content, it is possible to filter the signal by various high-pass filters, and choose a subset of the filters according to their responses. The samples in a signal can be grouped as

$$n \in \begin{cases} n_1, & \sum_{i=-l}^{l} h_k[i]x[n-i] > T_k \\ n_2, & else \end{cases}, n = 1, 2, ..., N. \tag{5.11}$$

where N, $2l+1$, are the length of the signal and the high-pass filter $\mathbf{h_k}$, respectively, and $k = 1, ..., N$ is the high-pass filter number. In this way, it is possible to generate a mask for each high-pass filter $\mathbf{h}_k$ that indicates edge or high-frequency content samples of the signal. The union of these masks of different high-pass filters gives an idea about the variation content of the whole signal. This procedure can also be considered as a FV constraint, and used together with the other FV constraints given in Chapter 3. For example, the samples that are classified as low-pass are updated through "Constraint II: Time and Space Domain Local Variational Bounds" defined in Section 3.1.2 with a low amplitude P parameter.

In the following experiment, this filter selection based Filtered variation idea is implemented and tested on 5 different images (Cameraman image and 4 different images from Kodak dataset). Constraints given in Sections 3.1.1,3.1.2,3.1.5, and 3.1.6 are used together with the above mentioned new FV constraint. Here the threshold value T_k given in (5.11) is taken as the variance of noise on the signal. Among $K = 15$ different high-pass filters, five filters, which gave the highest energy output, and their respective masks are used to group the signal samples.

The filter selective pixel grouping stage described above avoids smoothing out the edges of the test images. On the other hand, it smoothes the variation around the low-pass pixels by applying FV constraints on them. Some pixels in the processed image may wrongly be classified as high-pass pixels due to noise. The smoothing operation applied on the low-pass pixels also smoothes these isolated isolated high-pass pixels, which are located around the low pixels. As shown in Figure 5.6, as the iterations of the algorithm proceeds, these isolated pixels in the mask image are cleaned and the real edges in the original image remains untouched.

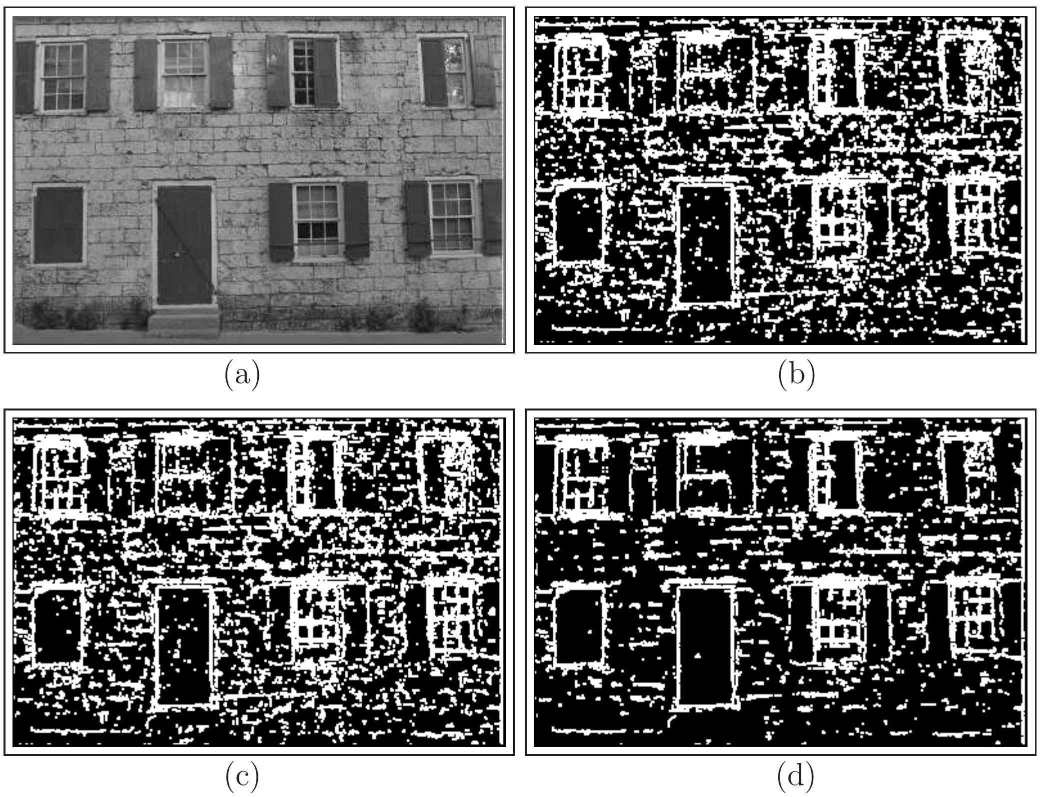

Figure 5.6: (a) The wall image from the Kodak dataset. The mask images regarding the Wall image after (b) 1, (c) 3, and (d)8 iterations of the algorithm. The masks are binary and white pixels represent the samples that are classified as high-pass.

Images reconstructed using TV based denoising [19] and the proposed methods results in similar SNR values. However, the proposed method preserves the edge content of the image while TV method smoothes out the edges in the image and leads to much blurred reconstructions. The blurring effect of the TV method can be seen in the detail at the right columns of Figures 5.7-5.11. For example, in Figure 5.7, the columns of the building at the background is blurred, but it is preserved by the proposed method. In Figures 5.8, 5.9, 5.10, and 5.11, same kind of an effect can be seen at the head of the parrots, the fences of the lighthouse, the texture on the wall and the window of the house respectively.

In this section, Filtered variation framework is applied to signal denoising problem. In the proposed algorithm, regularization is achieved by using discrete-time high-pass filters instead of taking the difference of neighboring signal samples as in the TV method. The FV based denoising problem is solved by making alternating projections in space and transform domains. It is experimentally observed that FV approach provides better denoising results compared to the TV approach. If some prior knowledge about the original signal exists, it is possible to design high-pass filters according to the signal and incorporate it to the FV framework.

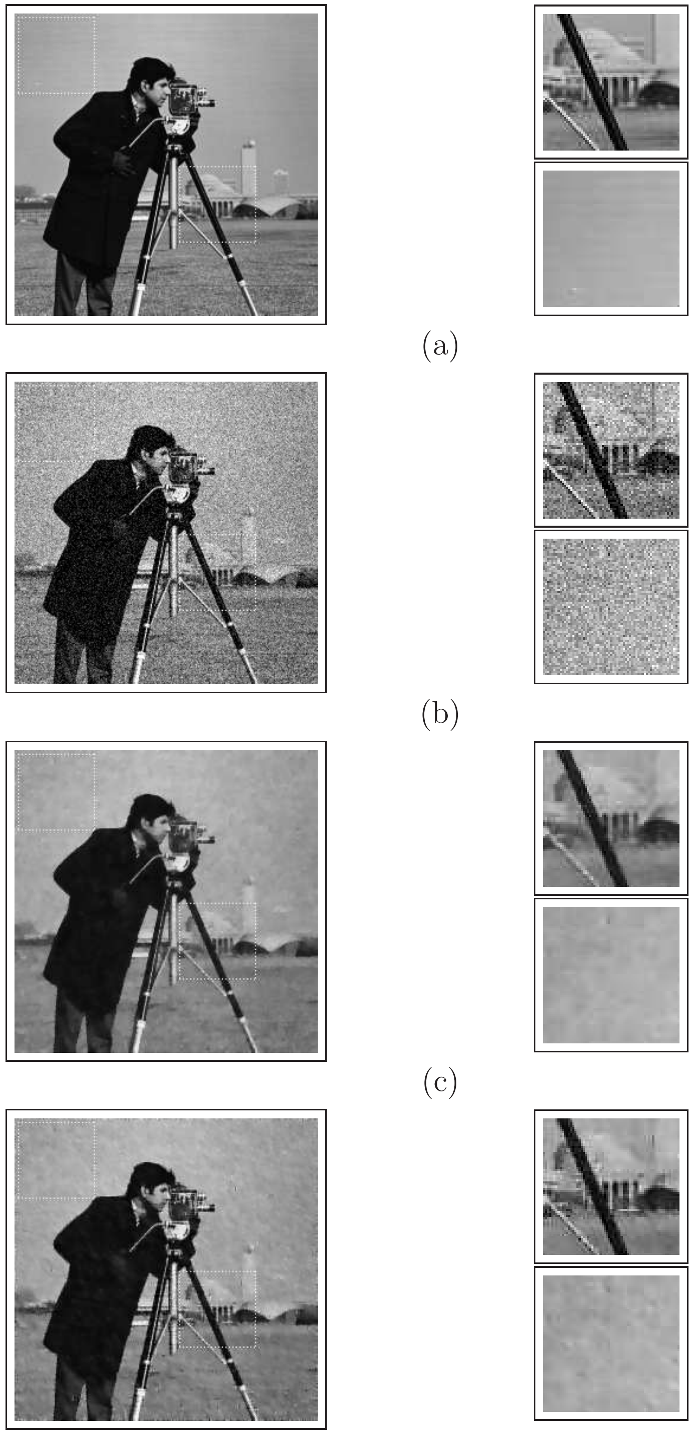

Figure 5.7: The (c) TV and (d) FV based denoising result for (b) the noisy version of the (a) 256-by-256 original cameraman image. Details that are extracted from the reconstruction results are also presented in the right column of the respective images. The original image is corrupted by Gaussian noise with a standard deviation $\sigma = 0.1$.

(a)

(b)

(c)

(d)

Figure 5.8: The (c) TV and (d) FV based denoising result for (b) the noisy version of the (a) 256-by-256 original kodim23 image from Kodak dataset. Details that are extracted from the reconstruction results are also presented in the right column of the respective images. The original image is corrupted by Gaussian noise with a standard deviation $\sigma = 0.1$.

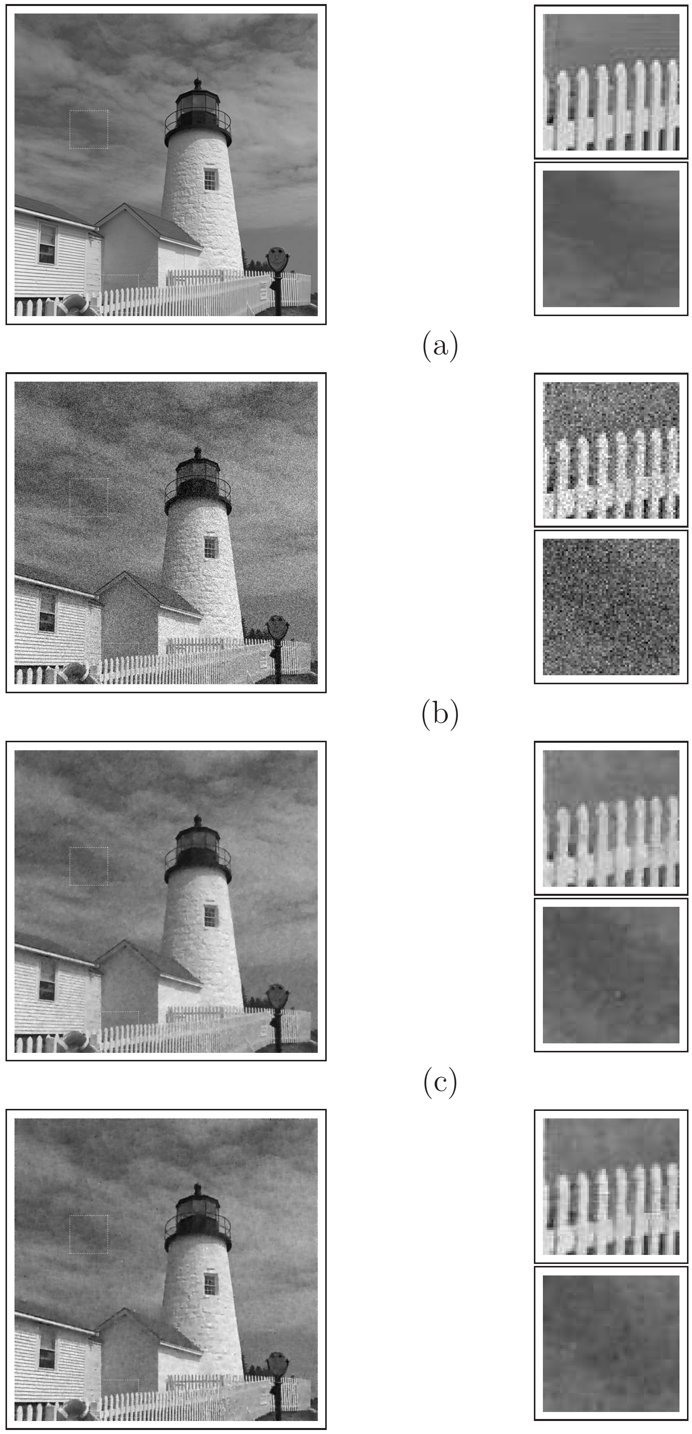

(a)

(b)

(c)

(d)

Figure 5.9: The (c) TV and (d) FV based denoising result for (b) the noisy version of the (a) 256-by-256 original kodim19 image from Kodak dataset. Details that are extracted from the reconstruction results are also presented in the right column of the respective images. The original image is corrupted by Gaussian noise with a standard deviation $\sigma = 0.1$.

(a)

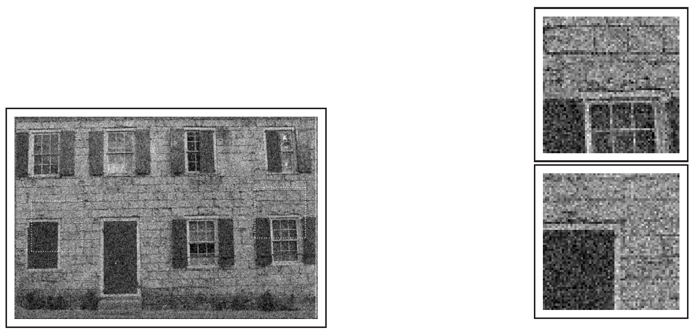

(b)

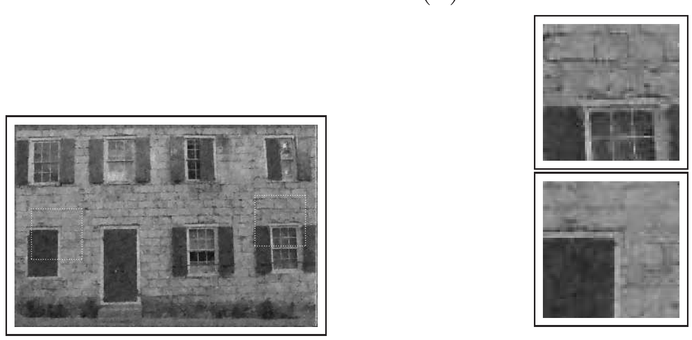

(c)

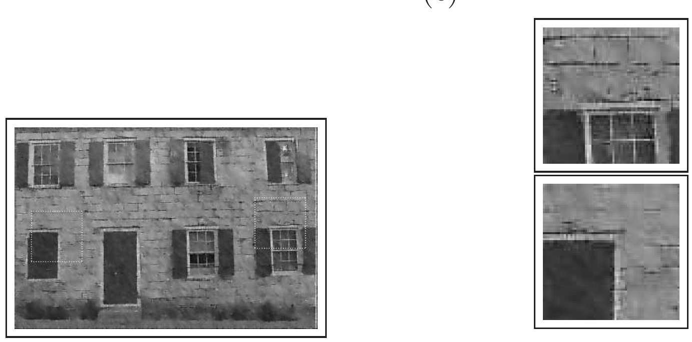

(d)

Figure 5.10: The (c) TV and (d) FV based denoising result for (b) the noisy version of the (a) 256-by-256 original kodim01 image from Kodak dataset. Details that are extracted from the reconstruction results are also presented in the right column of the respective images. The original image is corrupted by Gaussian noise with a standard deviation $\sigma = 0.1$.

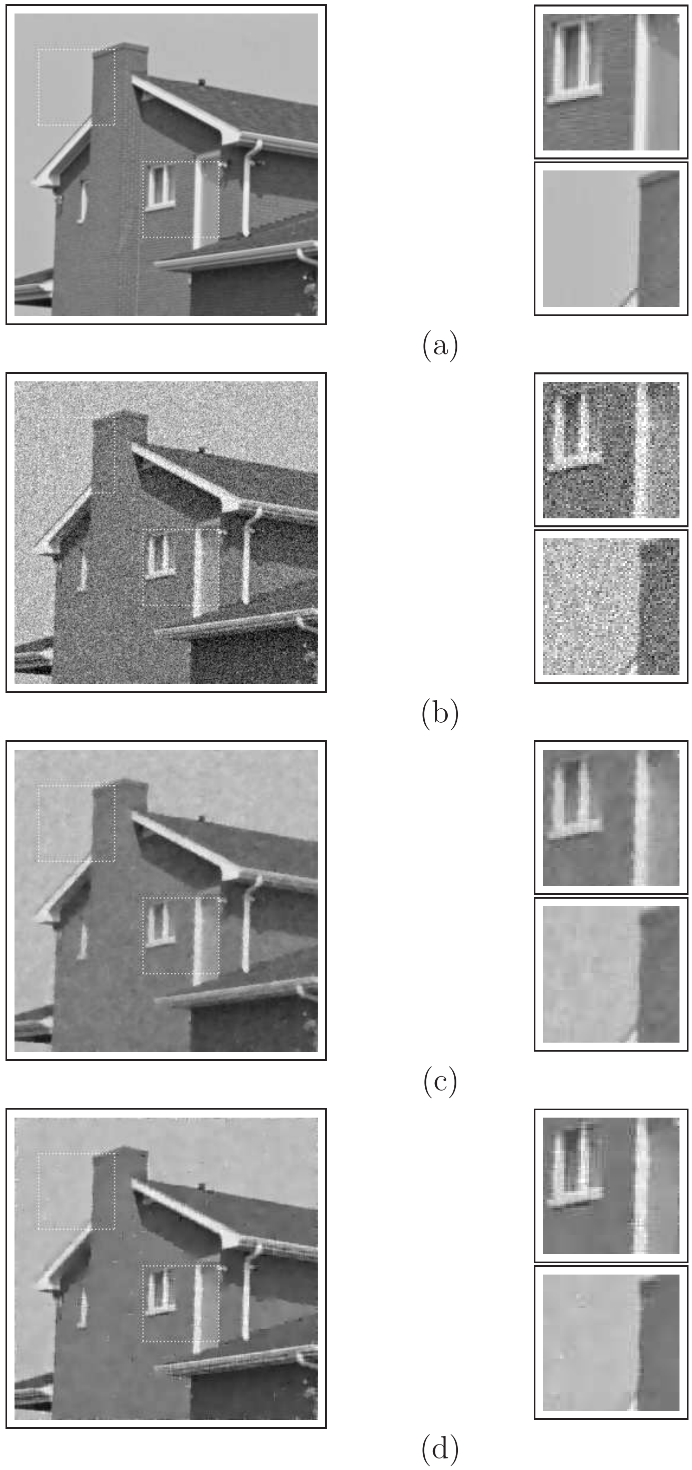

Figure 5.11: The (c) TV and (d) FV based denoising result for (b) the noisy version of the (a) 256-by-256 original House image. Details that are extracted from the reconstruction results are also presented in the right column of the respective images. The original image is corrupted by Gaussian noise with a standard deviation $\sigma = 0.1$.

Chapter 6

ADAPTATION AND LEARNING IN MULTI-NODE NETWORKS

In this chapter, we describe modified entropy, Total Variation (TV), and Filtered Variation (FV) functional based adaptation and learning algorithms for multi-node networks. New algorithms learn the environment and converge faster than ℓ_2-norm based algorithms under ε-contaminated Gaussian noise. The modified entropy functional based adaptive learning algorithms have two stages similar to the adapt and combine (ATC) and combine and adapt (CTA) frameworks introduced by Sayed et. al. [4]. In a multi-node network, each adaptation step in the original ATC and CTA frameworks consist of Least mean squares (LMS) or Normalized LMS (NLMS) algorithms, which are essentially an orthogonal projection operation onto the hyperplane defined by

$$d_{i,t} = \mathbf{h}_{i,t}\mathbf{u}'_{i,t}, \tag{6.1}$$

where d_t, $\mathbf{h}_t$, and $\mathbf{u}_t$ are the output of the $i^t h$ node, estimated node impulse response and the node input vector at time t, respectively. Bregman generalized the orthogonal projection concept by introducing the concept of D-projection in [13]. This allows the use of any convex function other than $g(x) = x^2$ as a distance or cost measure. In the adaptation stage of either of the algorithms, we replace the NLMS algorithm based update step with the Bregman's D-projection approach corresponding to a modified entropy functional based projections.

We also introduce TV and FV based schemes performing spatial and temporal updates to obtain the final filter updates of each node. The new set of algorithms are more robust against heavy tailed noise types such as ε-contaminated Gaussian noise.

This chapter is organized as follows. We will first give a short review of the adaptation and learning algorithms presented in [4], as well as the original ATC and CTA schemes. In Section 6.2, we will define a way to embed modified entropy functional based projection operator into the adaptation stage of the ATC and CTA schemes. In Section 6.3 we discuss the TV and FV based schemes that replaces the adaptation and combination steps in the reference algorithms. In the experimental results section of the paper, we demonstrate the performance of the proposed schemes using multi node network topologies under Gaussian and ε-contaminated Gaussian noise.

6.1 LMS-Based Adaptive Network Structure and Problem Formulation

Assume that we have a network with K nodes, which takes measurements according to a linear regression model (e.g., sensors on a wireless sensor network). The measurement $d_i[t]$ that are taken by node $i \in K$ at time t is given as

$$d_i[t] = \sum_{k=0}^{M-1} h_i[k]u_i[t-k] + n_i[t], \quad i = 1, 2, ..., K \tag{6.2}$$

where $u_i[t]$, $n_i[t]$ are the input and the noise signals for node i at time t, and $\mathbf{h}_i$ is the length-M impulse response of the nodes. The same system can be represented in vector form as

$$d_i[t] = \mathbf{h}_i\mathbf{u}'_{i,t} + n_i[t] \tag{6.3}$$

where $\mathbf{u}_t = [u[t], \ldots, u[t-M-1]]$.

Adaptive filtering algorithms are frequently used to estimate the node model and eliminate the noise at the output of the nodes [127, 128]. These algorithms start from an initial system using the current estimate and the real system output and update the system impulse response The simple adaptive filtering model is illustrated in Figure 6.1. The algorithm starts with an initial estimate of the node impulse response $\mathbf{h}_{i,0}$ and updates this estimate at every time instance t using the M regressive samples of the input signal $\mathbf{u}_{i,t}$, and the error ϵ_t between the real node output $d_i[t]$ and the estimated output $\tilde{d}_i[t]$ that can be calculated using (6.3).

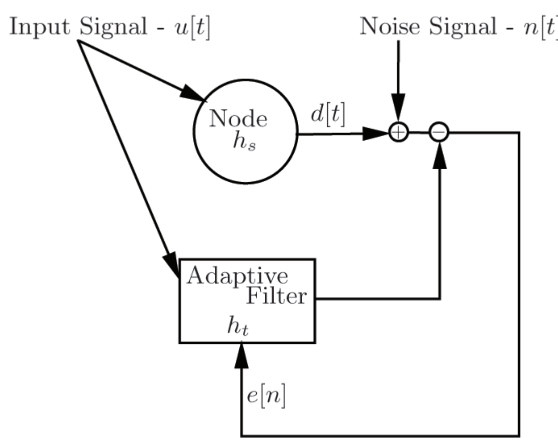

Figure 6.1: Adaptive filtering algorithm for the estimation of the impulse response of a single node.

Least Mean Squares (LMS) algorithm is one of the most well-known adaptive filtering algorithm in the literature. It initializes with an arbitrary length-M filter $\mathbf{h}_o$. Coefficients of this filter at time t are updated recursively as follows

$$\mathbf{h}_{t+1} = \mathbf{h}_t + \mu \boldsymbol{\epsilon}_t \mathbf{u}_t, \tag{6.4}$$

where $\mathbf{u}_t = [u[t], \ldots, u[t-M-1]]$, and ϵ_t is the error signal at time t respectively and μ is the learning constant of the adaptive filter. The error signal at time t is calculated as in [129, 130]

$$\epsilon_t = d[t] - \tilde{d}[t] = d[t] - \mathbf{h}_t\mathbf{u}'_t \tag{6.5}$$

In the LMS algorithm the main objective is to minimize the square norm of the error. It is well-known that the Normalized version of the LMS algorithm (NLMS) can be obtained by solving

$$\min_{\mathbf{h}_t} \ |\epsilon_t| \quad s.t. \quad d[t] = \mathbf{h}\mathbf{u}'_t, \ t = 0, 1, ... \tag{6.6}$$

which is the orthogonal projection onto the hyperplane $d[t] = \mathbf{h}\mathbf{u}_t$. If the learning parameter in LMS algorithm is selected as $\mu = \frac{1}{||\mathbf{u}_t||^2}$, then the solution is the same as (6.4). Using this recursive method, the coefficients of the adaptive filter at time $t+1$ can be estimated from the former set of coefficients at time t.

However, it is shown in [4] that, if the nodes in a network are able to interact with each other, then using diffusion adaptation based algorithms integrated with LMS type adaptive filtering increases the system performance compared to handling all the nodes individually. In [4], the authors presented ATC (Fig. 6.2(a)) and CTA (Fig. 6.2(b)) schemes in which the nodes are able to effect the estimation results of each other. A performance comparison of these adaptation schemes are presented in [4].

The update and combination equations for ATC scheme in a two node network are as follows

$$\textit{Node 1}: \begin{cases} \boldsymbol{\phi}_{1,t} = & \mathbf{h}_{1,t-1} + \mu\epsilon_{1,t}\mathbf{u}_{1,t} \\ \mathbf{h}_{1,t} = & \alpha\boldsymbol{\phi}_{1,t} + (1-\alpha)\boldsymbol{\phi}_{2,t} \end{cases} \tag{6.7}$$

$$\textit{Node 2}: \begin{cases} \boldsymbol{\phi}_{2,t} = & \mathbf{h}_{2,t-1} + \mu\epsilon_{2,t}\mathbf{u}_{2,t} \\ h_{2,t} = & \alpha\boldsymbol{\phi}_{2,t} + (1-\alpha)\boldsymbol{\phi}_{1,t} \end{cases} \tag{6.8}$$

In the CTA scheme, the update and combination steps become

$$\textit{Node 1}: \begin{cases} \boldsymbol{\phi}_{1,t-1} = & \alpha\mathbf{h}_{1,t-1} + (1-\alpha)\mathbf{h}_{2,t-1} \\ \mathbf{h}_{1,t} = & \boldsymbol{\phi}_{1,t-1} + \mu\epsilon_{1,t}\mathbf{u}_{1,t} \end{cases} \tag{6.9}$$

$$\textit{Node 2}: \begin{cases} \boldsymbol{\phi}_{2,t-1} = & \beta\mathbf{h}_{2,t-1} + (1-\beta)\mathbf{h}_{1,t-1} \\ \mathbf{h}_{2,t} = & \boldsymbol{\phi}_{2,t-1} + \mu\epsilon_{2,t}\mathbf{u}_{2,t} \end{cases} \tag{6.10}$$

It is important to note that, both ATC and CTA schemes, that are given in Eq. (6.7)-(6.10), use LMS algorithm at their adaptation stages.

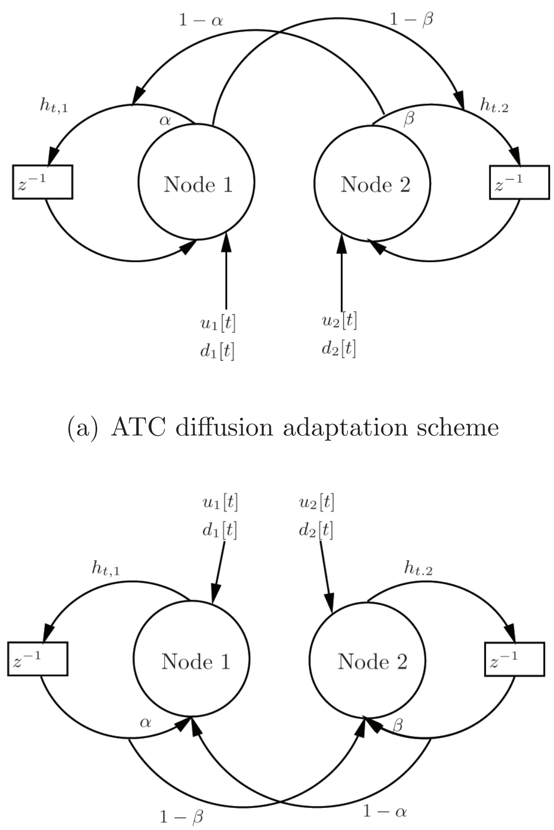

(a) ATC diffusion adaptation scheme

(b) CTA diffusion adaptation scheme

Figure 6.2: ATC and CTA diffusion adaptation schemes on a two node network topology [4].

6.2 Modified Entropy Functional based Adaptive Learning

In many cases, ℓ_1 optimization is more robust against heavy tailed noise compared to ℓ_2 norm based algorithms [131]. However, convex optimization tools can not be used to minimize the ℓ_1 norm based cost functions. As mentioned in Chapter 2, it is possible to replace the ℓ_2 norm based cost function with modified entropy cost functional and use Bregman's D-Projection operator to define entropic projection operator.

In our first algorithm, we replace the orthogonal projection operations in ATC and CTA schemes with the entropic functional based D-projection operation. In this way, we develop an adaptive learning algorithm, which is robust against the heavy tailed ε-contaminated Gaussian noise.

We use the same notation as in [4]. Instead of solving (6.4) or (6.6) as in [4], we reformulate the problem using D-projection operation, and solve

$$\min_{\boldsymbol{\phi}_{i,t}} \; D(\boldsymbol{\phi}_{i,t}, \mathbf{h}_{i,t-1}) \quad s.t. \quad d_i[t] = \boldsymbol{\phi}_{i,t}\mathbf{u}'_{i,t} \tag{6.11}$$

for each node at every time instant t to determine the next set of filter coefficients for the nodes. Using the Lagrange multipliers one can obtain

$$sgn(\boldsymbol{\phi}_{i,t}).ln(|\boldsymbol{\phi}_{i,t}|+\frac{1}{e})=sgn(\mathbf{h}_{i,t-1}).ln(|\mathbf{h}_{i,t-1}|+\frac{1}{e})+\lambda\mathbf{u}_{i,t} \tag{6.12}$$

and

$$d_i[t] = \boldsymbol{\phi}_{i,t}\mathbf{u}'_{i,t}, \tag{6.13}$$

which can be solved together numerically to obtain the new set of coefficients. Instead of (6.11), if we used the Euclidean norm, we would get the first step of the ATC algorithm.

Since the entropic cost function is convex, the filter coefficients obtained through the iterative algorithm converge to the actual filter coefficients as in the LMS algorithm [17, 90], provided that hyperplanes $d_i[t] = \boldsymbol{\phi}_{i,t}\mathbf{u}_{i,t}$ have a nonempty intersection. In general, this iterative process tracks the hyperplanes when we have a drifting scenario [90, 118, 132, 133]. This new filter update strategy is used in ATC or CTA frameworks. For example in a two node network that uses ATC framework, the next set of filter coefficients are obtained through the combination stage as

$$\mathbf{h}_{i,t} = (1-\alpha)\boldsymbol{\phi}_{j,t} + \alpha\boldsymbol{\phi}_{i,t} \tag{6.14}$$

where $\boldsymbol{\phi}_{j,t}$ is the intermediate filter coefficients of the neighboring node.

Consider the following experiments in which the parameters are as summarized in Table 6.1. We used two types of noise models in the experiments. One of them is zero mean, white Gaussian noise with a standard deviation of $\sigma_{d,i}$ that is

Table 6.1: Simulation parameters.

Filter Length M	μ	Node 1 $\sigma^2_{d,1}$	Node 2 $\sigma^2_{d,2}$	σ^2_u	α,β	Number of Iterations	Number of Trials
10	0.005	0.5	-	1	-	2000	1000
10	0.005	0.5	0.3	1	0.7	2000	1000

also used in [4]. In the second case we used ε-contaminated Gaussian noise, which is composed of two independent white Gaussian noise signals with standard deviation $\sigma_{d,i}$ and γ. The probability density function of the ε-contaminated noise is

$$\bar{N}_{\sigma_{d,i}} = (1-\varepsilon)N_{\sigma_{d,i}} + \varepsilon N_{\gamma} \tag{6.15}$$

where $\varepsilon << 1$ is a constant. We chose $\varepsilon = 0.01$ and $\gamma = 100$ in Table 6.1.

In the first set of experiments, we tested the proposed adaptation approach on a single node. We also compared our results with the results of the original ATC and CTA approaches [4]. We obtained the results presented in Figure 6.3. In our tests and comparisons, we used the EMSE error metric, which was defined in [4] as

$$EMSE_d \triangleq \lim_{t\to\infty} E|\mathbf{u}_i[t](\mathbf{h}_o - \mathbf{h}_{d,t-1})|^2 , \tag{6.16}$$

where $\mathbf{h}_o$ is the actual filter coefficients of the node of interest d. As shown in Figure 6.3(a), the proposed algorithm converges faster. However it can not achieve better EMSE value than the LMS based ATC original approach. However, as presented in Figure 6.3(b), the proposed adaptation method achieved better EMSE values under ε-contaminated noise.

In the second set of experiments, we test the entropy projection based adaptation method on a two node network, using the ATC scheme. We obtained similar results as in the single node case. As presented in Figure 6.4(a), the proposed algorithm could not achieve the EMSE level of the LMS based ATC algorithm under white Gaussian noise. However, the entropic projection based adaptation method achieved better EMSE values than the LMS based ATC method under ε-contaminated noise as shown in Figure 6.3(b).

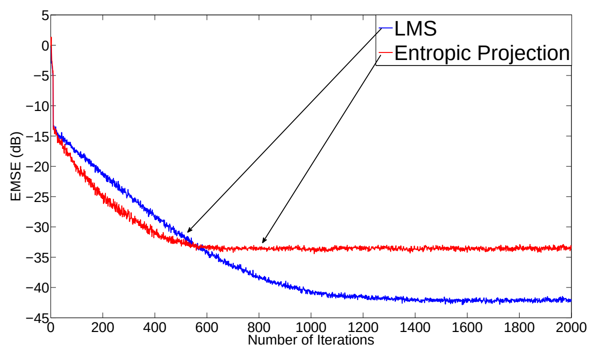

(a)

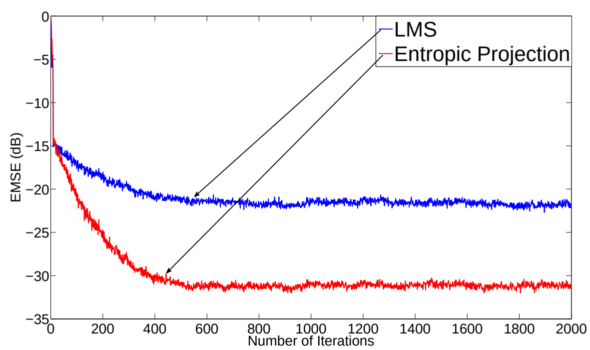

(b)

Figure 6.3: EMSE comparison between LMS and Entropic projection based adaptation in single node topologies under (a) ε-contaminated Gaussian, (b) white Gaussian noise. The noise parameters are given in Table 6.1, and 6.3

More detailed simulation results using various node topologies are presented in Section 6.3

6.3 The TV and FV based robust adaptation and learning

In this section, we introduce the Total Variation (TV) and Filtered Variation (FV) based diffusion adaptation methods in multi-node networks. The TV and FV based schemes automatically generate their own adaptation and combination stages (e.g. in FIRESENSE framework [134–136] the locations of the sensors are

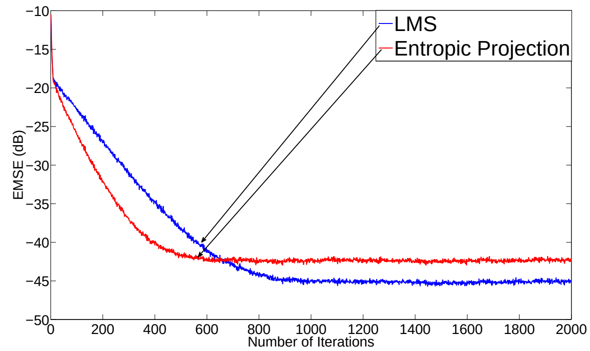

(a)

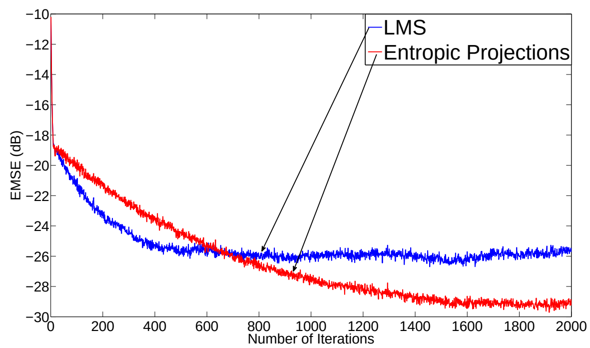

(b)

Figure 6.4: EMSE comparison between LMS and Entropic projection based ATC schemes in two node topologies under (a) ε-contaminated Gaussian, (b) white Gaussian noise.The noise parameters are given in Table 6.1, and 6.3

known beforehand). They also enable the user to add more functionalities to these stages.

For a K-node network, the diffusion adaptation problem can be solved by solving the following optimization problem

$$\begin{aligned} \min \qquad & \sum_i ||\mathbf{h}_{i,t} - \mathbf{h}_{i,t-1}|| + \lambda ||\mathbf{H}_t||_{TV} \\ \text{subject to} \quad & d_i[t] = \mathbf{h}_{i,t}\mathbf{u}_{i,t}, \quad i = 1, 1, \ldots, K, \end{aligned} \tag{6.17}$$

where $\mathbf{H}_t = [\mathbf{h}_{1,t}|\mathbf{h}_{2,t}|\ldots|\mathbf{h}_{K,t}]$, λ is the regularization parameter, and $||\mathbf{H}||_{TV}$ is the TV norm defined as follows

$$||\mathbf{H}||_{TV} = \sum_i |\mathbf{h}_i - \mathbf{h}_{i-1}|. \tag{6.18}$$

A related problem is

$$\begin{aligned} \min \quad & \sum_i ||\mathbf{h}_{i,t} - \mathbf{h}_{i,t-1}|| \\ \text{subject to} \quad & ||\mathbf{H}_t||_{TV} < \varepsilon_s \\ \text{and} \quad & d_i[t] = \mathbf{h}_{i,t}\mathbf{u}_{i,t} \quad , i = 1, 1, \ldots, K. \end{aligned} \tag{6.19}$$

The term $||\mathbf{h}_{i,t} - \mathbf{h}_{i,t-1}||$ in cost functions of (6.17), and (6.19) is a temporal constraint, which limits the new set of filter coefficients $\mathbf{h}_{i,t}$ with respect to the filter coefficients $\mathbf{h}_{i,t-1}$ at time instant $t-1$. The TV term $||\mathbf{H}_t||_{TV}$ in (6.17), and (6.19) is the spatial constraint, which represents the cooperation between the nodes. By minimizing this term, we allow neighboring nodes to behave in a similar manner. The regularization parameter λ determines the composition of the overall cost function in (6.17). For each λ one can find a corresponding ε_s because (6.17) is the Lagrangian version of (6.19).

Solving the optimization problems in (6.17), and (6.19) are not straightforward and various computational schemes are developed for this purpose [69,97]. On the other hand, the cost functions in (6.17), and (6.19) are convex and the constraints in the problems are closed and convex sets. Therefore, the problem can be divided into subproblems and each subproblem can be solved in an iterative manner using the Projection onto Convex sets (POCS) framework [3, 13, 17]. This approach leads to computationally efficient diffusion adaptation schemes for multi-node networks.

For each node of the network, the temporal constraint is:

$$||\mathbf{h}_{i,t} - \mathbf{h}_{i,t-1}|| \leq \varepsilon_t, \quad i = 1, 2, \ldots, K, \tag{6.20}$$

which limits the difference between the new update $\mathbf{h}_{i,t}$ and the previous set of coefficients $\mathbf{h}_{i,t-1}$. This means that $\mathbf{h}_{i,t}$ cannot be too far away from $\mathbf{h}_{i,t-1}$. Ordinary LMS type update schemes may produce large jumps due to impulsive noise. The temporal constraint (6.20) limits such behavior. The inequality (6.20) is a closed ball in $\mathbb{R}^N$ when the Euclidean norm is used. To obtain $\mathbf{h}_{i,t}$ we first project $\mathbf{h}_{i,t}$ onto the hyperplane $d_i[t] = \mathbf{h}_{i,t}\mathbf{u}_{i,t}$ and obtain a vector $\mathbf{v}_{i,t}$. This step is the LMS or the NLMS update in the adaptation stages of the ATC and

CTA methods. If the vector $\mathbf{v}_{i,t}$ satisfies the condition (6.20), then $\mathbf{h}_{i,t} = \mathbf{v}_{i,t}$. Otherwise, $\mathbf{v}_{i,t}$ is projected onto the ball defined by (6.20), and we obtain

$$\tilde{\mathbf{h}}_{i,t} = \alpha \mathbf{v}_{i,t} + (1-\alpha)\mathbf{h}_{i,t-1}, \tag{6.21}$$

where

$$\alpha = \frac{\varepsilon_s}{||\mathbf{v}_{i,t}||}. \tag{6.22}$$

It turns out that the orthogonal projection of $\mathbf{v}_{i,t}$ onto the convex set (ball) is the convex combination of $\mathbf{v}_{i,t}$ and $\mathbf{h}_{i,t}$ with α as given in (6.22).

When the norm is the ℓ_1 norm in (6.20), the solution will obtained using the orthogonal project onto the ℓ_1 ball centered at $\mathbf{h}_{i,t-1}$ with the largest dimension ε_t. This type of a projection turns out a sparse vector of filter coefficients [6, 11], and it can be determined as described in [137].

The next step is determined by the TV based spatial constraint for each node, which is defined as

$$||\mathbf{h}_{i,t} - \mathbf{h}_{i-1,t}|| < \varepsilon_s, \quad i = 1 \dots K, \tag{6.23}$$

where $\mathbf{h}_{i,t}$ and $\mathbf{h}_{i-1,t}$ are the filter coefficients of two-neighboring nodes. Instead of constraining the TV function for the entire network, it is easier to impose a bound for each node one by one. This constraint can also be solved in a similar way as the temporal constraint.

Using the constraints (6.20), and (6.23), we define a new adaptation diffusion algorithm in Algorithm 1. The first step of the algorithm can either be the LMS or the modified entropic projection based update. Both classes of algorithms are robust against heavy-tailed noise. The computational cost of the modified entropy functional based scheme is higher compared to the LMS type algorithms because a nonlinear equations has to be solved at each stage.

In TV approach only the difference between the two neighboring nodes is computed. The FV approach is a generalized version of the TV approach in which the differencing operator is replaced by a high pass filter [138]. In this case, the spatial constraint can be defined as

$$||\mathbf{h}_{i,t} - \sum_j \beta_j \mathbf{h}_{j,t}|| < \varepsilon_s, \quad i = 1 \dots K, i \neq j \tag{6.24}$$

Algorithm 1 Adaptation diffusion algorithm with temporal and spatial constraints

STEP 0: initialize t = 1, i=1

*STEP 1:*Adaptation step

$\epsilon_{i,t} = d[t] - \mathbf{h}_{i,t-1}\mathbf{u}_{i,t}$

$\mathbf{v}_{i,t} = \mathbf{h}_{i,t-1} + \mu\epsilon_{i,t}\mathbf{u}_{i,t},$

*STEP 2:***Temporal Constraint**: Projection onto (6.20)

If $||\mathbf{v}_{i,t} - \mathbf{h}_{i,t-1}|| \leq \varepsilon_t$

$\tilde{\mathbf{h}}_{i,t} = \mathbf{v}_{i,t}$

else

$\tilde{\mathbf{h}}_{i,t} = \alpha\mathbf{v}_{i,t} + (1-\alpha)\mathbf{h}_{i,t-1},\ \ \alpha = \frac{\varepsilon_t}{||\mathbf{v}_{i,t}||}$

STEP 3: **Spatial Constraint**: Projection onto (6.23)

If $||\tilde{\mathbf{h}}_{i,t} - \mathbf{h}_{i-1,t}|| \leq \varepsilon_s$

$\mathbf{h}_{i,t} = \tilde{\mathbf{h}}_{i,t}$

else

$\mathbf{h}_{i,t} = \alpha\tilde{\mathbf{h}}_{i,t} + (1-\alpha)\mathbf{h}_{i-1,t},\ \ \alpha = \frac{\varepsilon_s}{||\tilde{\mathbf{h}}_{i,t}||}$

STEP 4: $i = (i+1)$

If $i > N$

$i = 1, t = t+1$

end

Go to STEP 1

Table 6.2: Parameters of the additive white Gaussian noise on different topologies.

M:Filter Length	$\sigma^2_{d,1}$	$\sigma^2_{d,2}$	$\sigma^2_{d,3}$	$\sigma^2_{d,4}$	$\sigma^2_{d,5}$	σ^2_u	Topology
10	0.5	0.3	-	-	-	1	Fig.6.5-(c)
10	0.5	0.3	0.3	0.2	0.2	1	Fig.6.6-(c)
10	0.5	0.3	0.3	0.2	0.2	1	Fig.6.7-(c)
10	0.5	0.3	0.3	0.2	0.2	1	Fig.6.8-(c)

where $\mathbf{h}_{j,t}$ is the filter coefficients of the neighbors of the i^{th} node, and β_j are the coefficients of the high-pass filter. The neighborhood is defined by the high-pass filter. Both ℓ_1 and ℓ_2 norms can be used as in TV based spatial constraint and temporal constraint cases. Projection onto this set is not the same as the TV case, however they are similar in nature.

We tested the LMS based ATC, entropic projection based ATC, and the TV and FV based versions of Algorithm 1 using four different node topologies. The amount of interaction between the nodes of the multi-node test networks is a correlation matrix $\boldsymbol{A}$. The entries $\alpha_{i,j}$ of $\boldsymbol{A}$ corresponds to the effect of the j^{th} node at the combination stage of the i^{th} node. For example, when we want to calculate the filter coefficients $\mathbf{h}_{1,t}$ of node-1 from intermediate filter coefficients $\boldsymbol{\phi}_{j,t}$ at time t in an ATC based diffusion adaptation problems, the corresponding combination equation at time t is

$$\mathbf{h}_{1,t} = \sum_j \alpha_{1,j} \boldsymbol{\phi}_{j,t}. \tag{6.25}$$

It should also be mentioned that the rows of the correlation matrix $\boldsymbol{A}$ must add up to one.

The topologies and their corresponding node correlation matrices are shown in Figures 6.5(b)-(a), 6.6(b)-(a), 6.8(b)-(a), 6.8(b)-(a), respectively. We tested each node topology under seven different noise models. These noise models consist of ε-contaminated Gaussian noise with 6 different parameter sets (rows 1-6 in Table 6.3) and white Gaussian noise. The parameters of the white Gaussian output noise $\sigma^2_{d,i}$ for each node in the network is given in Table 6.2.

Table 6.3: ε-contaminated Gaussian noise parameters in the simulations

Noise No	ε	γ
1	0.01	100
2	0.01	50
3	0.1	100
4	0.05	50
5	0.01	10
6	0.05	100
7 (WGN)	0	N.A.

We selected $\beta_j = -1/2$ in (6.24), which corresponds to the high pass filter with coefficient $[-1/2, 1, -1/2]$. We only consider the FV scheme in spatial adaptation stage. In the FV scheme that we implemented, a node can only cooperate with the closest two nodes in its one-hop-neighborhood. One important implementation detail about the FV scheme that we used in our tests is about that we have to maintain a scanning order of the nodes during the implementation. When we process the node i, the impulse response of node $i-1$ has already been calculated. On the other hand, this is not the case for node $i+1$. Therefore, we use the filter coefficients of $i+1^{st}$ node from time instant $t-1$ instead of using its intermediate filter coefficients. As a result, the new spatial constrain becomes

$$||\mathbf{h}_{i,t} - \left(\frac{1}{2}\mathbf{h}_{i-1,t} + \frac{1}{2}\mathbf{h}_{i+1,t-1}\right)|| < \varepsilon_s, \quad i = 1 \ldots K \tag{6.26}$$

in our experiments. The last implementation detail that we need to mention is that, we selected $\varepsilon_s = \varepsilon_t = 0.5$ throughout the experiments.

The bounds ε_s, and ε_t are correlated with the noise level. They should be selected such that they should block the effects due to impulsive component of the ε-contaminated Gaussian noise. Since, in our tests, we select the original node-filter coefficients ($\mathbf{h}_i$) from an uniform distribution between 0 and 1, we arbitrarily set ε_s, and ε_t in that range. In our simulation we used $\varepsilon_s = \varepsilon_t = 0.5$ bound, which correspond to 10% variation in each filter coefficient. We did not make any assumptions about the noise level. If the noise levels are known, more educated guesses can be made for ε_s, and ε_t.

Figures 6.5-(c), 6.6-(c), 6.8-(c), 6.8-(c) are obtained by testing the respective topologies under ε-contaminated Gaussian noise with parameters given in the first row of Table 6.3. We use (6.15) to generate the ε-contaminated Gaussian noise. In all cases, the entropic projection based method achieves lower EMSE values compared to the LMS based ATC algorithm under ε-contaminated noise. In general, the FV based diffusion adaptation algorithm achieved the best EMSE results in such cases. The node correlation in the network topology given in Fig. 6.7 is very similar to the FV based diffusion adaptation. Even in that case, the other algorithms could not achieve the EMSE level of the FV algorithm. The node correlation in the network topology in Fig. 6.8 is similar to TV based diffusion adaptation model. In that case, TV achieved better results than both LMS and entropic projection based algorithms.

In the second set of experiments, we tested the performance of the algorithm under white Gaussian noise. As shown in the previous section, the entropic projection based algorithm achieves slightly worse results compared to the LMS based ATC algorithm. As shown in Figs. 6.5-(d), 6.6-(d), 6.8-(d), 6.8-(d), entropic projection based algorithm catches the EMSE level of the LMS based algorithm, however, the convergence speed of the entropic projection based algorithm is slow. Under white Gaussian noise, the best performance is achieved by the LMS based ATC algorithm.

We conducted another series of experiments using different ε-contaminated Gaussian noise parameters, given in Table 6.3. We could not present graphical results for these test due to lack of space. In Table 6.4, we present the EMSE levels that each algorithm achieved after 2000 iterations. In most of the cases FV based algorithm achieved the best results under ε-contaminated Gaussian noise. However, under noise model 5 in Table 6.3, LMS based ATC achieved better results than FV. In this case the γ value, which is the variance of the impulsive component, is small and the ε values is high. Therefore this noise model is much like a mixture of two ordinary white Gaussian noises. Due to this reason, the LMS based ATC performed better in this case.

As a final test, we embed entropic projection based adaptation into the FV based version of Algorithm 1. In this case, the LMS based update stage is replaced by the entropic projection operation. In the experiment, we used the topology in Fig. 6.7 under ε-contaminated noise, whose parameters are as given in the first row of Table 6.3. As shown in Fig. 6.9 entropic projection based version of the algorithm leads to slightly better EMSE results, and faster convergence rates, at the expense of increased computational complexity.

In this section, we present two new diffusion adaptation algorithms for cooperative multi-node networks. We first integrate the modified entropy functional based, entropic projection operator into the adaptation stage of the ATC and CTA schemes. As the modified entropy functional approximates the ℓ_1 norm, entropic projection operator based algorithm turns out to be more robust against the effects of heavy-tailed impulsive noise. We tested the proposed adaptation scheme using various multi-node cooperative networks under ε-contaminated gaussian noise, and it turns out better EMSE results compared to the LMS based ATC and CTA schemes.

In the second part of the section, we introduced TV, and FV based combination stages, which can be used both with LMS, and Entropic projection based adaptation stages. We redefine the whole diffusion adaptation problem as a minimization problem and use TV and FV based regularization terms to define a new combination stage. Since, both the proposed adaptation and the combination stages are composed of closed and convex constraint sets, it became possible to solve the diffusion adaptation problem by performing successive projections on these constraint sets. The experimental results indicate that the proposed FV based scheme gives the best perfomance among a group of algorithms including LMS and Entropic projection based ATC schemes as well as the TV based approach.

Nodes	1	2
1	0.7	0.3
2	0.3	0.7

(a)

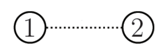

(b)

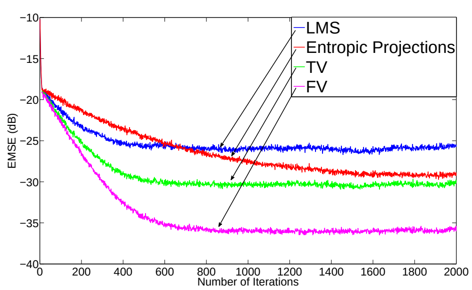

(c)

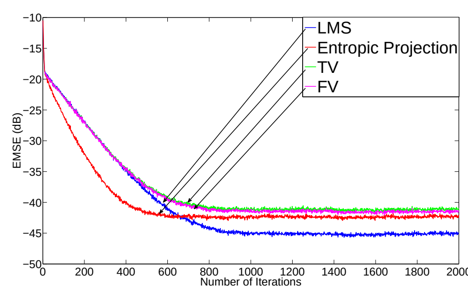

(d)

Figure 6.5: (a) Correlation between the nodes ($\boldsymbol{A}$) in the network topology shown in (b). EMSE comparison between two node topologies under (c) ε-contaminated Gaussian (first row in Table 6.3), and (d) white Gaussian noise (seventh row in Table 6.3). The proposed robust methods produce better EMSE results under ε-contaminated Gaussian noise.

Nodes	1	2	3	4	5
1	0.5	0.25	0.25	0	0
2	0.25	0.5	0.25	0	0
3	0.15	0.15	0.5	0.1	0.1
4	0	0	0.125	0.5	0.375
5	0	0	0.125	0.375	0.5

(a)

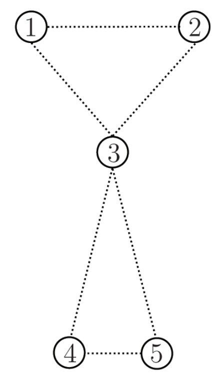

(b)

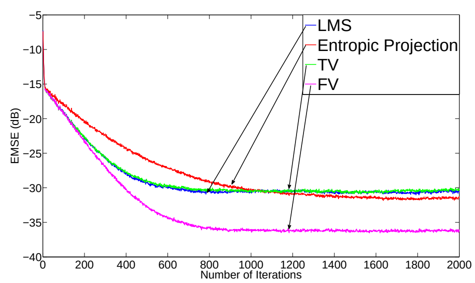

(c)

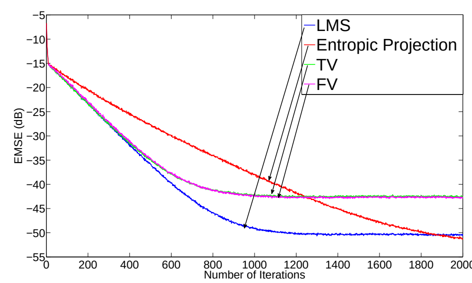

(d)

Figure 6.6: (a) Correlation between the nodes ($\boldsymbol{A}$) in the network topology shown in (b). EMSE comparison between five node topologies under (c) ε-contaminated Gaussian (first row in Table 6.3), and (d) white Gaussian noise (seventh row in Table 6.3). The proposed robust methods produce better EMSE results under ε-contaminated Gaussian noise.

Nodes	1	2	3	4	5
1	0.5	0.25	0.25	0	0
2	0.25	0.5	0.25	0	0
3	0	0.25	0.5	0.25	0
4	0	0	0.25	0.5	0.25
5	0	0	0	0.5	0.5

(a)

(b)

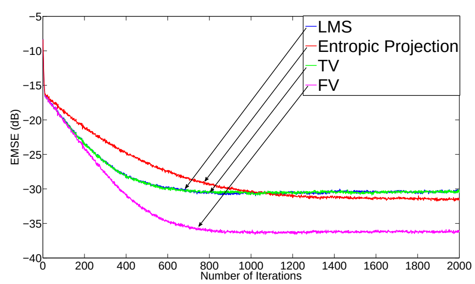

(c)

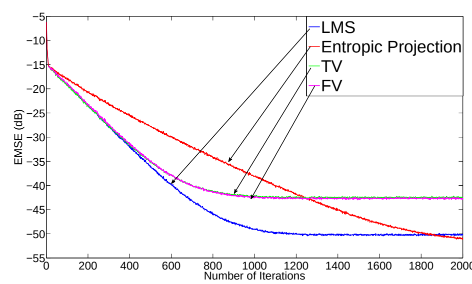

(d)

Figure 6.7: (a) Correlation between the nodes ($\boldsymbol{A}$) in the network topology shown in (b). EMSE comparison between five node topologies under (c) ε-contaminated Gaussian (first row in Table 6.3), and (d) white Gaussian noise (seventh row in Table 6.3). The proposed robust methods produce better EMSE results under ε-contaminated Gaussian noise.

Nodes	1	2	3	4	5
1	0.5	0.5	0	0	0
2	0	0.5	0.5	0	0
3	0	0	0.5	0.5	0
4	0	0	0	0.5	0.5
5	0	0	0	0	0.5

(a)

(b)

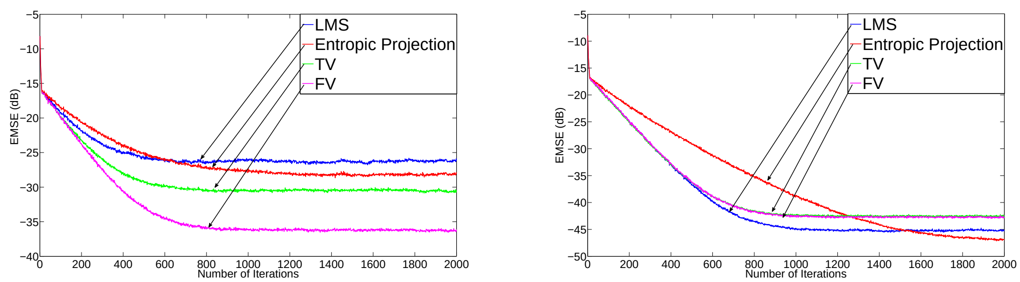

(c) (d)

Figure 6.8: (a) Correlation between the nodes ($\boldsymbol{A}$) in the network topology shown in (b). EMSE comparison between five node topologies under (c) ε-contaminated Gaussian (first row in Table 6.3), and (d) white Gaussian noise (seventh row in Table 6.3). The proposed robust methods produce better EMSE results under ε-contaminated Gaussian noise.

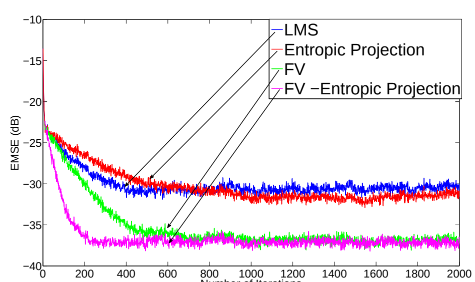

Figure 6.9: EMSE comparison between LMS and Entropic projection based adaptation schemes in Algorithm 1. Node topology shown in Fig. 6.7 (b) under ε-contaminated Gaussian, is used in the experiment. The noise parameters are given in Tables 6.1 and 6.3

Table 6.4: EMSE comparison for different topologies under various noise modes that are given in Table 6.3

Noise Model	1	2	3	4	5	6	Average (1-6)	7
Topology in Fig 6.5								
LMS based ATC	-25	-31	-15	-24	-44	-18	-26.17	-45
Entropy	-26	-32	-16	-26	-45	-19	-27.33	-45.5
TV	-29	-31.5	-20	-25	-39	-23	-27.92	-40.5
FV	-35.5	-36.5	-27.5	-30	-40	-30.5	-33.33	-40.5
Topology in Fig 6.6								
LMS based ATC	-30	-36.5	-20	-28.5	-48	-22	-30.83	-50
Entropy	-30.5	-37.5	-17.5	-29.5	-49	-22	-31	-50.5
TV	-30	-32.5	-19.5	-25	-39	-22	-28	-40.5
FV	-35.5	-37.5	-27.5	-31.5	-40	-30	-33.67	-40.5
Topology in Fig. 6.7								
LMS based ATC	-30	-35.5	-20	-39	-48	-23.5	-32.67	-50
Entropy	-31	-37.5	-18	-30	-49	-22.5	-31.33	-50.5
TV	-30	-32.5	-19.5	-35.5	-39	-23.5	-30	-40.5
FV	-36	-37.5	-27.5	-32	-40	-30.5	-33.92	-40.5
Topology in Fig 6.8								
LMS based ATC	-25	-32	-13	-24.5	-43	-16.5	-25.67	-45
Entropy	-26	-35	-17	-26	-39	-19.5	-27.08	-46.5
TV	-29.5	-32.5	-19.5	-25	-40	-22.5	-28.17	-41.5
FV	-36	-37.5	-28	-32	-44.5	-30	-34.67	-41.5

Chapter 7

CONCLUSIONS

In many signal processing problems, it is possible to have blurred, noisy and/or irregularly sampled versions of a signal or an image. The inverse problem of restoring the original signal or image is studied in this thesis. It is assumed that the signal is sparse in some transform domain such as Fourier, DCT or wavelet domain. This means that the signal or image can be accurately represented with some large valued transform coefficients. This assumption has also been used in transform domain digital waveform coding since 1960's. In this thesis, inverse signal processing methods are developed based on sparsity and interval convex programming.

Inverse signal processing problems are solved by minimizing the ℓ_1 norm or the Total Variation (TV) based cost functions in the literature. In this thesis, a modified entropy functional approximating the absolute value function is defined. This functional is also used to approximate the ℓ_1 norm, which is the most widely used cost function in sparse signal processing problems. The modified entropy functional is continuous, differentiable and convex. As a result a globally convergent iterative compressive sensing (CS) method using the modified entropy functional is developed. This method is computationally superior to other CS algorithms because it divides the large inverse problem into smaller problems defined by the rows of the CS measurement matrix. At each step of the algorithm a D-projection is performed on a hyperplane defined by a row of the measurement matrix. In this way it is possible to solve very large CS problems. Moreover the solution can be updated online, if a new measurement comes.

Total Variation (TV) based cost functions became recently popular in inverse signal processing problems using sparsity assumption. We are able to solve the TV based cost functions using Bregman's interval convex programming methods and projection onto convex sets (POCS) theory. Using TV based cost function, a locally adaptive TV denoising method is developed. The main feature of the method is that it can relax the TV based cost bound when there is an edge in the local analysis window. In this way, it is possible to achieve smoothing the image without blurring the edges.

We generalized the TV concept to Filtered Variation approach by replacing the differencing operator with a discrete-time high-pass filter. This allows us to use filters according to the frequency content of the signal, which is more or less available in some problems.

In this thesis, we also developed two new diffusion adaptation algorithms for cooperative multi-node networks. The first algorithm uses the modified entropy functional as the cost functional and the projection operator based on this functional defines an adaptation strategy. We then integrate the entropic projection operator into the adaptation stage of the problem. According to the experimental results, the new adaptation scheme turns out to be more effective than the ordinary LMS algorithm against impulsive noise, such as the ϵ-contaminated Gaussian noise. Since the entropy functional approximates the ℓ_1 norm, it is more robust against the effects of heavy tailed impulsive noise.

In the second class of algorithms, the TV and FV concepts are used to develop diffusion adaptation methods in multi-node networks. By minimizing the TV and FV cost functions, new adaptation and spatial combination stage equations in both temporal and spatial dimensions are obtained. In [4], the spatial combination stage was achieved using alpha-blending. Here the relation between the alpha-blending and the similarity between the filters of the neighboring nodes or the similarity between the old set of filter coefficients and the new ones are established using closed and convex sets, which limit the deviation between the node filters.

Since the adaptation, temporal and spatial combination constraints that are used in the diffusion adaptation problem are closed and convex sets, it is possible to solve the individual subproblems in an iterative manner by performing successive orthogonal projections onto the sets. Moreover, this approach enables the users to insert any other convex and closed constraint into the diffusion adaptation problem, according to their needs. It is possible to embed the entropy functional based algorithm into adaptation stage if the TV and FV based frameworks. The experimental results indicate that the new class of the algorithms perform similar to ATC and CTA methods [4] under white Gaussian noise. They perform better under ε-contaminated Gaussian noise. As in the original ATC and CTA frameworks, when the cooperation between the nodes increases, the performance of the proposed algorithms also increases.

Sparsity assumption is a reasonable assumption and it helps the signal interpolation, reconstruction, and restoration process in inverse problems. However, it sometimes oversimplifies or oversmoothes the signal because practical signals cannot be represented with a couple of transform domain coefficients in general. For example in transform domain signal, image, and video coding, the signal is divided into blocks and some smooth blocks are represented with a few transform domain coefficients. On the other hand, some block contain high-frequency information and the coder may even have to use all the transform domain coefficients to represent the block. In signal interpolation problem, a signal with sharp edge is used as an example. Interpolators using the sparsity assumption do not produce any good interpolation results. To solve this problem, transition band and stopband concepts from the discrete-time filtering theory is used. In this way, the reconstructed signal is allowed to have some high-frequency coefficients in transform domain. This led to better interpolation results than sparsity assumption.

APPENDIX A

Proof of Convergence of the Iterative Algorithm

The problem described in (2.2) and(2.8) is a convex programming problem

$$\begin{aligned} &\min_{\mathbf{s}\in H} \qquad g(\mathbf{s}) \\ &\text{subject to} \quad \theta_i.\mathbf{s} = y_i \quad for \quad i = 1, 2, ..., M \ , \end{aligned} \tag{A.1}$$

where $g(\mathbf{s})$ is a strictly convex and differentiable cost function in $\mathbb{R}^N$, H is the intersection of M hyperplanes $\theta_i.\mathbf{s} = y_i$, and $\mathbf{s} \in \mathbb{R}^N$. In [13], Bregman solved the convex optimization problem (A.1) using D-Projections. He proved in [13](Theorem 3) that starting from an initial point $s_0 = 0$, and making successive D-projections on convex hyperplanes as defined by $\theta_i.\mathbf{s} = y_i$ (Chapter 3), converges to the solution of the convex optimization problem, provided that H is non empty.

Statement 1: The function $g(x) = (|x| + \frac{1}{e})\log(|x| + \frac{1}{e}) + \frac{1}{e}$ is continuously differentiable in $\mathbb{R}$.

Proof: The derivative of the cost function $g(x)$ can be computed using the chain rule. The first derivative of the cost function $g(x)$ is

$$g'(x) = sign(x)\left[log\left(|x| + \frac{1}{e}\right) + 1\right], \tag{A.2}$$

which is a continuous function in $\mathbb{R}$. The plot of the function is shown in Figure A.1. Extension to $\mathbb{R}^N$ is straightforward.

Statement 2: The function $g(x)$ is a strictly convex function.

Proof: The second derivative of the cost function $g(x)$ is

$$g''(x) = \frac{1}{|x| + \frac{1}{e}} > 0, \tag{A.3}$$

where $g(x) > 0, \forall x \in \mathbb{R}$ The one-dimensional plot of the function is shown in Figure A.1. The cost function is strictly convex because its second derivative is non-negative $\forall x \in \mathbb{R}$.

The problem described in (4.19) is also a convex programming problem. The convergence of this optimization problem can also be proven using Theorem 4 of [13] because $g(\mathbf{s})$ is a strictly convex and differentiable function in $\mathbb{R}^N$.

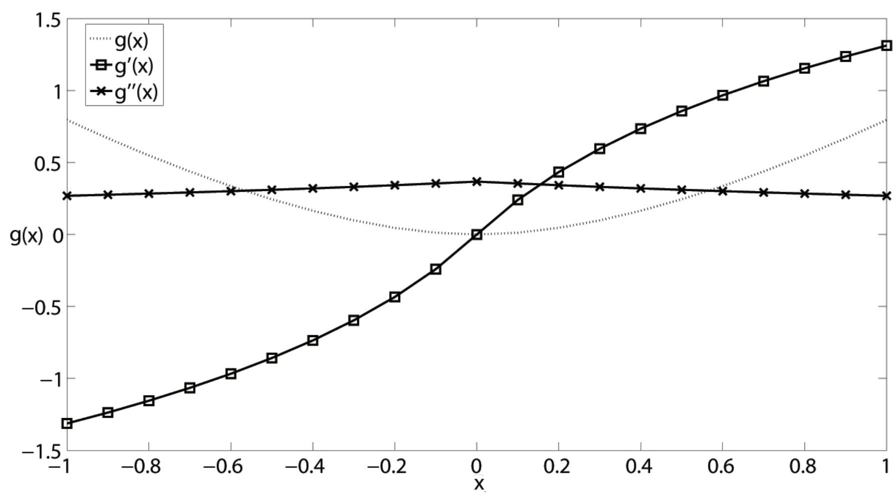

Figure A.1: The plot of the entropic cost function, its first, and second derivatives.

APPENDIX B

Proof of Convexity of the Filtered Variation Constraints

B.1 ℓ_1 Filtered Variation Bound

The set

$$C_1 = \left\{ \mathbf{x} : \sum_{k=0}^{N-1} |H[k]X[k]| \leq \varepsilon_1 \right\} \tag{B.1}$$

defines the ℓ_1 filtered variation bound constraint set. Let's assume that $\mathbf{X}_1, \mathbf{X}_2 \in C_1$. To prove the convexity of set C_1, we need to check if

$$\mathbf{X}_3 = \alpha \mathbf{X}_1 + (1-\alpha)\mathbf{X}_2,\ \forall \alpha \in [0,1] \tag{B.2}$$

satisfies the following condition

$$\sum_{k=0}^{N-1} |H[k]X_3[k]| \leq \varepsilon_1. \tag{B.3}$$

Using (B.2), one can rewrite (B.3) as follows

$$\begin{aligned} |H[k]X_3[k]| &= \sum_{k=0}^{N-1} |H[k](\alpha X_1[k] + (1-\alpha)X_2[k]))| && \text{(B.4)} \\ &= \sum_{k=0}^{N-1} |(\alpha H[k]X_1[k]) + ((1-\alpha)H[k]X_2[k]))| && \text{(B.5)} \end{aligned}$$

. Using triangle inequality in (B.5)

$$
\begin{aligned}
|H[k]X_3[k]| \leq & \sum_{k=0}^{N-1} \alpha \left|(H[k]X_1[k])\right| + (1-\alpha) \left|(H[k]X_2[k]))\right| && \text{(B.6)} \\
=& \alpha \left(\sum_{k=0}^{N-1} |(H[k]X_1[k])| \right) + (1-\alpha) \left(\sum_{k=0}^{N-1} |(H[k]X_2[k])| \right) && \text{(B.7)} \\
\leq & \varepsilon_1. && \text{(B.8)}
\end{aligned}
$$

Therefore, C_1 is a convex constraint set.

B.2 Time and Space Domain Local Variation Bounds

Let's consider the time and space domain local variation bound

$$
C_2 = \left\{ \mathbf{x} : \left| \sum_{i=-l}^{l} h[i]x[n-i] \right| \leq P \right\}, \tag{B.9}
$$

Let's assume that $\mathbf{x}_1, \mathbf{x}_2 \in C_2$. We would like to check if $\mathbf{x}_3 = \alpha \mathbf{x}_1 + (1-\alpha)\mathbf{x}_2 \in C_2,\ \forall \alpha \in [0,1]$. If this condition is satisfied, then C_2 defines a convex constraint set.

For the convexity of C_2 set, $\mathbf{x}_3$ should satisfy the condition (B.9) as

$$
\left| \sum_{i=-l}^{l} h[i]x_3[n-i] \right| \leq P. \tag{B.10}
$$

It is possible to rewrite (B.10) as

$$
\begin{aligned}
\left| \sum_{i=-l}^{l} h[i]x_3[n-i] \right| &= \left| \sum_{i=-l}^{l} h[i](\alpha x_1[n-i] + (1-\alpha)x_2[n-i] \right|. && \text{(B.11)} \\
&= \left| \sum_{i=-l}^{l} (\alpha h[i]x_1[n-i]) + ((1-\alpha)h[i]x_2[n-i]) \right|. && \text{(B.12)}
\end{aligned}
$$

. Using triangle inequality in (B.12)

$$\leq \alpha \left| \sum_{i=-l}^{l} (h[i] x_1[n-i]) \right| + (1-\alpha) \left| \sum_{i=-l}^{l} (h[i] x_2[n-i]) \right|. \tag{B.13}$$

$$\leq P \tag{B.14}$$

Therefore, C_2 is a convex constraint.

B.3 Bound on High Frequency Energy

Let's consider the bound on high frequency energy

$$C_3 = \left\{ \mathbf{x} : \sum_{k=k_0}^{N-k_0} |X[k]|^2 \leq \varepsilon_3 \right\}. \tag{B.15}$$

Let's assume that $\mathbf{X}_1, \mathbf{X}_2 \in C_3$. we would like to check if $\mathbf{X}_3 = \alpha \mathbf{X}_1 + (1-\alpha)\mathbf{X}_2 \in S_3,\ \forall \alpha \in [0, 1]$. If this condition is satisfied, then C_3 is a convex constraint set.

For the convexity of C_3 set, $\mathbf{X}_3$ should satisfy the condition (B.15) as

$$\sum_{k=k_0}^{N-k_0} |X_3[k]|^2 \leq \varepsilon_3 \tag{B.16}$$

It is possible to rewrite (B.16) as

$$\sum_{k=k_0}^{N-k_0} |X_3[k]|^2 = \sum_{k=k_0}^{N-k_0} |\alpha X_1[k] + (1-\alpha) X_2[k]|^2 \tag{B.17}$$

Since $|.|^2$ is a convex function, using definition of convexity of a function given in (3.1) of [139], one can rewrite (B.17) as

$$\sum_{k=k_0}^{N-k_0} |\alpha X_1[k] + (1-\alpha) X_2[k]|^2 \leq \alpha \left(\sum_{k=k_0}^{N-k_0} |X_1[k] \right) + (1-\alpha) \left(\sum_{k=k_0}^{N-k_0} |X_2[k] \right) \tag{B.18}$$

$$\leq \varepsilon_3 \tag{B.19}$$

Therefore, C_3 is a convex constraint.

B.4 Sample Value Locality Constraint

The Sample Value Locality Constraint is defined as

$$C_7 = \{\mathbf{x} : |x[n] - y[n]| < \delta\}\,, \tag{B.20}$$

where $x[n]$ and $y[n]$ are n^{th} samples from the signals $\mathbf{x}$, and $\mathbf{y}$. Let's assume that for $x_1[n], x_2[n] \in C_7$. Let's assume that $x_1[n], x_2[n] \in C_7$. We would like to check if $x_3[n] = \alpha x_1[n] + (1-\alpha)x_2[n] \in C_7,\ \forall\alpha \in [0,1]$. If this condition is satisfied, then C_7 is a convex constraint set.

Therefore, one needs to check if the following condition holds:

$$|x_3[n] - y[n]| << \delta. \tag{B.21}$$

It is possible to rewrite (B.21) as

$$|x_3[n] - y[n]| = \quad |\alpha x_1[n] + (1-\alpha)x_2[n] - y[n]| \tag{B.22}$$

$$= \quad |\alpha(x_1[n] - y[n]) + (1-\alpha)(x_2[n] - y[n])| \tag{B.23}$$

$$= \quad \alpha\,|(x_1[n] - y[n])\,| + (1-\alpha)|\,(x_2[n] - y[n])| \tag{B.24}$$

$$\leq \quad \delta \tag{B.25}$$

Therefore, C_7 is a convex constraint.

Bibliography

[1] G. Gilboa, "Shock Filters" Accessed at September 2012. [Online]. Available: http://visl.technion.ac.il/~gilboa/PDE-filt/shock_filters.html

[2] J. E. Fowler, S. Mun, and E. W. Tramel, "Block-based compressed sensing of images and video," *Foundations and Trends in Signal Processing*, vol. 4, no. 4, pp. 297–416, March 2012.

[3] P. L. Combettes and J. Pesquet, "Image restoration subject to a total variation constraint," *IEEE Transactions on Image Processing*, vol. 13, pp. 1213–1222, 2004.

[4] X. Zhao and A. H. Sayed, "Performance limits of lms-based adaptive networks," in *International Conference on Acoustics, Speech and Signal Processing (ICASSP), IEEE*, May 2011, pp. 3768 –3771.

[5] C. E. Shannon, "Communication in the presence of noise," *Proceedings of the Institute of Radio Engineers*, vol. 37, no. 1, pp. 10–21, 1949. [Online]. Available: http://ieeexplore.ieee.org/xpls/abs_all.jsp?arnumber=1697831

[6] E. Candes, "Compressive sampling," in *Proceedings of International Congress of Mathematics*, vol. 3, 2006, pp. 1433–1452.

[7] J.-L. Starck and F. Murtagh, *Astronomical Image and Data Analysis.* Springer-Verlag, 2006.

[8] W. Hardle, G. Kerkyacharian, D. Picard, and A. Tsybakov, *Wavelets, Approximation and Statistical Applications*, W. Hardle, G. Kerkyacharian, D. Picard, and A. Tsybakov, Eds. Springer, 1998.

[9] I. M. Johnstone, "Wavelets and the theory of nonparametric function estimation," *Philosophical Transactions of the Royal Society of London*, vol. 357, pp. 2475–2493, September S1999.

[10] J.-L. Starck, M. F., and J. M. Fadilli, *Sparse Image and Signal Processing: Wavelets, Curvelets, Morphological Diversity*. Cambridge University Press, 2010.

[11] E. J. Candes and T. Tao, "Near-optimal signal recovery from random projections: Universal encoding strategies?" *IEEE Transactions on Information Theory*, vol. 52, no. 12, pp. 5406–5425, 2006. [Online]. Available: http://ieeexplore.ieee.org/lpdocs/epic03/wrapper.htm?arnumber=4016283

[12] Y. Censor and A. Lent, "An iterative row-action method for interval convex programming," *Journal of Optimization Theory and Applications*, vol. 34, no. 3, pp. 321–353, 1981.

[13] L. M. Bregman, "The Relaxation Method of Finding the Common Point of Convex Sets and Its Application to the Solution of Problems in Convex Programming," *USSR Computational Mathematics and Mathematical Physics*, vol. 7, pp. 200–217, 1967.

[14] S. Osher, Y. Mao, B. Dong, and W. Yin, "Fast linearized bregman iteration for compressive sensing and sparse denoising," *Communications in Mathematical Sciences*, vol. 8(1), pp. 93–111, 2010.

[15] J.-F. Cai, S. Osher, and Z. Shen, "Linearized bregman iterations for compressed sensing," *Mathematics of Computation*, vol. 78, no. 267, pp. 1515–1536, 2009.

[16] L. I. Rudin, S. Osher, and E. Fatemi, "Nonlinear total variation based noise removal algorithms," *Phys. D*, vol. 60, pp. 259–268, November 1992. [Online]. Available: http://dx.doi.org/10.1016/0167-2789(92)90242-F

[17] D. C. Youla and H. Webb, "Image restoration by the method of convex projections, part i-theory," *IEEE Transactions on Medical Imaging*, vol. MI-I-2, pp. 81–94, 1982.

[18] D. Needell and J. A. Tropp, "CoSaMP: Iterative signal recovery from incomplete and inaccurate samples," 2008, arXiv:0803.2392v2.

[19] A. Chambolle, "An algorithm for total variation minimization and applications," *Journal of Mathematical Imaging and Vision*, vol. 20, pp. 89–97, 2004.

[20] K. Kose, A. Cetin, and O. Gunay, "Entropy minimization based robust algorithm for adaptive networks," in *Proceedings of Signal Processing and Communications Applications Conference (SIU)*, April 2012, pp. 1 –4.

[21] G. Baraniuk, "Compressed sensing [lecture notes]," *IEEE Signal Processing Magazine*, vol. 24, no. 4, pp. 118–124, 2007.

[22] E. J. Candes, J. Romberg, and T. Tao, "Robust uncertainty principles: exact signal reconstruction from highly incomplete frequency information," *IEEE Transactions on Information Theory*, vol. 52, no. 2, pp. 489–509, February 2006. [Online]. Available: http://dx.doi.org/10.1109/TIT.2005.862083

[23] Y. Tsaig and D. L. Donoho, "Compressed sensing," *IEEE Transaction on Information Theory*, vol. 52, pp. 1289–1306, 2006.

[24] R. Baraniuk, V. Cevher, M. Duarte, and C. Hegde, "Model-based compressive sensing," *IEEE Transactions on Information Theory*, vol. 56, no. 4, pp. 1982 –2001, April 2010.

[25] S. S. Chen, "Basis pursuit," Ph.D. dissertation, Stanford University, 1995.

[26] S. S. Chen, D. L. Donoho, and M. A. Saunders, "Atomic decomposition by basis pursuit," *SIAM Review*, vol. 43, pp. 129–159, 2001.

[27] A. Beck and M. Teboulle, "A fast iterative shrinkage-thresholding algorihm for linear inverse problems," *SIAM Journal of Imaging Sciences*, vol. 2, no. 1, pp. 183–202, 209.

[28] M. A. T. Figueiredo, D. R. Nowak, and S. J. Wright, "Gradient projection for sparse reconstruction: Application to compressed sensing and other

inverse problems," *IEEE Journal of Selected Topics in Signal Processing*, vol. 1, no. 4, pp. 586 –597, December 2007.

[29] J. Friedman, T. Hastie, and R. Tibshirani, "Regularization paths for generalized linear models via coordinate descent," *Journal of Statistical Software*, vol. 33(1), pp. 1–22, 2010.

[30] E. T. Hale, W. Yin, and Y. Zhang, "A fixed-point continuation method for l1 -regularized minimization with applications to compressed sensing," Rice University, Technical Report, TR07-07, 2007.

[31] T. Blumensath and M. E. Davies, "Iterative hard thresholding for compressed sensing," *Applied and Computational Harmonic Analysis*, vol. 27 (3), pp. 265–274, November 2009.

[32] J. A. Tropp, Anna, and C. Gilbert, "Signal recovery from random measurements via orthogonal matching pursuit," *IEEE Trans. Inform. Theory*, vol. 53, pp. 4655–4666, 2007.

[33] D. L. Donoho, Y. Tsaig, I. Drori, and J. luc Starck, "Sparse solution of underdetermined linear equations by stagewise orthogonal matching pursuit," Technical Report, 2006.

[34] D. Needell and R. Vershynin, "Signal recovery from incomplete and inaccurate measurements via regularized orthogonal matching pursuit."

[35] M. Pilanci, A. C. Gurbuz, and A. O., "Expectation maximization based matching pursuit," in *IEEE International Conference on Acoustics, Speech and Signal Processing (ICASSP)*, March 2012.

[36] D. Mark A., D. Marco F., E. Yonina, and K. Gitta, *Compressed Sensing: Theory and Applications*, E. Yonina and G. Kutyniok., Eds. Cambridge University Press, June, 2012.

[37] A. C. Gilbert, M. J. Strauss, J. A. Tropp, and R. Vershynin, "One sketch for all: fast algorithms for compressed sensing," in *Proceedings of the Thirty-Ninth Annual ACM Symposium on Theory of Computing*, ser.

STOC '07. New York, NY, USA: ACM, 2007, pp. 237–246. [Online]. Available: http://doi.acm.org/10.1145/1250790.1250824

[38] M. A. Iwen, "Combinatorial sublinear-time fourier algorithms," *Foundations of Computational Mathematics*, vol. 10 (3), pp. 303–338, 2010.

[39] M. F. Duarte, M. A. Davenport, D. Takhar, J. N. Laska, T. Sun, K. F. Kelly, and R. G. Baraniuk, "Single-pixel imaging via compressive sampling," *IEEE Signal Processing Magazine*, vol. 25, no. 2, pp. 83 –91, 2008.

[40] M. B. Wakin, J. N. Laska, M. F. Duarte, D. Baron, S. Sarvotham, D. Takhar, K. F. Kelly, and R. G. Baraniuk, "An architecture for compressive imaging," in *Proceedings of IEEE International Conference on Image Processing (ICIP)*, 2006, pp. 1273–1276.

[41] ——, "Compressive imaging for video representation and coding," in *Proceedings of Picture Coding Symposium (PCS)*, 2006.

[42] V. Cevher, A. Sankaranarayanan, M. F. Duarte, D. Reddy, and R. G. Baraniuk, "Compressive sensing for background subtraction," in *Proceedings of European Conference on Computer Vision (ECCV)*, 2008, pp. 155–168.

[43] M. Lustig, J. M. Santos, J. hyung Lee, D. L. Donoho, and J. M. Pauly, "Application of compressed sensing for rapid MR imaging," in *Proceedings of Signal Processing with Adaptative Sparse Structured Representations (SPARS)*, 2005.

[44] J. Trzasko and S. Member, "Highly undersampled magnetic resonance image reconstruction via homotopic ℓ_0-minimization," *IEEE Trans. Med. Imaging*, pp. 106–121, 2009.

[45] T. Cukur, M. Lustig, E. Saritas, and D. Nishimura, "Signal compensation and compressed sensing for magnetization-prepared mr angiography," *IEEE Transactions on Medical Imaging*, vol. 30, no. 5, pp. 1017–1027, May 2011.

[46] T. Cukur, M. Lustig, and D. Nishimura, "Improving non-contrast-enhanced steady-state free precession angiography with compressed sensing," *Magnetic Resonance Med.*, vol. 61, no. 5, pp. 1122–1131, May 2009.

[47] J. Provost and F. Lesage, "The application of compressed sensing for photo-acoustic tomography," *Medical Imaging, IEEE Transactions on*, vol. 28, no. 4, pp. 585 –594, april 2009.

[48] J. Choi, M. W. Kim, W. Seong, and J. C. Ye, "Compressed sensing metal artifact removal in dental ct," in *Proceedings of IEEE International Symposium on Biomedical Imaging: From Nano to Macro*, 2009.

[49] R. Willettt, M. Gehm, and D. Brady, "Multiscale reconstruction for computational spectral imaging," in *SPIE Electronic Imaging, Computational Imaging V.*, vol. 6498, 2007, p. 64980L.

[50] S. Gazit, A. Szameit, Y. C. Eldar, and M. Segev, "Super-resolution and reconstruction of sparse sub-wavelength images," *Optics Express*, vol. 17, no. 26, pp. 23 920–23 946, December 2009.

[51] A. Bourquard, F. Aguet, and M. Unser, "Optical imaging using binary sensors," *Optics Express*, vol. 18, no. 5, pp. 4876–4888, March 2010.

[52] D. J. Brady, K. Choi, D. L. Marks, R. Horisaki, and S. Lim, "Compressive holography," *Optics Express*, vol. 17, no. 15, pp. 13 040–13 049, July 2009.

[53] Y. Rivenson, A. Stern, and J. Rosen, "Compressive multiple view projection incoherent holography," *Optics Express*, vol. 19, no. 7, pp. 6109–6118, March 2011.

[54] L. Denis, D. Lorenz, E. Thiébaut, C. Fournier, and D. Trede, "Inline hologram reconstruction with sparsity constraints," *Optics Letters*, vol. 34, no. 22, pp. 3475–3477, November 2009.

[55] W. Dai, M. A. Sheikh, O. Milenkovic, and R. G. Baraniuk, "Compressive sensing dna microarrays," *EURASIP Journal on Bioinformatics and Systems Biology*, vol. 2009, no. 1, 2009.

[56] A. Griffin, T. Hirvonen, C. Tzagkarakis, A. Mouchtaris, and P. Tsakalides, "Single-channel and multi-channel sinusoidal audio coding using compressed sensing," *IEEE Transactions on Audio, Speech, and Language Processing*, vol. 19, no. 5, pp. 1382 –1395, July 2011.

[57] R. Baraniuk, "Compressive radar imaging," in *Proceedings of IEEE Radar Conference*, 2007, pp. 128–133.

[58] J. H. Ender, "On compressive sensing applied to radar," *Signal Processing*, vol. 90, no. 5, pp. 1402 – 1414, 2010.

[59] R. Moses, M. Cetin, and L. Potter, "Wide angle SAR imaging," in *Proceedings of SPIE Algorithms for Synthetic Aperture Radar Imagery XI*, 2004.

[60] J. Ma, "Improved iterative curvelet thresholding for compressed sensing and measurement," *IEEE Transactions on Instrumentation and Measurement*, vol. 60, no. 1, pp. 126 –136, January 2011.

[61] ——, "Single-pixel remote sensing," *IEEE Geoscience and Remote Sensing Letters*, vol. 6, no. 2, pp. 199 –203, April 2009.

[62] M. Mishali and Y. C. Eldar, "Wideband spectrum sensing at sub-nyquist rates [Applications Corner]," *IEEE Signal Processing Magazine*, vol. 28, no. 4, pp. 102–135, 2011.

[63] C. R. Berger, Z. Wang, J. Huang, and S. Zhou, "Application of compressive sensing to sparse channel estimation," *IEEE Communications Magazine*, vol. 48, no. 11, pp. 164–174, 2010.

[64] C. R. Berger, S. Zhou, J. C. Preisig, and P. Willett, "Sparse channel estimation for multicarrier underwater acoustic communication: from subspace methods to compressed sensing," *IEEE Transactions on Signal Processing*, vol. 58, no. 3, pp. 1708–1721, 2010.

[65] D. Gross, Y.-K. Liu, S. T. Flammia, S. Becker, and J. Eisert, "Quantum state tomography via compressed sensing," *Physical Review Letters*, vol. 105, p. 150401, October 2010.

[66] A. Shabani, R. L. Kosut, M. Mohseni, H. Rabitz, M. A. Broome, M. P. Almeida, A. Fedrizzi, and A. G. White, "Efficient measurement of quantum dynamics via compressive sensing," *Physical Review Letters*, vol. 106, March 2011.

[67] L. Rudin, "Images, Numerical Analysis of Singularities and Shock Filters," Ph.D. dissertation, California Institute of Technology, Pasadena, California, 1987.

[68] S. Osher and L. I. Rudin, "Feature oriented image enhancement using shock filters," *SIAM Journal of Numerical Analysis*, vol. 27, p. 919, 1990.

[69] S. Osher, M. Burger, D. Goldfarb, J. Xu, and W. Yin, "An iterative regularization method for total variation-based image restoration," *Multiscale Modelling and Simulation*, vol. 4, pp. 460–489, 2005.

[70] P. Combettes, "The foundations of set theoretic estimation," *Proceedings of the IEEE*, vol. 81, no. 2, pp. 182 –208, February 1993.

[71] D. Butnariu, R. Davidi, G. Herman, and I. Kazantsev, "Stable convergence behavior under summable perturbations of a class of projection methods for convex feasibility and optimization problems," *IEEE Journal of Selected Topics in Signal Processing*, vol. 1, no. 4, pp. 540 –547, December 2007.

[72] F. Malgouyres, "Minimizing the total variation under a general convex constraint for image restoration," *IEEE Transactions on Image Processing*, vol. 11, no. 12, pp. 1450 – 1456, December 2002.

[73] M. Persson, D. Bone, and H. Elmqvist, "Total variation norm for three-dimensional iterative reconstruction in limited view angle tomography," *Physics in Medicine and Biology*, vol. 46, no. 3, p. 853, 2001.

[74] T. F. Chan, S. Esedoglu, F. Park, and A. Yip, *Mathematical Models in Computer Vision: The Handbook, ch. Recent developments in total variation image restoration.* Springer, 2005.

[75] B. R. Frieden, "Restoring with maximum likehood and maximum entropy," *Journal of Optical Society of America*, vol. 62, p. 511, 1972.

[76] D. L. Phillps, "A technique for numerical solution of certain integral equations of the first kind," *Journal of ACM*, vol. 9, p. 84, 1962.

[77] S. .Twomey, “On the numerical solution of fredholm integral equations of the first kind by the inversion of the linear system procduced by quadratures,” *Journal of ACM*, vol. 10, p. 97, 1963.

[78] G. Gilboa, N. Sochen, and Y. Zeevi, “Image enhancement and denoising by complex diffusion processes,” *IEEE Transactions on Pattern Analysis and Machine Intelligence*, vol. 26, no. 8, pp. 1020 –1036, August 2004.

[79] C. Li, “An efficient algorithm for total variation regularization with applications to the single pixel camera and compressive sensing,” Ph.D. dissertation, Rice University, September 2009.

[80] D. Goldfarb and W. Yin, “Second-order cone programming methods for total variation-based image restoration,” *SIAM Journal of Scientific Computing*, vol. 27, pp. 622–645, 2004.

[81] E. Candes and T. Tao, “Decoding by linear programming,” *IEEE Transactions on Information Theory*, vol. 51, no. 12, pp. 4203 – 4215, December 2005.

[82] S. Becker, J. Bobin, and E. J. Candes, “Nesta: A fast and accurate first-order method for sparse recovery,” *SIAM Journal on Imaging Sciences,*, vol. 4 (1), pp. 1–39, 2011.

[83] Y. Nesterov, “Smooth minimization of non-smooth functions,” *Mathematical Programming*, vol. 103, pp. 127–152, 2005.

[84] G. T. Herman, “Image reconstruction from projections,” *Real-Time Imaging*, vol. 1, no. 1, pp. 3–18, 1995.

[85] H. Trussell and M. R. Civanlar, “The landweber iteration and projection onto convex set,” *IEEE Transactions on Acoustics, Speech and Signal Processing*, vol. 33, no. 6, pp. 1632–1634, 1985.

[86] I. Sezan and H. Stark, “Image restoration by the method of convex projections: Part 2-applications and numerical results,” *IEEE Transactions on Medical Imaging*, vol. 1, no. 2, pp. 95–101, 1982.

[87] A. E. Çetin, "An iterative algorithm for signal reconstruction from bispectrum," *IEEE Transactions on Signal Processing*, vol. 39, no. 12, pp. 2621–2628, 1991.

[88] A. E. Çetin and R. Ansari, "Signal recovery from wavelet transform maxima," *IEEE Transactions on Signal Processing*, vol. 42-1, pp. 194–196, 1994.

[89] ——, "Convolution-based framework for signal recovery and applications," *Journal of the Optical Society of America*, vol. 5, pp. 1193–1200, 1988.

[90] K. S. Theodoridis and I. Yamada, "Adaptive learning in a world of projections," *IEEE Signal Processing Magazine*, vol. 28, no. 1, pp. 97–123, 2011.

[91] R. Chartrand, "Exact reconstruction of sparse signals via nonconvex minimization," *IEEE Signal Processing Letters*, vol. 14, no. 10, pp. 707 –710, oct. 2007.

[92] M. Ehler, "Shrinkage rules for variational minimization problems and applications to analytical ultracentrifugation," *Journal Inverse Ill-Posed Problems*, vol. 19, pp. 593–614, 2011.

[93] K. Bredies and D. A. Lorenz, "Minimization of non-smooth, non-convex functionals by iterative thresholding," submitted (DFG SPP 1324 Preprint 10), April 2009.

[94] H. T. Lent, "An iterative method for the extrapolation of band-limited functions," *Journal of Mathematical Analysis and Applications, 83 (2), pp.1981*, vol. 83, pp. 554–565, 1981.

[95] J.-B. Hiriart-Urruty and C. Lemarechal, *Convex Analysis and Minimization Algorithms II.* Springer, October 1993.

[96] M. C. Pinar and S. A. Zenios, "An entropic approximation of ℓ_1 penalty function," *Transactions on Operational Research*, pp. 101–120, 1995.

[97] R. Davidi, G. Herman, and Y. Censor, "Perturbation-resilient block-iterative projection methods with application to image reconstruction from

projections," *International Transactions in Operational Research*, vol. 16, no. 4, pp. 505–524, 2009.

[98] A. E. Çetin, "Reconstruction of signals from fourier transform samples," *Signal Processing*, vol. 16, pp. 129–148, 1989.

[99] M. Elad and A. Feuer, "Restoration of a single superresolution image from several blurred, noisy, and undersampled measured images," *IEEE Transactions on Image Processing*, vol. 6, no. 12, pp. 1646 –1658, December 1997.

[100] Y.-H. Dai, "Fast algorithms for projection on an ellipsoid," *SIAM Journal on Optimization*, vol. 16, no. 4, pp. 986–1006, 2006.

[101] E. Margolis and Y. Eldar, "Nonuniform sampling of periodic bandlimited signals," *IEEE Transaction on Signal Processing*, vol. 56, no. 7, pp. 2728–2745, July 2008.

[102] K. Yao and J. Thomas, "On some stability and interpolatory properties of nonuniform sampling expansions," *IEEE Transactions on Circuit Theory*, vol. 14, no. 4, pp. 404 –408, December 1967.

[103] J. Yen, "On nonuniform sampling of bandwidth-limited signals," *IEEE Transactions on Circuit Theory*, vol. 3, no. 4, pp. 251 – 257, December 1956.

[104] A. Jerri, "The shannon sampling theorem - its various extensions and applications: A tutorial review," *Proceedings of the IEEE*, vol. 65, no. 11, pp. 1565 – 1596, nov. 1977.

[105] R. Prendergast, B. Levy, and P. Hurst, "Reconstruction of band-limited periodic nonuniformly sampled signals through multirate filter banks," *IEEE Transactions on Circuits and Systems I: Regular Papers*, vol. 51, no. 8, pp. 1612 – 1622, August 2004.

[106] H. Johansson, P. Lowenborg, and K. Vengattaramane, "Least-squares and minimax design of polynomial impulse response fir filters for reconstruction of two-periodic nonuniformly sampled signals," *IEEE Transactions on*

Circuits and Systems I: Regular Papers, vol. 54, no. 4, pp. 877 –888, April 2007.

[107] F. Marvasti, M. Analoui, and M. Gamshadzahi, "Recovery of signals from nonuniform samples using iterative methods," *IEEE Transactions on Signal Processing*, vol. 39, no. 4, pp. 872 –878, April 1991.

[108] H. G. Feichtinger, K. Grchenig, and T. Strohmer, "Efficient numerical methods in non-uniform sampling theory," *Numerical Mathematics*, vol. 69, pp. 423–440, 1995.

[109] T. E. Tuncer, "Block-based methods for the reconstruction of finite-length signals from nonuniform samples," *IEEE Transactions on Signal Processing*, vol. 55, no. 2, pp. 530 –541, February 2007.

[110] H. Choi and R. Baraniuk, "Interpolation and denoising of nonuniformly sampled data using wavelet-domain processing," in *Prooceedings of IEEE International Conference on Acoustics, Speech, and Signal Processing*, vol. 3, March 1999, pp. 1645 –1648.

[111] A. Ozbek, "Adaptive seismic noise and interference attenuation method," US Patent 6 446 008, 2002.

[112] A. Papoulis, "A new algorithm in spectral analysis and band-limited extrapolation," *IEEE Transactions on Circuits and Systems*, vol. 22, no. 9, pp. 735–742, September 1975.

[113] W. Lertniphonphun and J. McClellan, "Complex frequency response fir filter design," in *Proceedings of the 1998 IEEE International Conference on Acoustics, Speech and Signal Processing*, vol. 3, May 1998, pp. 1301 –1304 vol.3.

[114] J. Munson, D. and E. Ullman, "Support-limited extrapolation of offset fourier data," in *Proceedings of IEEE International Conference on Acoustics, Speech, and Signal Processing (ICASSP)*, vol. 11, April 1986, pp. 2483–2486.

[115] K. Haddad, H. Stark, and N. Galatsanos, "Constrained fir filter design by the method of vector space projections," *IEEE Transactions on Circuits and Systems II: Analog and Digital Signal Processing*, vol. 47, no. 8, pp. 714–725, August 2000.

[116] A. Cetin, O. Gerek, and Y. Yardimci, "Equiripple fir filter design by the fft algorithm," *IEEE Signal Processing Magazine*, vol. 14, no. 2, pp. 60–64, March 1997.

[117] A. E. Cetin and R. Ansari, "Signal recovery from wavelet transform maxima," *IEEE Transactions on Signal Processing*, vol. 42, pp. 194–196, 1994.

[118] K. Slavakis, S. Theodoridis, and I. Yamada, "Online kernel-based classification using adaptive projection algorithms," *IEEE Transactions on Signal Processing*, vol. 56, pp. 2781–2796, 2008.

[119] S. Alliney, "A property of the minimum vectors of a regularizing functional defined by means of the absolute norm," *IEEE Transactions on Signal Processing*, vol. 45, no. 4, pp. 913–917, April 1997.

[120] M. Nikolova, "A variational approach to remove outliers and impulse noise," *J. Math. Imaging Vis.*, vol. 20, no. 1-2, pp. 99–120, Jan. 2004. [Online]. Available: http://dx.doi.org/10.1023/B:JMIV.0000011920.58935.9c

[121] C. Micchelli, L. Shen, Y. Xu, and X. Zeng, "Proximity algorithms for the l1/tv image denoising model," *Advances in Computational Mathematics*, pp. 1–26, 2011.

[122] G. Pierra, "Decomposition through formalization in a product space," *Mathematical Programming*, vol. 28, pp. 96–115, 1984, 10.1007/BF02612715. [Online]. Available: http://dx.doi.org/10.1007/BF02612715

[123] V. Cevher, C. Hegde, M. F. Duarte, and R. G. Baraniuk, "Sparse signal recovery using markov random fields," in *Proceedings of the Workshop on Neural Information Processing Systems (NIPS)*, 2008.

[124] J. A. Tropp, “Just relax: Convex programming methods for subset selection and sparse approximation,” Univ. Texas at Austin, Technical Report ICES Report 04-04, February 2004.

[125] J.-J. Fuchs, “On sparse representations in arbitrary redundant bases,” *IEEE Transactions on Information Theory*, vol. 50, no. 6, pp. 1341–1344, June 2004.

[126] K. Kose and A. Cetin, “Low-pass filtering of irregularly sampled signals using a set theoretic framework,” *IEEE Signal Processing Magazine*, vol. 28, no. 4, pp. 117 –121, July 2011.

[127] M. H. Hayes, *Statistical Digital Signal Processing and Modeling*. Wiley, 1996.

[128] A. H. Sayed, *Adaptive Filters*. John Wiley & Sons, 2008.

[129] N. Bershad, “Analysis of the normalized lms algorithm with gaussian inputs,” *IEEE Transactions on Acoustics Speech and Signal Processing*, vol. 34, no. 4, pp. 793–806, 1986.

[130] A. Weiss and D. Mitra, “Digital adaptive filters: Conditions for convergence, rates of convergence, effects of noise and errors arising from the implementation,” *IEEE Transactions on Information Theory*, vol. 25, no. 6, pp. 637–652, November 1979.

[131] O. Arikan, M. Belge, A. Cetin, and E. Erzin, “Adaptive filtering approaches for non-gaussian stable processes,” in *Proceedings of IEEE International Conference on Acoustics, Speech, and Signal Processing (ICASSP)*, vol. 2, May 1995, pp. 400–14 031.

[132] O. Gunay, B. Toreyin, K. Kose, and A. Cetin, “Entropy-functional-based online adaptive decision fusion framework with application to wildfire detection in video,” *IEEE Transactions on Image Processing*, vol. 21, no. 5, pp. 2853–2865, May 2012.

[133] K. Slavakis, S. Theodoridis, and I. Yamada, “Adaptive constrained learning in reproducing kernel hilbert spaces: the robust beamforming case,” *IEEE*

Transactions on Signal Processing, vol. 57, no. 12, pp. 4744–4764, Dec. 2009. [Online]. Available: http://dx.doi.org/10.1109/TSP.2009.2027771

[134] N. Grammalidis, A. E. Cetin, and et al., "Fire detection and management through a multi-sensor network for the protection of cultural heritage areas from the risk of fire and extreme weather conditions (FIRESENSE)," Grant no: FP7-ENV-2009-1-244088: EC FP7 Project.

[135] K. Dimitropoulos, K. Kose, N. Grammalidis, and E. Çetin, "Fire detection and 3-d fire propagation estimation for the protection of cultural heritage areas," *ISPRS Technical Commission VIII Symposium*, vol. 38, pp. 620–625, 2010.

[136] N. Grammalidis, A. E. Cetin, K. Dimitropoulos, F. Tsalakanidou, K. Kose, O. Gunay, B. Gouverneur, D. Torri, E. Kuruoglu, S. Tozzi, A. Benazza, F. Chaabana, B. Kosucu, and C. Ersoy, "A multi-sensor network for the protection of cultural heritage," in *Proceedings of European Signal Processing Conference (EUSIPCO)*, 2011.

[137] J. Duchi, S. S. Shwartz, Y. Singer, and T. Chandra, "Efficient projections onto the l1-ball for learning in high dimensions," in *Proceedings of the 25th International Conference on Machine Learning*, ser. ICML. ACM, 2008, pp. 272–279.

[138] K. Kose, V. Cevher, and A. E. Cetin, "Filtered variation method for denoising and sparse signal processing," in *Proceedings of IEEE International Conference on Acoustics, Speech and Signal Processing (ICASSP)*, March 2012.

[139] S. Boyd and L. Vandenberghe, *Convex Optimization*, S. Boyd and L. Vandenberghe, Eds. Cambridge University Press, 2004.